EFFECTIVE DEPTH OF SOIL COMPACTION UNDER A CONTROLLED COMPACTIVE EFFORT AT LABORATORY SCALE

By

Andres R. Tascon

A dissertation submitted in partial fulfillment of the requirements for the degree of

MASTER OF SCIENCE (GEOLOGICAL ENGINEERING)

at the

University of Wisconsin- Madison

2011

EFFECTIVE DEPTH OF SOIL COMPACTION UNDER A CONTROLLED COMPACTIVE EFFORT AT LABORATORY SCALE

Approved

Dante O. Fratta, Associate Professor
08/26/2011

ABSTRACT

EFFECTIVE DEPTH OF SOIL COMPACTION UNDER A CONTROLLED COMPACTIVE EFFORT AT LABORATORY SCALE

Andres R. Tascon

Under supervision of Associate Professor Dante Fratta
Geological Engineering Program
University of Wisconsin - Madison

Embankment construction specifications in the State of Wisconsin indicate that compaction lifts cannot be thicker than 20 cm. This specification was established several years ago based on field experience when compactors were lighter and smaller than the equipment used today. Lift thickness may be increased to save construction time and cost when heavier and larger compaction equipment is used. In this research effort, the possibility of increasing lift thickness specifications in the construction industry without compromising the embankment stability is explored by developing a methodology to evaluate engineering properties of compacted soils.

A laboratory soil compaction test was designed to compact soil under controlled compactive efforts while monitoring mechanical soil properties before, during and after compaction. The soil underwent eight compaction passes. The soil properties were monitored using techniques including nuclear density gauge (NDG), soil stiffness gauge (SSG), dynamic cone penetrometer (DCP), P-wave velocity tests, and MEMS-accelerometers rotations. Soil density, stiffness, shear strength, and deformation profiles were thus measured as a function of the compactive effort, soil type, water content, and lift thickness.

Thicker lifts results in greater soil surface displacement but less volume change and less uniform compaction than thin lifts. Furthermore, thin lifts undergo larger strains and yield greater stiffnesses than thick lifts. A comparison of the laboratory tests performed in this study with a real soil compaction monitoring experiment shows that, despite the differences in scale, density in thick lifts decreases with depth, and shows regions of low density at the bottom of the lift. Soils with larger shear strength results when are compacted closer of the optimum water content. Analysis of the stiffness measurements shows that the use of the SSG in embankment construction using thin lift should consider the influence of the stiffness ratio between the lift and the underlying layer. The effective depth of influence of the compactor used in this laboratory study reached about 15 cm; where, as for field operations using a compactive force that is 22 times larger, the influence reaches 30 to 40 cm.

ACKNOWLEDGMENTS

I would like to express my gratitude to all the people who help me to make my stay in USA a wonderful experience. I would like to especially thank my advisor Dante Fratta for all his support and guidance through my research; also for his kind hospitality in many familiar diners. Work under his supervision, it has being an unbelievable experience where I have learned not just engineering knowledge but also how to grow as a professional.

Also, I would like to thank my parents, Ricardo Tascon and Maria Antonieta Sturla, and my sister, Camila Tascon, for their support and for always being there in moments when I needed them.

I wish to express my sincere thanks to professors Tuncer Edil and James Tinjum, for being part of my defense committee, and professor Herb Wang for giving me the opportunity of visiting the Homestake Mine at Lead, South Dakota. It was a great professional experience. Finally, I want to express my gratitude to all my friends here at Wisconsin, especially to Vonmarie Martinez, Ozlem Bozyurt, Ali Ebrahimi, Marcos Montoro, and Erica Hagen for sharing with me wonderful moments as fellow students.

TABLE OF CONTENT

LIST OF FIGURES

LIST OF TABLES

1. INTRODUCTION

1.1. Motivation

This research is a part of an experimental investigation with the objective to evaluate the potential of increasing lift thicknesses in embankment construction. This document presents a laboratory testing program, designed and conducted to make a comparative analysis with field-scale embankment constructions and to support the possibility of increasing the lift thicknesses in soil compaction specifications.

1.2. Context

In embankment construction, an appropriate selection of the lift thickness has important engineering and economic implications in the design, construction and performance of road, levees, and dams (Kim et al. 2011). Currently, the standard specification from the Department of Transportation in the State of Wisconsin (WisDOT) for road construction recommends a lift thickness less than 20 cm (8 in - Standard Specifications for Highway and Structure Construction – WisDOT 1996). This recommendation was based on the size and weight of 90's era compaction equipment that were smaller than the current compactors, which induce larger compactive energies (Kim et al. 2011). Contractors and WisDOT officials are willing to consider increasing maximum allowable lift thicknesses to reduce construction time and total cost if the engineering properties of the embankments are not compromised. The concern is that a large increment in lift thicknesses may also produce mechanically unstable embankments due to the reduction of compaction effectiveness, thus leaving regions with low density and poor engineering properties (Kim et al. 2011).

Therefore, the increase of maximum lift thicknesses has to be technically justified to guarantee the mechanical performance of soil embankments.

1.3. Objective

The objective of this experimental research is to evaluate, at laboratory-scale, the engineering properties of soil under a controlled compactive effort for different lift thicknesses, soil type, and molding water content. The results of these experiments are then related to field tests performed as part of a larger research program at the University of Wisconsin-Madison.

1.4. Scope

The research of soil compaction monitoring at laboratory-scale consists of:

- Designing and building an experimental program to evaluate soil compaction at laboratory-scale using different lift thickness, soil type, water content, and energy levels (as represented by number of passes).
- Designing and implementing a methodology to evaluate the engineering soil properties before, during and after compaction.
- Analyzing and interpreting experimental data to make a comparative analysis with field-scale soil compaction situations.

2. BACKGROUND

Engineering projects such as foundations, earth dams, slope stability, highway and railway fills or landfills barriers require soils with minimum engineering properties. Generally, natural soil does not have the engineering properties required by the project; therefore, most soils have to be stabilized or improved to accomplish the desired engineering properties. Soil improvement may consist of mechanical, chemical, thermal or electrical stabilization (Lambe and Whitman 1969; Bowels 1979). These improvements may consist of increasing soil density to reduce settlements by increasing stiffness, improving shear strength by chemical or physical changes, and enhancing drainage by removing or replacing poor performing soils. Increasing the soil density by mechanical compaction is one of the most widely used methods to improve the engineering properties of soil (Lambe and Whitman 1969; Holtz 1990; Rollings and Rollings 1996). This section describes the main aspects of soil compaction.

2.1. General compaction characteristics, procedures and specifications

Soil compaction is defined as a method for mechanically increasing the density of soil by reducing the air volume from the pore space. The main objective of the compaction process is to increase the strength and stiffness of soils by reducing the compressibility and to decrease the permeability of the soil mass by reducing its porosity (Lambe and Whitman 1969; Rollings and Rollings 1996; Holtz et al. 2010).

Proctor (1933) proposed a procedure to determine the maximum density of the soil as a function of the water content and compactive effort (Lambe and Whitman 1969; Bowles

1979; Rollings and Rollings 1996). This procedure is described in ASTM D 698 and ASTM D 1557 standards. These standards describe procedures that use different energy levels to better represent field conditions when heavy machinery are used (Holtz et al. 2010). Figure 2.1 shows the typical compaction relationship found by Proctor (1933) for different compaction energies. This relationship shows how dry density initially increases when the water content increases until reaching the maximum dry density at the optimum water content. When soil is compacted at water content greater than optimum water content, the dry density decreases. As the energy of compaction increases, similar convex curves are obtained by the curves are shifted to the left and up. That is, increasing compaction energies yield higher dry densities and lower optimal water contents. The figure also presents the zero air void line and line of optimums. The zero air void line associates the dry unit weight that corresponds to soil fully saturated with water. This line represents a boundary state that cannot be crossed by the compactive process. The line of optimums joins the points that correspond to the maximum dry density and optimum water content for different compaction efforts. The line of optimums corresponds to approximately 85 to 90% degree of saturation (Rollings and Rollings 1996).

2.2. Fabrics in compacted soils

When soils are compacted, the compactive effort displaces soil particles thus reducing the air void volume and increasing the density of the soil. As compaction progresses, the soil deforms reducing its porosity and increasing the interlocking and contact forces between particles until the soil has sufficient shear strength to resists the compactive effort. After the compactive effort is released, the soil slightly expands vertically, which reduces the lateral

pressure and produces negative water pore pressure within the soil. The negative water pore pressure in addition to the lateral pressure and the soil interlocking, produce enough effective stress to maintain the soil deformation and thus the soil density (Olson 1963).

The rearrangement of particles is different for soil compacted at water content less than optimal water content (i.e., dry side on the compaction curve) than for soil compacted at water content higher than the optimal water content (i.e., the wet side of the compaction curve - Daniel and Benson 1990; Holtz el al. 2010). The compaction method, compaction effort and strength of the preexisting fabric affect the final soil particle arrangement during compaction. This phenomenon is more clearly observed in fine-grained soils compacted at the wet side of optimum (Mitchell and Soga 2005). When soils are compacted at the wet side of optimum, an alignment of particles or particle groups are produced along the horizontal plane whereas particles compacted at the dry side tend to be more flocculated (Lambe and Whitman 1969). Furthermore, higher compactive efforts disperse the soil particles if the soil is compacted on the dry side and produces more particle alignment along the horizontal plane that a low compactive effort on the wet side of optimum (Lambe and Whitman 1969). While fine graded soils compacted dry of optimum, the risk of swelling usually increases due to the tendency to absorb water (Holtz et al. 2010). Moreover, soil compressibility increases when soils are compacted wet of optimum (Bowels 1979; Holtz et al. 2010). Figures 2.2 and 2.3 schematically show the fabric of compacted soils as a function of the water content and compactive effort. Figure 2.4 shows how the molding water content at compaction influences the permeability of the soil due to changes in the soil fabric (Lambe and Whitman 1969; Mitchell and Soga 2005). The permeability may change by one order of magnitude if the soil

is compacted at the same density on the dry side or on the wet side of optimum (Holtz et al. 2010).

2.3. Factors affecting compaction

Researchers such as Turnbull and Foster (1956), D'Appolonia et al. (1969), Bowels (1979), and Holtz et al. (2010) have identified method, molding water content, effort and the soil type as the main parameters controlling the compaction behavior of soils. This section describes the influence of these factors on the process of compaction and on the final performance of the compacted fill.

2.3.1. Compaction method

Different compaction methods yield different results. Seed and Chan (1959) indicate that significantly different shear strength and volumetric stability are produced when soils are compacted using different compaction methods and water content as shown figure 2.5. The influence of the compaction method can be observed in figure 2.6 as well, where the same soil was compacted using different methods of compaction. The differences observed are produced by factors acting at laboratory scale for design, and at field scale during compaction (Holtz et al. 2010). As example, one of these factors is the presence of oversize material in the field that is not considered in laboratory tests. Furthermore, particles of soil may break down or degrade under the compaction hammer at test scale, increasing the fine content in the specimen (Holtz et al. 2010).

The selection of the compaction method depends mainly on the soil type and the equipment availability at the site (Bowels 1979 and Holtz et al. 2010). However there are no fixed rules for selecting the most appropriate compaction method, just guidelines justified on field experiences. In the literature, pounding, kneading, pressure, vibration, and dynamic compaction may be recognized as the most common compaction methods used in the construction industry. Rollings and Rollings (1996) suggest using dynamic forces such as vibration or impact for coarse grained soils and sheepfoot rollers for fine graded soils. Also Holtz et al. (2010) give some recommendations on the compaction method selection according to the applications of the soil improvement. As an example, Holtz et al. (2010) suggest vibrating rollers to compact coarse granular soils to be used in base and subbase for highway construction, parking areas, etc. Zou et al. (2005) evaluate the use of dynamic compaction on high road embankments and suggest that the construction rate and degree of compaction are higher when dynamic compaction is used rather than when roller compaction is used. Table 2.1 summarizes recommendations of compaction methods and compaction equipment for different types of soils.

Table 2.1: Compaction method and type of compactor recommended by Rollings and Rollings (1996)

Soil	First choice	Second choice	Comment
Rock fill	Vibratory roller	Pneumatic roller	-
Plastic soils – CH, MH	Sheepsfoot or pad foot roller	Pneumatic roller	Thin lifts usually needed
Low plasticity soils – CL, ML	Sheepsfoot or pad foot roller	Pneumatic vibratory roller	Moisture control often critical for silty soils
Plastic sands and gravels – GC, SC	Vibratory, pneumatic roller	Pad foot roller	-
Silty sands and gravels – SM, GM	Vibratory roller	Pneumatic, pad foot roller	Moisture control often critical
Clean sands – SW, SP	Vibratory roller	Impact, pneumatic roller	-

2.3.2. Molding water content

One variable which may be controlled during soil compaction operations is the amount of molding water. Generally to accomplish the standard specifications (95% of the maximum dry density measured by the ASTM D 1556 sand cone method as is required by WisDOT 1996), the optimum water content determined by Proctor test, is added to the soil. However in some cases it is recommendable to compact soils using different molding water contents than the optimum water content, since different water contents may give a range of soil properties (Mitchell and Soga 2005). As is discussed in section 2.2, compacting the soil at the dry or wet side of the optimum water content yields different soil fabric configurations which allow a range of suction and conduction phenomena such as hydraulic and thermal conductivity. Daniel and Benson (1990) propose different ranges of water content and dry density for a compacted soil to be used as a impervious barrier or liner (low hydraulic

conductivity) or zones where may be used as embankment where low compressibility and high shear strength are needed. Figure 2.7 shows schematically different ranges of molding water content in terms of soil properties and applications.

The matric suction of a compacted soil changes the shape of the soil water characteristic curve (SWCC) due to different pore structures or soil fabrics created during the compaction process (Tinjum et al. 1997). Figure 2.8 shows the differences in the SWCC for a clay soil CL and for a CH compacted at the dry side, wet side and optimum water content using different compactive effort. As matric suction and thus the long-term water content of the fill is affected by the molding water content at compaction, other soil properties such as the small strain shear modulus and the thermal conductivity are affected in long-term as well.

The small strain shear modulus is used in the mechanistic empirical design method for pavement systems described by Schuettpelz et al. (2009). Figure 2.9 presents a sketch showing how the shear modulus changes as a function of the water content.

Thermal conductivity of soils is also an important parameter in underground power installation because controlling the thermal conductivity of the soil may helps to control the energy losses in the power transmission industry. Thermal conductivity of soil is affected by dry density and water content as is reported by Campbell and Bristow (2002). Therefore an appropriate management of the molding water content during compaction may results in a range of thermal conductivity of the compacted soil, as is shown in figure 2.10 (Mitchell and Soga 2005).

2.3.3. Soil type

Soil parameters such as initial dry density, grain size distribution, particle shape and molding water content are important material properties in controlling how well the soil can be compacted (Rollings and Rollings 1996; Holtz et al. 2010). Different soils may show different compaction curves as is shown in figure 2.11.

Coarse graded soils like well graded sand (SW) and well graded gravel (GW), are easier and more efficient to compact using vibration due the particles are large and gravity forces are greater than surface forces (Holtz et al. 2010). Furthermore they may have two peaks in the compaction curve, this mean that a complete dry soil can be compacted at the same density using two different optimum water contents (Rollings and Rollings 1996). Also coarse grained soils tend to have a steeper compaction curve making them more sensitive to changes in molding water content (figure 2.11).

The compaction method and the compactive effort have higher influence in the final dry density of fine graded soils, than in coarse graded soils (Bowels 1979). As is shown in figure 2.11 the shape of the compaction curve when the soil has larger content of silt or clay has a sharp peak. When the soil is more plastic the difference of compaction curves for standard effort and modified effort is larger (Rollings and Rollings 1996). Furthermore, when the soil has fine content, the soil structure and fabric becomes of the molding water content.

2.3.4. Compaction effort

The compactive effort is perhaps one of the most important variables that control the final reduction of void ratio during compaction. This is because the compactive effort is the

amount of energy or work necessary to induce an increment in the density of the soil. The compactive effort is controlled by a combination of the parameters such as weight and size of the compactor, the frequency of vibration, the forward speed, the number of roller passes, the lift height (D'Appolonia et al. 1969), and falling high and dropping weight in dynamic compaction (Zou et al. 2005).

Figure 2.12 shows how the weight of the compactor increases the effectiveness of densification for different types of soils, frequencies and lift thicknesses (Rollings and Rollings 1996). Turnbull and Foster (1956) also discuss the relationship between the dry density and compaction variables such as the number of roller passes, the variation in size of the footprint of the roller, variation in tire pressure of rubber–tired rollers, and the lift thickness. Figure 2.13 documents how the tire pressure or compactor weight and number of passes increase the dry density of a compacted soil for a given water content.

In addition to the influence of the compactor weight D'Appolonia et al. (1969) reports that operating frequencies have a large effect on the efficiency of a compactor. Figure 2.14 shows how the compacted dry density, ground accelerations and dynamic stresses increase with the operative frequency of the compactor. D'Appolonia et al. (1969) reports that as the number of roller passes increases, the compactive effort and depth of influence increase as well; however the compaction efficiency and depth of compaction start to decrease after a certain number of passes. Figure 2.15 shows how the density changes as a function of depth for different roller passes. These results indicate that the rate of density gains decrease with the number of passes.

In dynamic compaction the amount of energy applied to the soil and therefore to its degree of compaction and depth of influence is directly related with the drop high, falling weight and number of impacts (Zou et al. 2005). Figure 2.16 shows how the degree of compaction increases with the number of impacts and it decreases with depth for a 10 ton weight and falling high of 10 m (Cui 2010).

2.3.5. Effect of Lift Thickness

The weight, size, number of passes, and operative frequency are important parameters which depends of the compactor equipment used; however after selecting the compactor method and equipment, the final results of compaction is principally influenced by the construction procedures (Holtz et al. 2010). This is why the appropriate selection of the lift thickness during compaction operations is a critical point that has to be analyzed.

Turnbull and Foster (1956) evaluated the effect of the lift thickness on the density gradient versus depth in a lean clay (CL) as is shown in figure 2.17 where the dry density gradient is steeper for 0.3 m than for 0.6 m lift thicknesses for soils compacted at the wet side of optimum.

D'Appolonia et al. (1969) evaluate the effective depth of influence of a vibratory roller (1.2 m diameter, 2 m width and pressure of 86 MPa) in a coarse graded soil. They suggest that the appropriate selection of the lift thickness may be determined taking the density profile of a thick lift compacted using a given compactor with five number of passes. The density within the lift thickness has to be larger than the 75% of relative density. The scheme of the

procedure is shown in figure 2.18. The density profile increases with depth until reach a maximum to then decrease to the bottom of the layer. The upper part of the lift is not well compacted due to an overvibration of the soil particles which vibrate loose due to a small effective stress close to the surface; besides an increment in relative densities at larger depths are not feasible regardless the number of passes (D'Appolonia et al. 1969).

2.4. Compaction energy propagation in soils

When the soil is compacted, the static or dynamic energy of the compactor is transmitted to the soil by a combination of P, S and Rayleigh waves that travels in radial directions from the compactor (Richart et al. 1970). As the wavefront moves away from the compactor, the damping of the soil decreases the wave energy until it is dissipated. When the wave interacts with the soil, produces compression and distortion between particles rearranging them and increasing its density. Figure 2.19 shows schematically how P, S, and Rayleigh waves propagate away from a surface soil. Santamarina (2001) reports that the horizontal particle motion diminishes faster with depth than the vertical particle motion as is shown in figure 2.20.

D'Appolonia et al. (1969) suggests that the compaction equipment parameters which determine the soil compaction are the maximum and minimum dynamic stress produced by the compactor. Figure 2.21 shows the contours of equal dynamic stress and acceleration beneath the compactor as a function of the vertical and horizontal position. This figure indicates that stress distribution beneath the roller is a function of the dynamic stresses

produced by the compactor, and these dynamic stresses are function of the weight and size of the compactor as well as the operative frequency.

2.5. Typical compactors equipment

In soil compaction operations, there are compactor-controlled parameters that are involved with the final efficiency of the compaction operations. These parameters include roller size and weight, roller operating frequency, amplitude of vibration, and speed of displacement (D'Appolonia et al. 1969). The appropriate selection of the compactor equipment plus the soil parameters control how well a soil can be compacted. This section, describes the typical compactor equipment used in the construction industry.

2.5.1. Smooth wheel rollers

These rollers are the most common rollers used in the construction industry (Rollings and Rollings 1996) and consist in a single steel drum with two rubber-tire wheels as is shown in figure 2.22. These rollers may be used for all types of soils, but they are most efficient in coarse grained soils. They provide a 100 % of coverage beneath the steel wheel, reaching contact pressures of up to 400 kPa (Holtz et al. 2010). The steel drum may vibrate in order to generate additional dynamic loads to help overcome the interparticle friction and facilitate the densification of coarse-grained soils (Rollings and Rollings 1996). Figure 2.23 shows how the dynamic component of compaction of coarse-grained materials helps to gain dry density over compaction without vibration. The vibration is generated by the rotation of eccentric weights inside the drum.

The mechanics of vibrating compactors-soils is often analyzed using nonlinear models of soil – machine. These models are used to evaluate and control the compactive effort in response to the degree of compaction of the soil measured as the material stiffness in intelligent compaction (Yoo and Selig 1979; Anderegg and Kaufmann 2004; Rahman et al. 2008). These models represent soil compaction operations using the dynamic properties of the soil-machine interaction system shown in figure 2.24. The compactor equipment is modeled as two spring-damping systems connected in series to model de compactor dynamic behavior. The first spring-damping system is connected in parallel and represent the compactor and the frame where the drum roller is located. The second spring-damping system is also connected in parallel and represents the vibrating drum roller. Finally the soil is modeled as third spring-damping system connected in parallel as is shown in figure 2.24.

As the passes of the compactor increases, the soil gain density and the stiffness increase but the damping decreases (Anderegg and Kaufmann 2004). The dynamical properties of soil (i.e., stiffness and damping) are determined by the resulting dynamic response of the compactor when interacts with the soil. In the literature there are a large number of investigations aiming to reduce the uncertainty in evaluating the soil stiffness (k_s) or modulus (E_{viv}) for compaction control in a layered media (Anderegg and Kaufmann 2004; Mooney and Rinehart 2009 and 2007; Rinehart and Mooney 2009).

2.5.2. Rubber – tired roller

These rollers consist of a two-axis roller with four or three wheels per axis as is shown if figure 2.25. The weight of the compactor may range between 490 and 590 kN. These rollers

provide an 80 % of coverage with tire pressure of about 700 kPa (Holtz et al. 2010). They can be used to compact coarse and fine graded soils in highway and earth dam construction. However for fine-grained soils lamination between lift can be a problem, especially if the soil is compacted at the wet side of optimum (Rollings and Rollings 1996). In some cases the tires may be tilted or wobbly in order to produce an effect of kneading to the soil (Bowels 1979).

2.5.3. Padfoot rollers

Padfoot rollers are mainly used to compact fine graded soils. They consist of a steel drum with protruding feet (figure 2.26). The drum may vibrate or not to induce more dynamic effort. Due to its protruding feet, these rollers have 8 to 12% of coverage with pressures between 1400 to 7000 kPa depending on the roller size. The padfoot roller starts to compact the soil from the bottom of the lift to the top until the roller 'walks out' of the lift when the upper part of the lift is compacted (Holtz et al. 2010).

2.5.4. Dynamic compaction equipment

The dynamic compaction method uses a dropping weight which generally is a steel plate, sand or concrete filled steel shell or reinforced concrete (Mayne et al. 1984). The dropping weight ranges from 60 to 400 kN and the falling high is typically between 10 to 40 m, depending of the soil type and the crane available. The depth of influence depends on the dropping weight, the falling high and type of soil, but can reaches up to 40 m (Zou et al. 2005). Dynamic compaction is mainly used in large areas of granular soils, where the use of

rollers is economically unfeasible to reach larges depth of compaction. The dynamic compaction method allows increasing the soil density at larger depths than the roller compactors (Holtz at al. 2010).

2.6. Compaction control and monitoring

After the soil is compacted, it is necessary to verify if the density of the compacted soil accomplish the standard specifications for the project. To do this, several tests allow determining through index correlation or directly, the density or stiffness of the compacted soil layer. These tests must be performed after compaction in a representative location of the compacted lift. The following table shows the most used test for compaction control.

Table 2.2: Typical test to compaction control and monitoring

Test Name	Index or measurement	Reference
Nuclear density gauge	Dry density – water content	ASTM D 6938
Soil stiffness gauge	Stiffness	ASTM D 6758
Sand cone	Density	ASTM D 1556
TDR	Water content	ASTM D 6565
Dynamic cone penetrometer	Blow count	ASTM D 6951
CBR	CBR index	ASTM D 4429

2.7. Specifications on Lift Thickness in the United States

Bowles (1979) proposed recommendations to select the lift thicknesses, number of passes, compaction method, and compaction equipment based on the Unified Soil Classification system. These recommendations are shown in table 2.3. The lift thickness, compaction method and equipment recommendations are generally based in field experiences, furthermore the lift thickness and the percent compaction requirement changes from state to state varying from 10.2 cm to 30.5 cm as is shown in table 2.4 (Hoope 1999). These differences in lift thickness come from different experiences compacting soils for road construction. These recommendation may be compared to dynamic compaction that may allow a lift thickness of the order of 4 m depending of the falling weight and drop high (Zou et al. 2005).

Table 2.3: Recommendations of lift thickness, compaction equipment, number of passes, degree of compaction as a function of compaction condition and soil type (Bowels 1979).

Soil group	Soil type	Compaction condition	Degree of compaction	Compaction equipment	No. of passes	Lift thickness	Moisture control	Unit weight	Field control
Pervious	GW GP SW SP	Compacted	95 to 105% of standard compaction test or 70 to 85% of relative density	Vibratory roller Rubber-tired roller Crawler-type tractor	As required 2 to 5 2 to 5	As required 0.30 m (12 in) 0.20 cm (8 in)	Saturate by flooding	17-21 kN/m^3 (108-134 pcf)	Field density test at random locations
		Semi-compacted	90 to 95% of standard compaction test or 60 to 70% of relative density	Rubber-tired roller Crawler-type tractor	2 to 5 1 to 2	0.35 m (14 in) 0.25 m (10 in)	Saturate by flooding	16-20 kN/m^3 (102-127 pcf)	Field density test at random locations
Semi-impervious to impervious	GM GC SM SC ML CL MH CH	Compacted	95 to 105% of standard compaction test	Rubber-tired roller Padfoot roller	2 to 5 4 to 8	0.20 m (8 in) 0.15 m (6 in)	OMC based on lab compaction test	16-20 kN/m^3 (102-127 pcf)	Field density test at random locations to determine relative compaction
		Semi-compacted	90 to 95% of standard compaction test	Rubber-tired roller Padfoot roller Crawler-type tractor	2 to 4 4 to 8 2 to 4	0.25 m (10 in) 0.20 m (8 in) 0.15 m (6 in)		14-19 kN/m^3 (89-121 pcf)	

Table 2.4: Compaction specifications in the US (Hoppe 1999; modified by Kim et al. 2011)

State	Loose lift thickness cm (in)	% compaction	Remark
Alabama	0.20 (8)	95	
Arizona	0.20 (8)	100	
California	0.20 (8)	95	For top 0.75 m (30 inch)
Connecticut	0.15 (6)	100	Compacted lift indicated
Delaware	0.20 (8)	95	
Florida	0.20 (8)	100	
Georgia		100	
Idaho	0.20 (8)	95	
Illinois	0.20 (8)	95	For top; remainder varies with embankment depth
Indiana	0.20 (8)	95	
Iowa	0.20 (8)	None	One roller pass per inch thickness
Kansas	0.20 (8)	90	
Kentucky	0.15 (6)	95	Compacted lift indicated; water +2% / -4% of optimum
Louisiana	0.30 (12)	95	
Maine	0.20 (8)	-	At or near optimum water
Maryland	0.15 (6)	97	For top 0.30 m (12 in); remainder is 92%
Massachusetts	0.15 (6)	95	
Michigan	0.23 (9)	95	
Minnesota	0.20 (8)	95	
Mississippi	0.20 (8)	-	
Missouri	0.20 (8)	95	
Montana	0.15 (6)	95	At or near optimum water
Nebraska		95	
Nevada		95	
New Hampshire	0.30 (12)	98	
New Jersey	0.30 (12)	95	
North Dakota	0.15 (6)	-	
Ohio	0.15 (6)	-	
Oklahoma	0.15 (6)	95	
Oregon	0.20 (8)	95	For top 0.90 m (36 in); remainder is 90%
South Carolina	0.20 (8)	95	
South Dakota	0.20-0.30 (8–12)	97	0.20 m (8 in) for embankment; 0.30 m (12 in) for bridge end backfill
Texas	0.30 (12)	-	
Vermont	0.20 (8)	90	
Virginia	0.20 (8)	95	+ or - 20% of optimum water
Washington	0.10 (4)	95	Top 24 in are 0.10 m (4 in) lifts; remainder are 0.20 m (8 in) lifts
Wisconsin	0.20 (8)	95	Top 1.8 m (6 ft), within 30 m (200 ft) of abutment; remainder is 90%
Wyoming	0.30 (12)	-	Use of reinforced geotextile layers

Note: New York DOT specifies lift thickness as function of soil and compaction equipment (State of New York 2008).

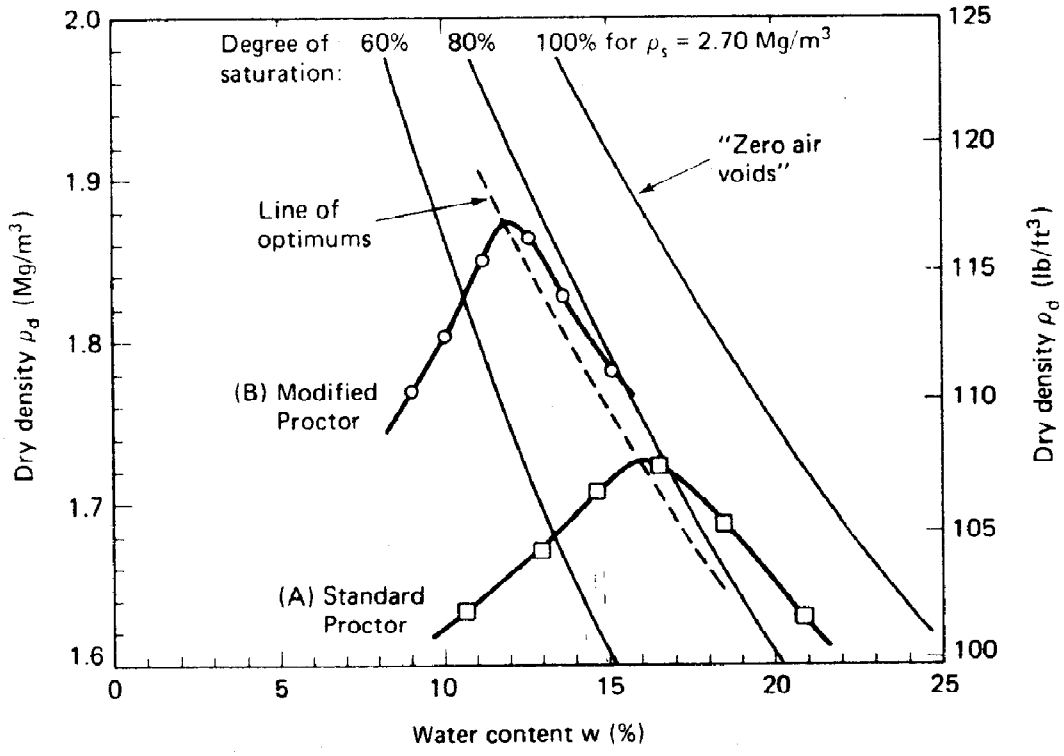

Figure 2.1: Typical compaction curve proposed by Proctor (1933) with the zero air void line, line of optimum and with different energies supply for a glacial till (Holtz et al. 2010)

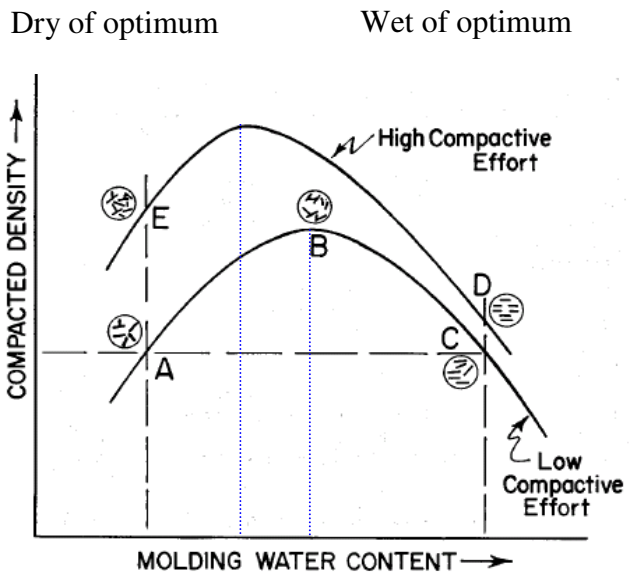

Figure 2.2: Particle fabrics as a function of water content and compactive effort (Lambe and Whitman 1969)

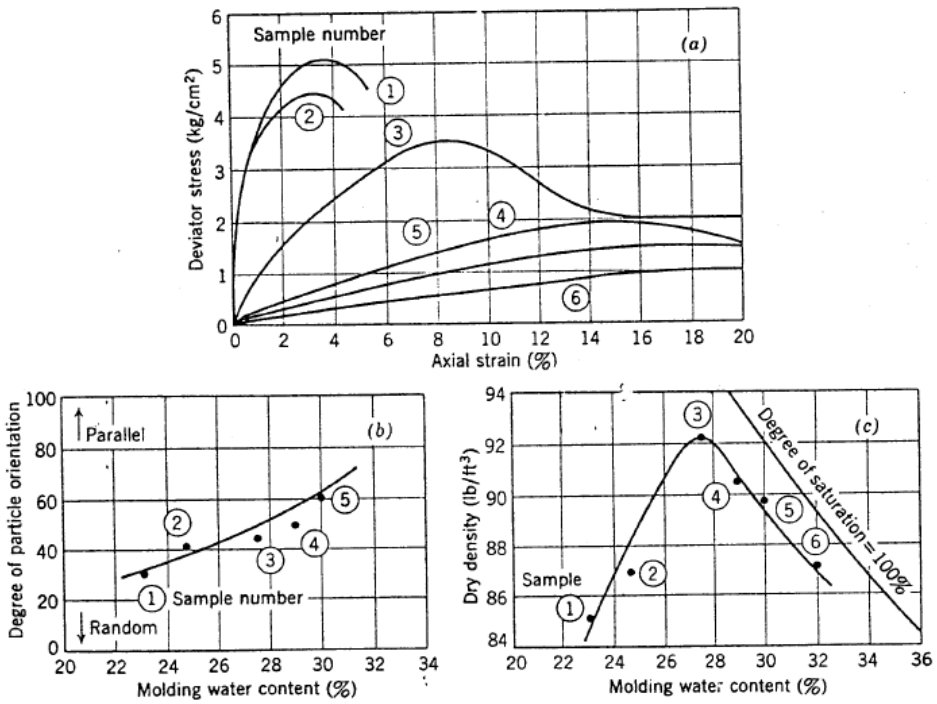

Figure 2.3: Particle orientation of kaolinite as a function of molding water content and compactive effort. (a) stress v/s strain relationship; (b) Particle orientation v/s water content; (c) dry density v/s water content (Seed and Chan 1959)

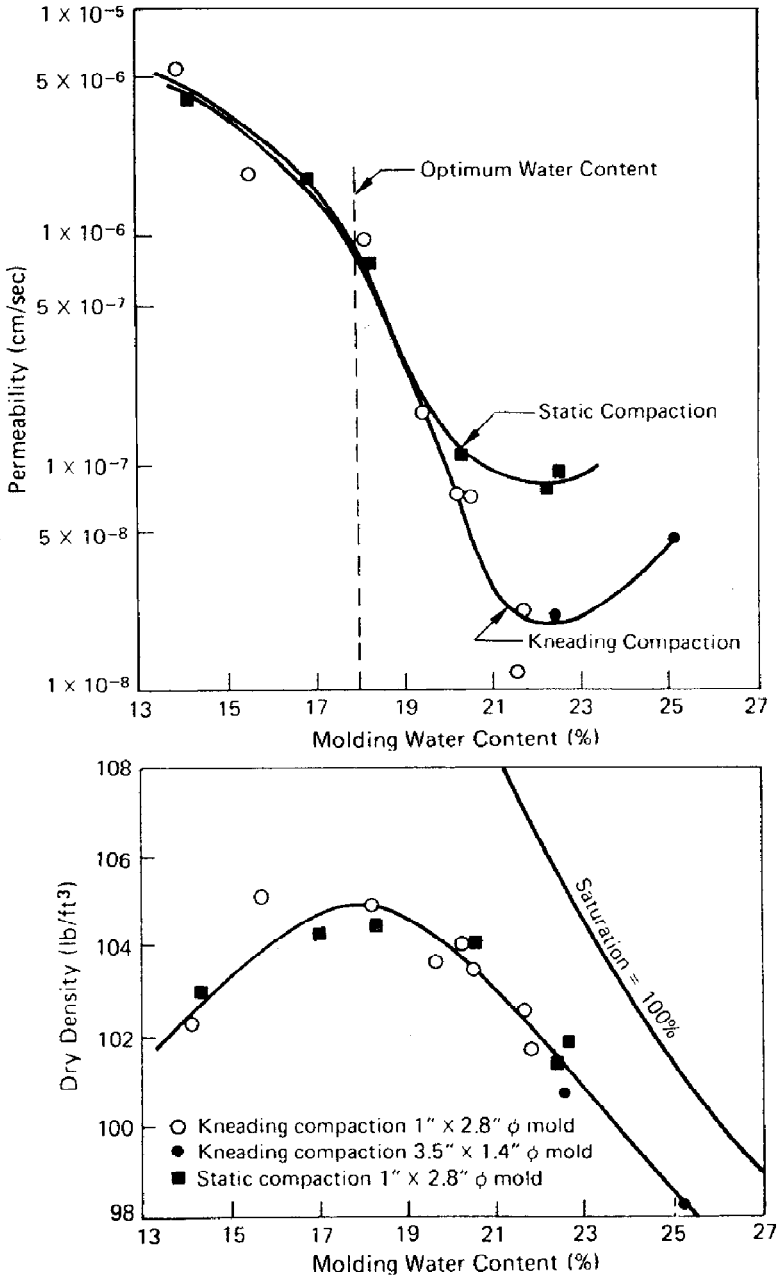

Figure 2.4: Permeability as a function of the molding water content in a compacted soil (Mitchell and Soga 2005)

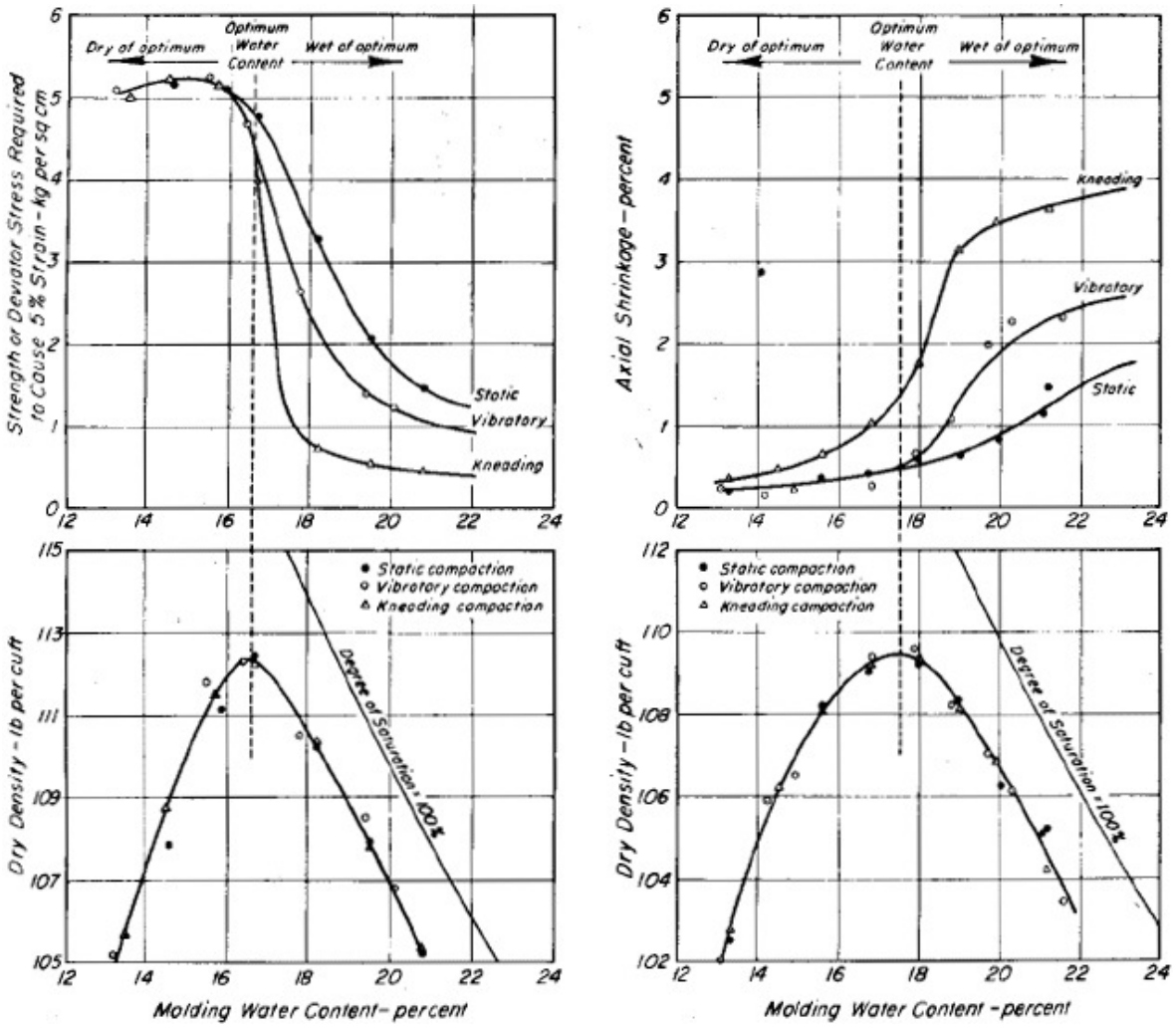

Figure 2.5: Strength and volumetric stability as a function of water content and compaction methods (Seed and Chan 1959)

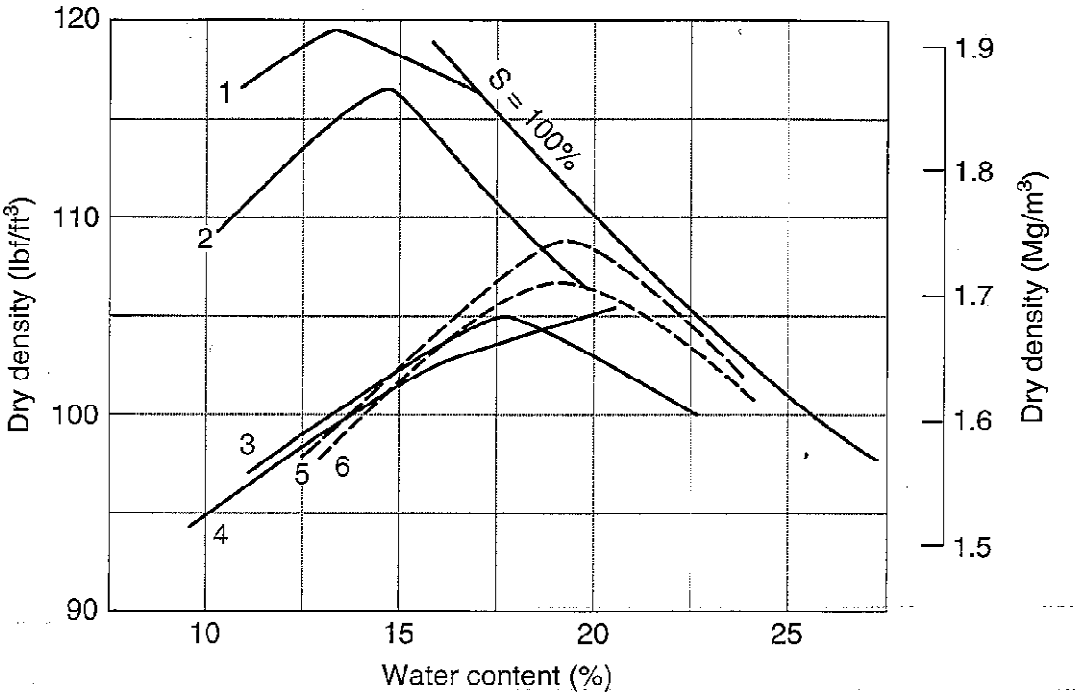

Figure 2.6: Compaction curves obtained by (1) laboratory static compaction, 13700 kPa; (2) Modified effort; (3) standard effort; (4) laboratory static compaction 1370 kPa; (5) field compaction rubber – tire load after 6 coverages; (6) field compaction sheepsfoot roller after 6 passes (Holtz et al. 2010 after Turnbull 1950)

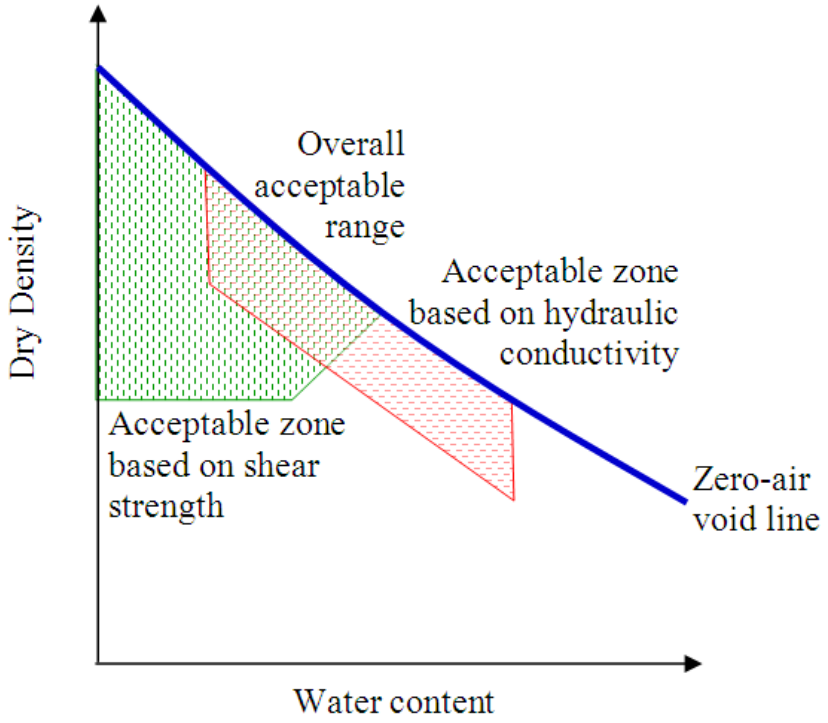

Figure 2.7: Scheme of ranges of soil properties and applications as a function of molding water content (after Daniel and Benson 1990)

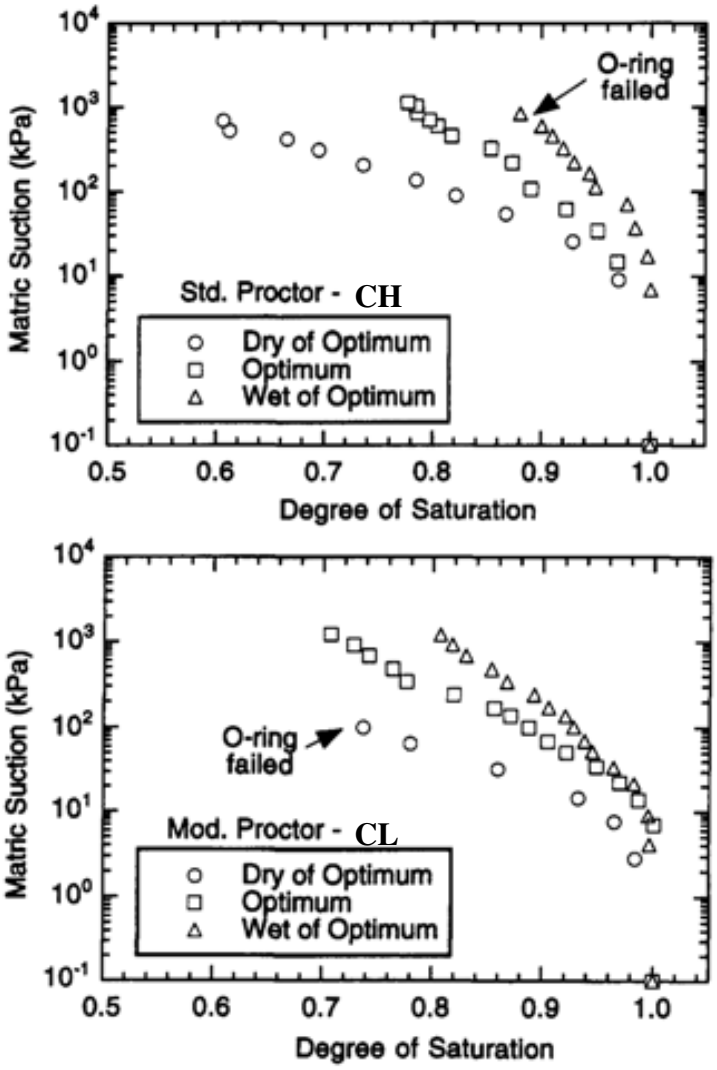

Figure 2.8: SWCC for a CH and CL soil compacted at dry of optimum, wet of optimum and optimum water content (Tinjum et al. 1997)

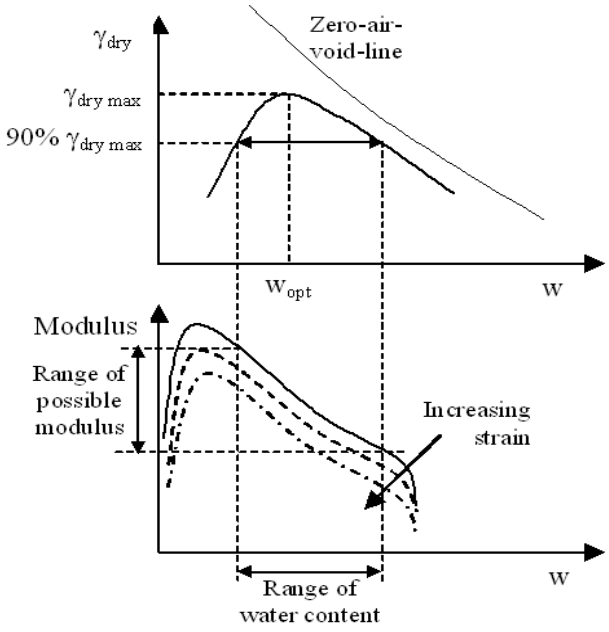

Figure 2.9: Small strain shear modulus as a function of soil water content

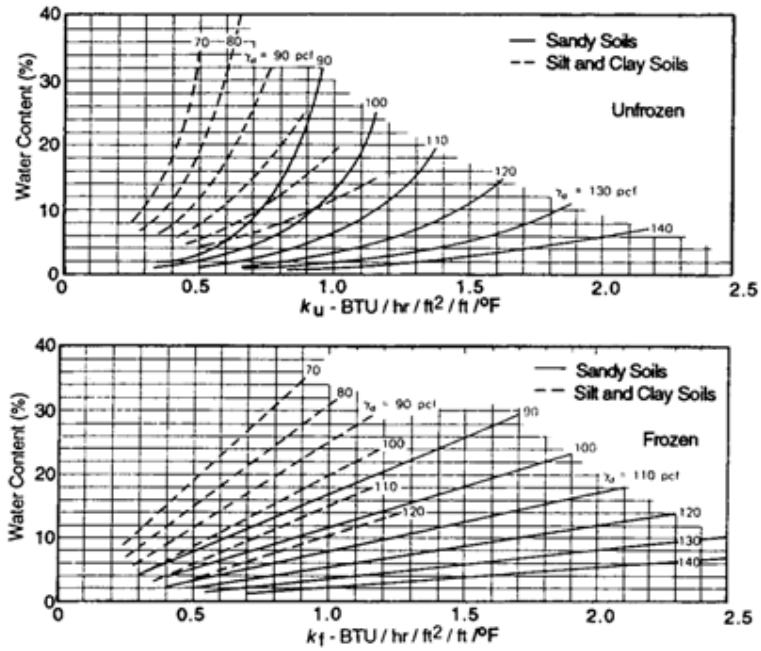

Figure 2.10: Thermal conductivity of the soil as a function of the water content and dry density (Mitchell and Soga 2005)

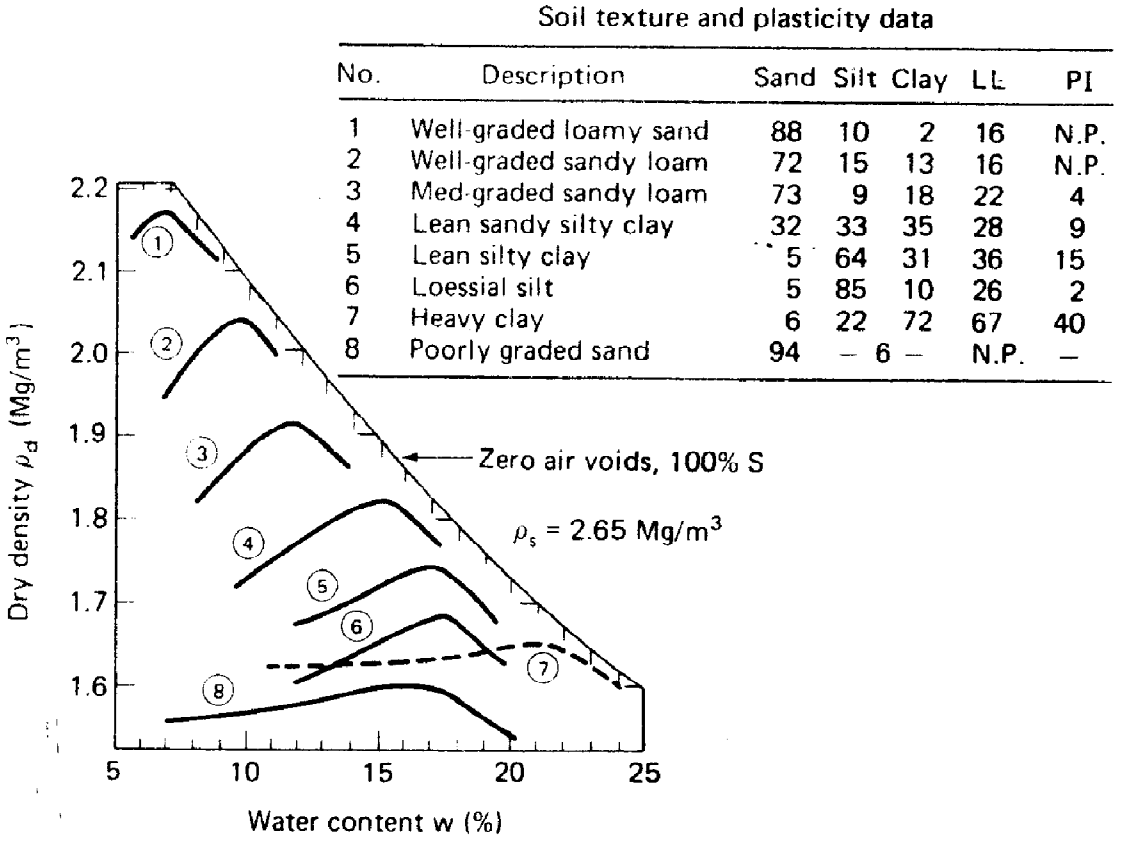

Figure 2.11: Compaction curves for different types of soils using the standard effort (Holtz et al. 1996)

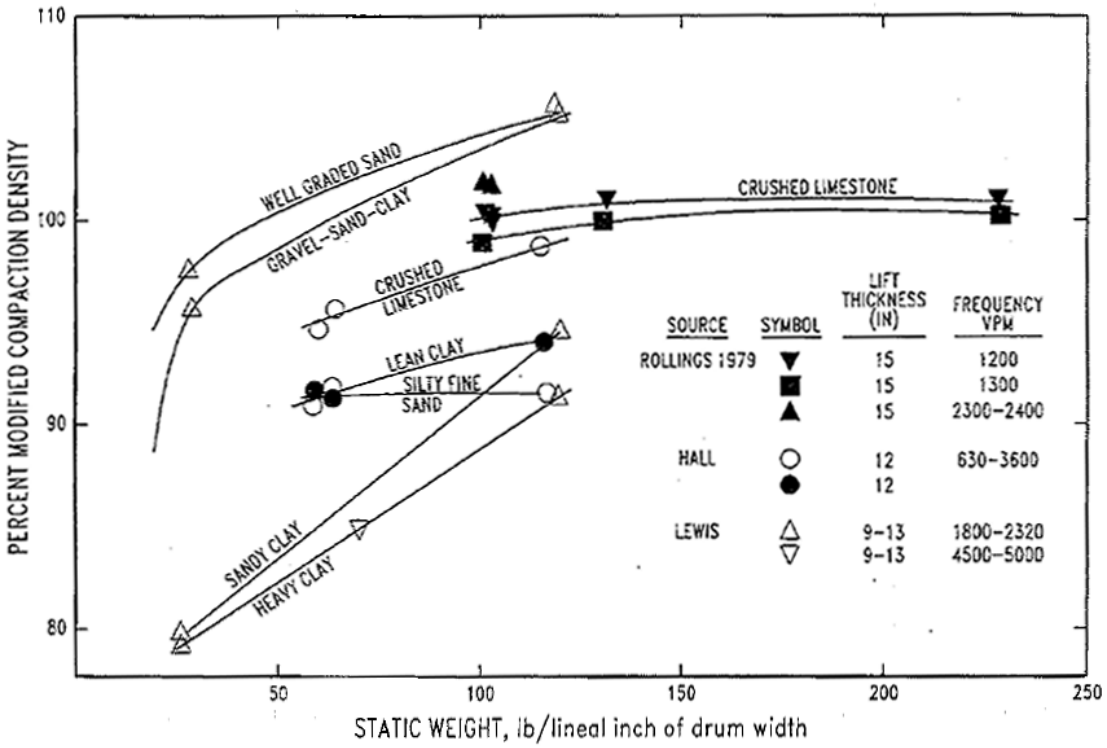

Figure 2.12: Influence of the compactor weight, frequency and lift thickness in density of different soils (Rollings and Rollings 1996)

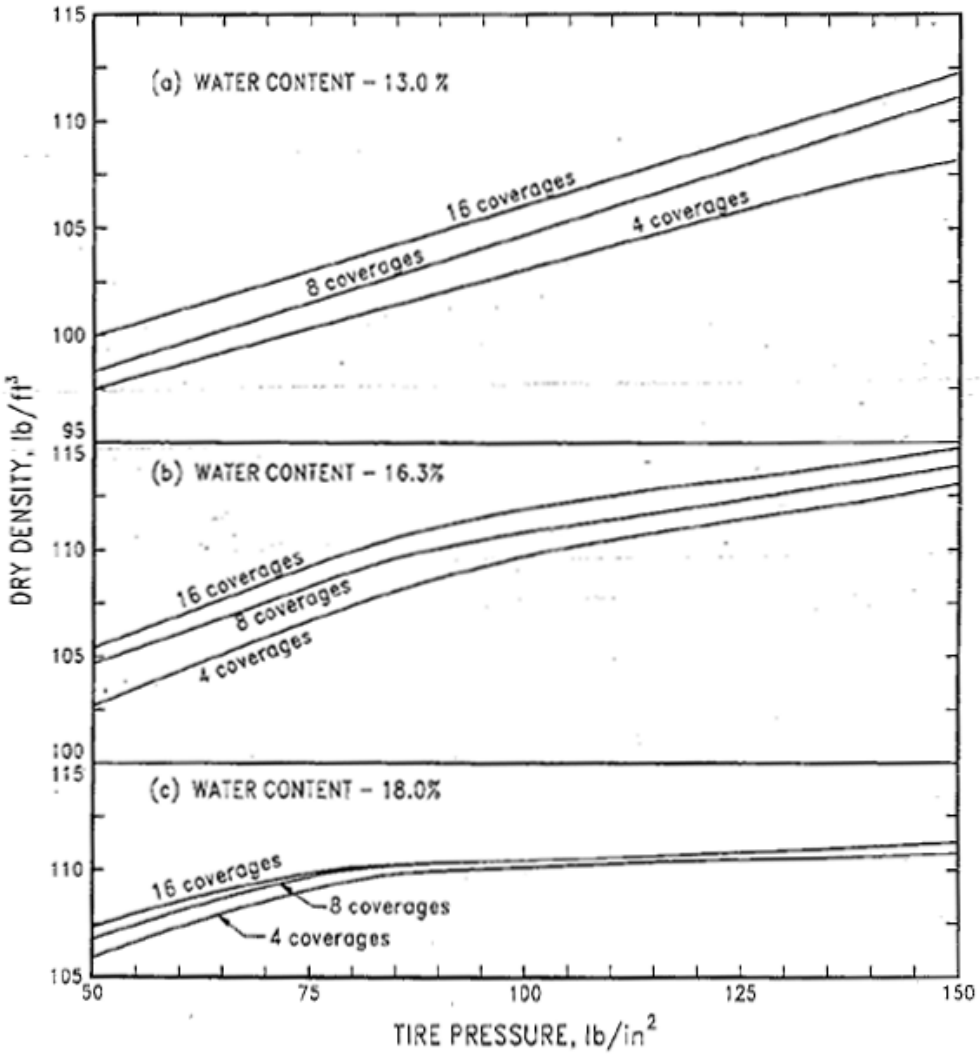

Figure 2.13: Influence of the tire pressure, number of passes (or number of coverages) and water content on the dry density of a lean clay (CL) compacted at dry side of optimum (a) close to the optimum (b), and wet side of optimum (c) using a rubber tired roller (Turnbull and Foster 1956)

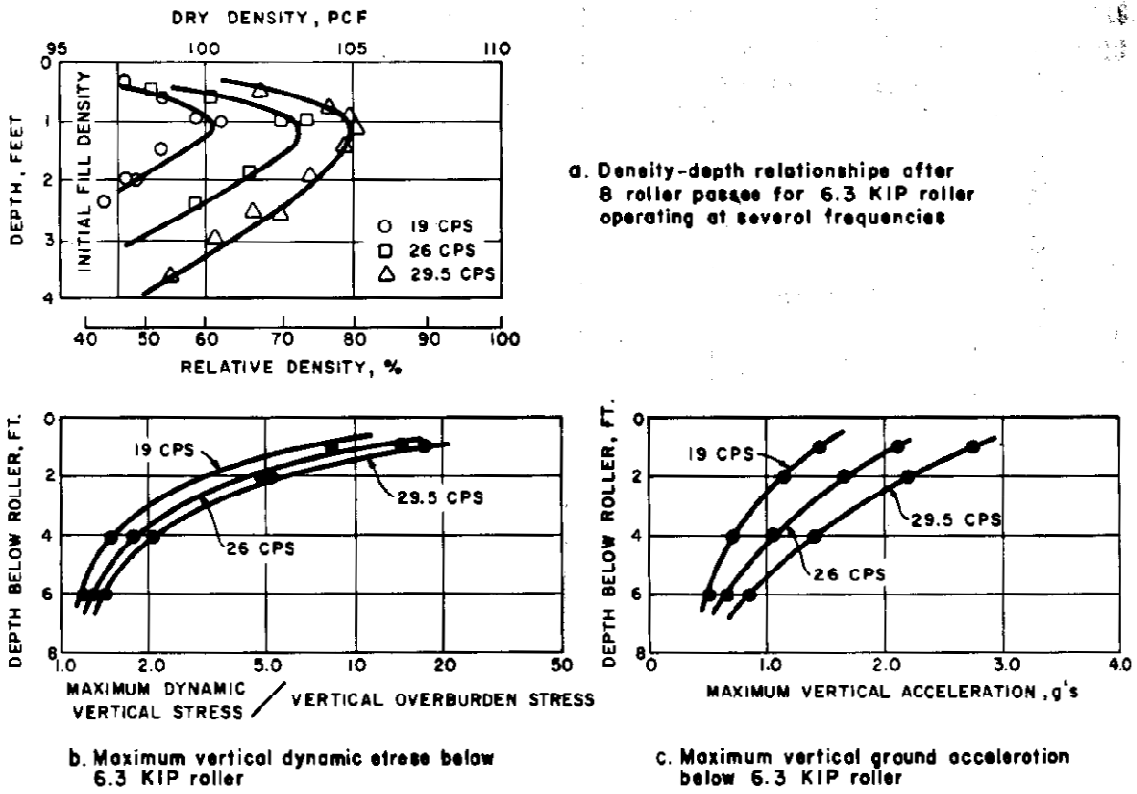

Figure 2.14: Influence of the operative frequency of a vibratory roller (1.1 m diameter, 1.67 m width and pressure of 43 MPa) after 8 passes in the dry density, dynamic stresses and ground accelerations of a poorly graded dune sand (D'Appolonia et al. 1969)

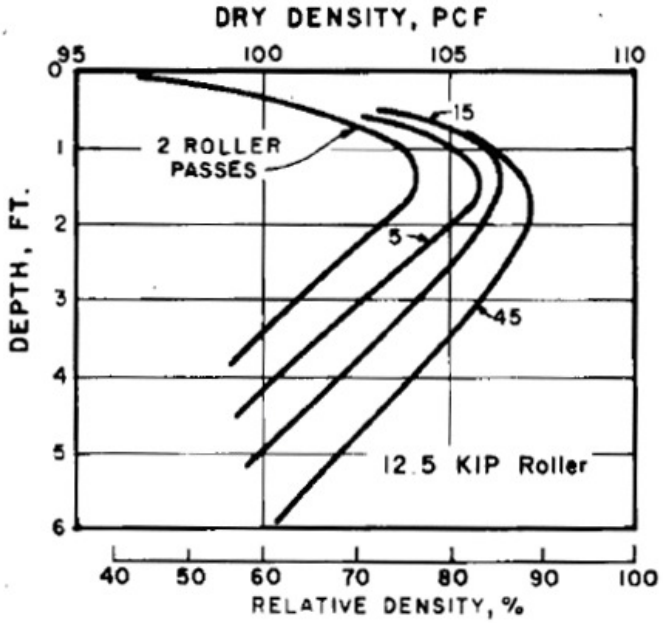

Figure 2.15: Influence of number of roller passes of a vibratory roller (1.2 m diameter, 2 m width and pressure of 86 MPa) in the density profile of a poorly graded dune sand (D'Appolonia et al. 1969)

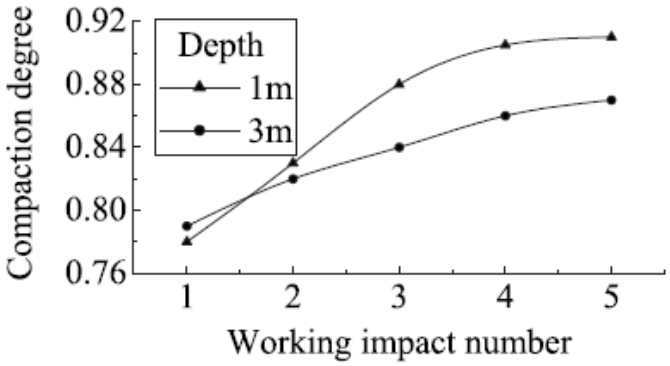

Figure 2.16: Compaction degree as a function of depth and number of impact of a tamper (10000 Kg weight 4 m^2 circular area, released at 10 m) in a 0- 2.5 m layer of clay and gravels underlying by a 2.5 – 7 m sand with silt layer (Cui 2010)

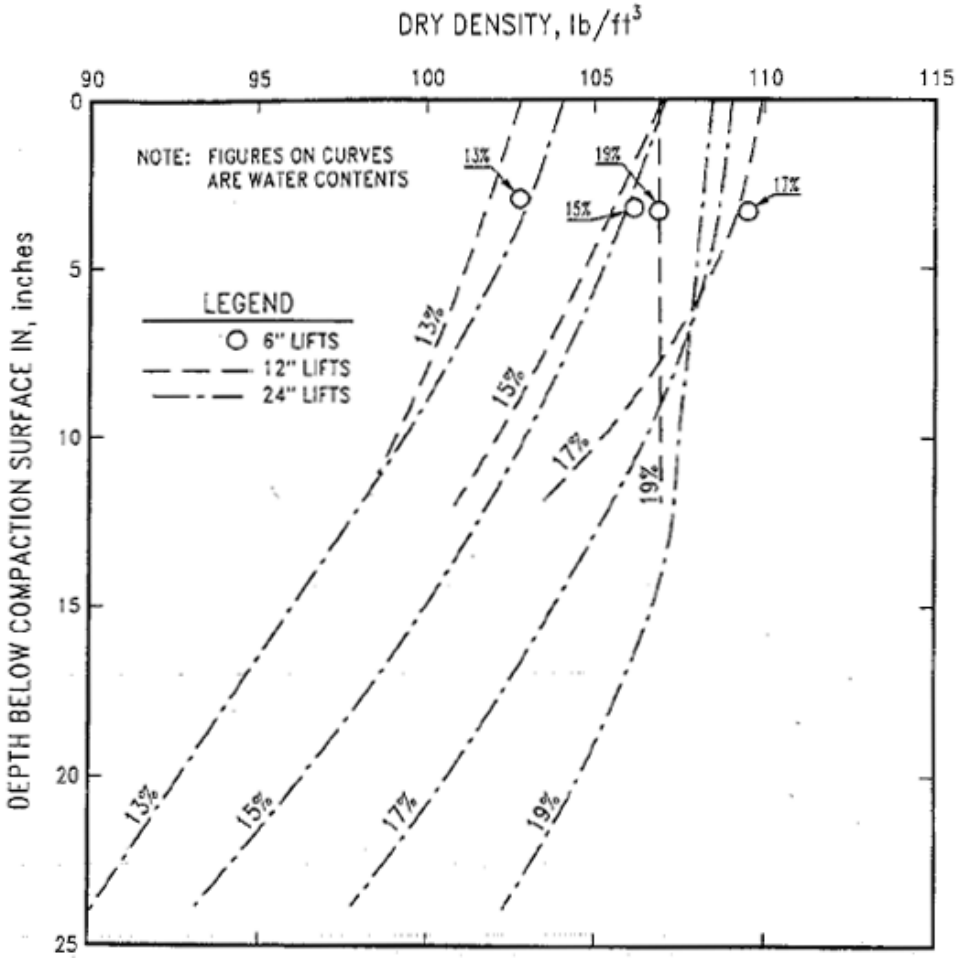

Figure 2.17: Density profile as a function of water content and lift thickness for a lean clay (CL) compacted using a 620 kPa rubber tired roller (Turnbull and Foster 1956)

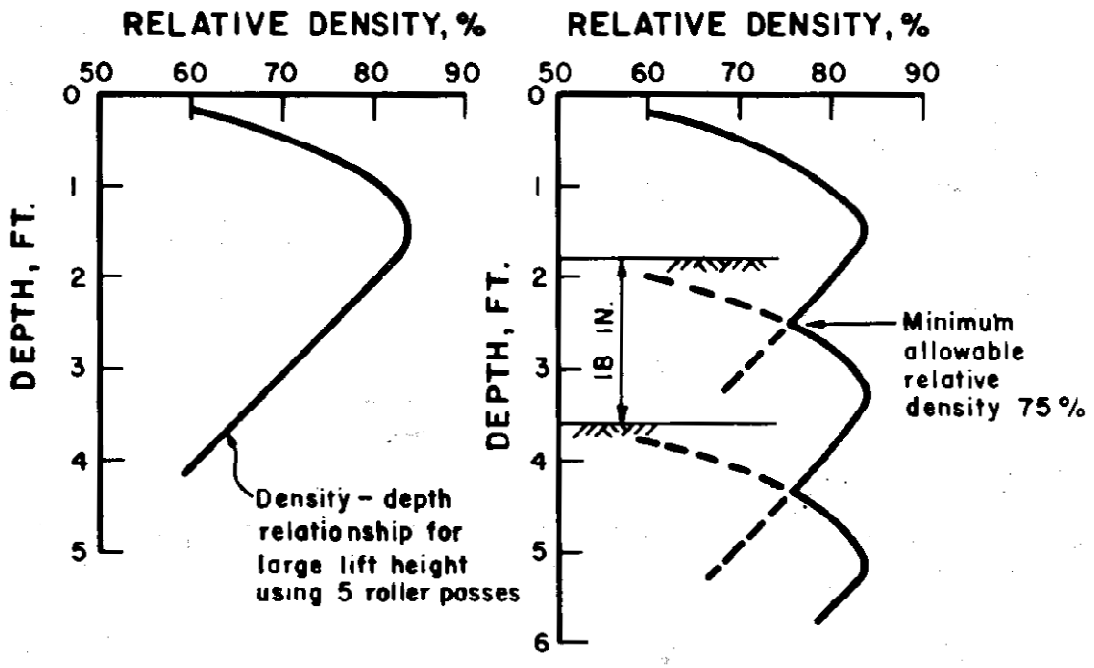

Figure 2.18: Scheme of the procedure to determine the appropriate lift thickness from the density profile of a thick lift described by D'Appolonia et al. (1969)

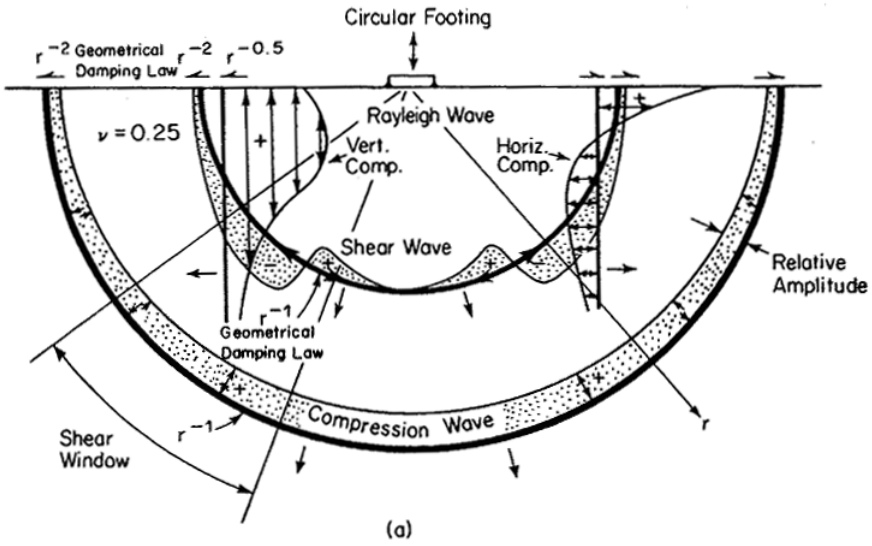

Wave Type	Per Cent of Total Energy
Rayleigh	67
Shear	26
Compression	7

Figure 2.19: Scheme of how the elastic wave interact with the soil media in radial direction (Richart et al. 1970)

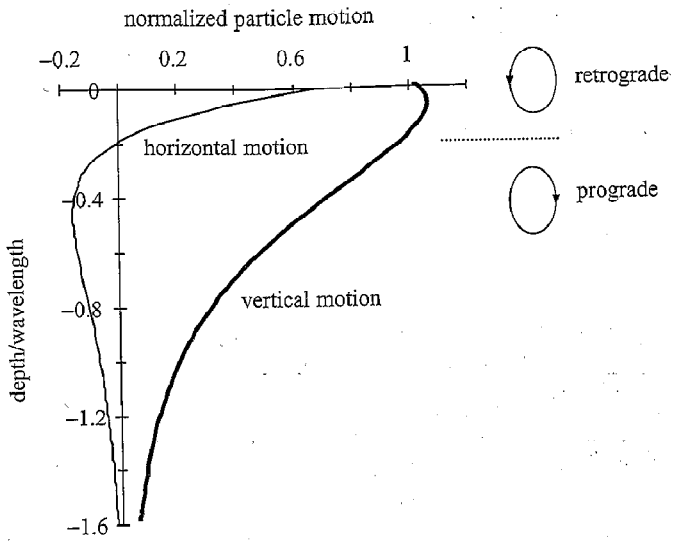

Figure 2.20: Vertical and horizontal particle motion as a function of depth (Santamarina 2001)

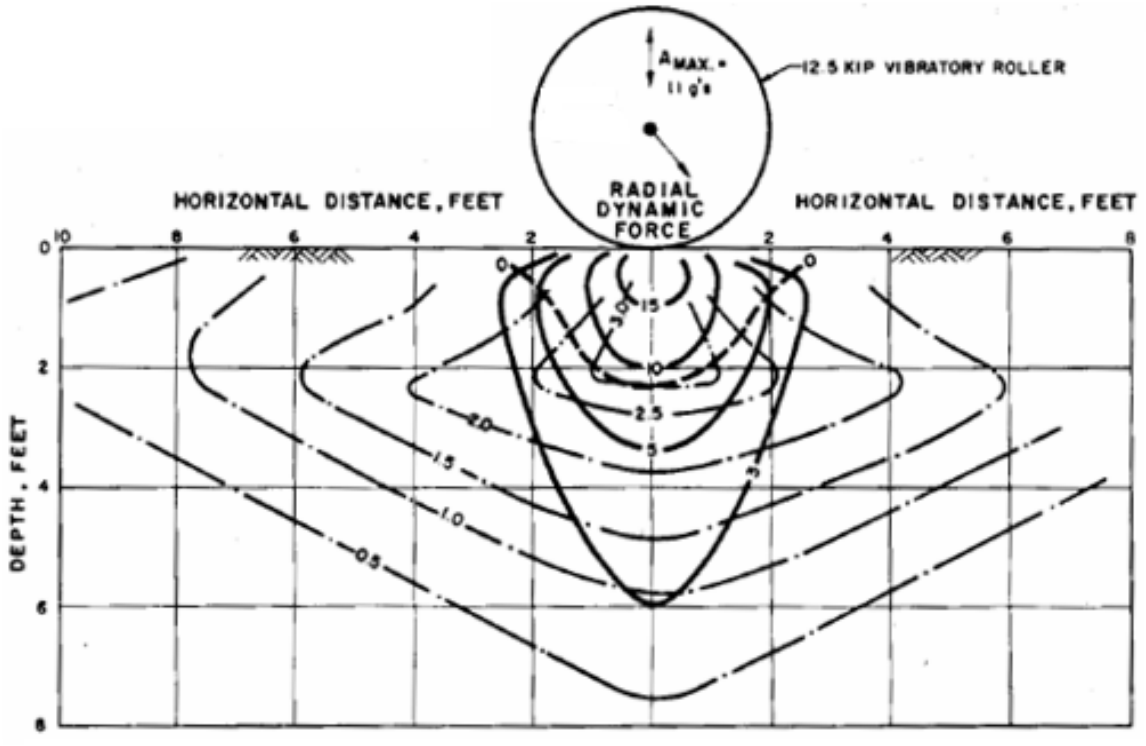

Figure 2.21: Dynamic stresses and acceleration profile under a vibrating roller (1.2 m diameter, 2 m width and pressure of 86 MPa) over a poorly graded sand dune (D'Appolonia et al. 1969)

Figure 2.22: Caterpillar™ CS76 smooth-drum vibratory roller (Operating equipment mass is 16,757 kg – 36,945 lb. Operating drum mass at drum is 10,750 kg (23,700 lb) (Source: Caterpillar 2011)

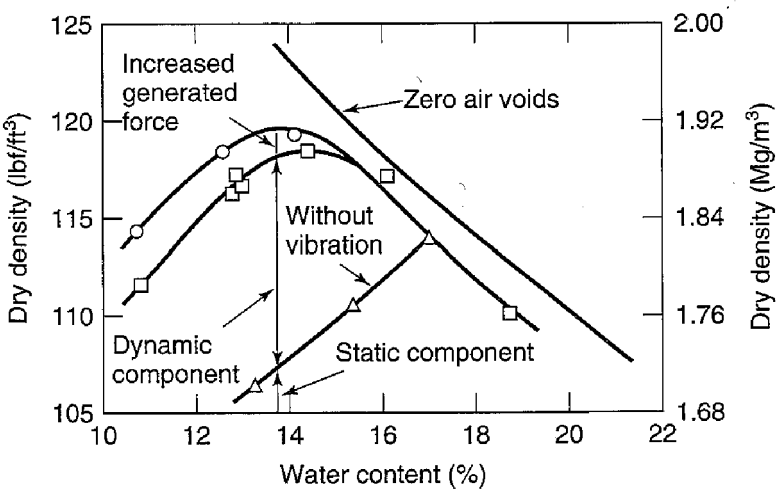

Figure 2.23: Compaction curve of a soil compacted with and without the dynamic component (Holtz et al. 2010)

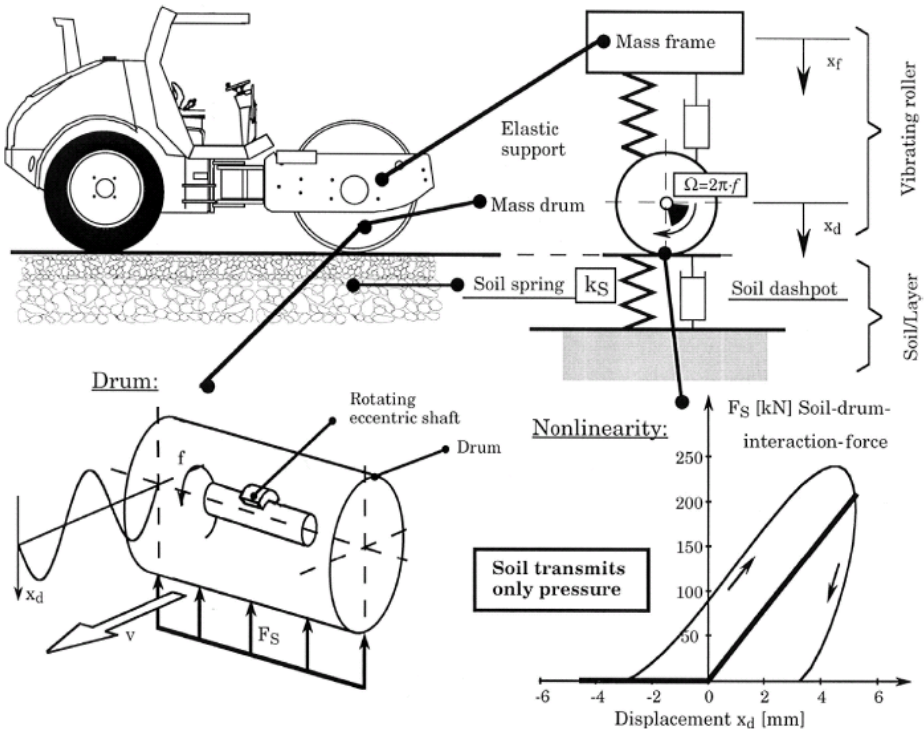

Figure2.24: Nonlinear model soil – compactor used in intelligent compaction (Anderegg and Kaufmann 2004)

Figure 2.25: Caterpillar™ PS-150C pneumatic compactor (Operating equipment mass is 4887 kg (10775 lb) (Source: Caterpillar 2011)

Figure 2.26: Caterpillar™ 815F padfoot roller (Operating equipment mass is 20,758 kg (45,765 lb). (Source: Caterpillar 2011)

Figure 2.27: Dynamic compactor equipment, crane, and reinforced concrete falling weight (Source: TerraSystem 2011)

3. MEASUREMENT TECHNIQUES, MATERIALS AND METHODS

An experimental program is designed to evaluate in the laboratory the effects of lift thickness and number of passes on the compaction characteristics and engineering response of different type of soils. The laboratory tests consist on compacting different soils in a large box in the laboratory and to monitor its engineering properties before, during and after compaction for different soil types, lift thickness and water content. This chapter describes the laboratory compaction experiments, procedures as well as the materials and measurement methods used.

3.1. Materials and materials properties

Two types of soils were tested in the laboratory. The first soil is a well-graded sand with clay or silty clay. The fine content is 5% with a plasticity index of 6. The second soil corresponds to a low plasticity silty sand (plasticity index PI=2). The physical properties of the soils are determined using ASTM (D 421; D 854; D 4318) standards.

Table 3.1 presents the physical properties of the tested soils and their classification according to the unified soil classification system (USCS –ASTM D 2487). Figure 3.1 shows the particle size distribution and the standard effort compaction curve (25 blows/layer) as well as 15 and 20 blows/layer are shown in figure 3.2.

Table 3.1: Physical properties of tested soils

Soil Name	C_u	C_c	Percent Fines	PI	G_s	γ_{dmax}	ω_{op}	USCS symbol
			%	%		kN/m^3	%	
Sand with clay or silty clay	10.8	1.0	5.4	6	2.612	16.7	12.5	SW-SC
Silty sand	-	-	15.7	2	2.720	19.7	10.5	SM

3.2. Compaction monitoring at laboratory

The selected soils are compacted and the physical and mechanical response during the compaction process is monitored for different lift thicknesses and water contents. The engineering soil properties are measured before, during and after compaction in order to document how the mechanical behavior improves for each soil, water content and lift thickness when the compactive effort is supplied. The measured engineering soil properties are density, water content, stiffness, dynamic penetration (using the dynamic cone penetrometer), rotations within the soil mass and P-wave velocity. A total of 15 tests were performed at the University of Wisconsin-Madison. Table 3.2 shows the laboratory testing program performed.

Table 3.2: Laboratory testing program

Soil type	Compaction method	Water content		Lift thickness
USCS		%		cm
SW-SC	Pounding	12.5	OMC	15 - 20 - 25
	Vibratory compaction plate	11.5	OMC – 1%	15 - 20 - 35
		15.2	OMC + 2.8%	15 - 20 - 35
SM	Vibratory compaction plate	10	OMC – 0.5%	15 - 20 - 35
		12.3	OMC + 2.3	15 - 20 - 35

3.2.1. Testing Cell

A wooden box 60-cm high, 90-cm long and 60-cm wide is built to contain the soil and perform the compaction monitoring test. The dimensions of the box were proposed and evaluated by Schuettpelz et al. (2009) to minimize edge effect during P-wave velocity measurements, to accommodate MEMS accelerometer separations of 5 cm in depth and to accommodate different lift thicknesses. At the bottom of the wooden box, a 15-cm thick soil layer of the same material being tested is compacted at 95% of the maximum dry unit weight (Standard Proctor effort – ASTM D 698) to represent a previous compacted lift. Figure 3.3 shows the wooden test cell, its dimensions and the bottom layer compacted at 95% of the standard effort.

3.2.2. Testing method and procedure

Different testing methods are tested, reduced, corrected, and analyzed to assess the physical and mechanical properties of soil during the compaction process. Two compaction methods are implemented. In the first method the soil first is compacted using a free-fall dropping 6.1-kg mass steel plate. The plate is instrumented with a MEMS accelerometer to monitor the kinetic energy of the steel plate when it reaches the surface of the ground (i.e., energy supplied to the soil). The steel plate is released from a height of 1.7 m with respect at the bottom of the wooden box as is shown in figure 3.4. A pressure plate is placed at the boundary of the compacted lift with the soil layer being tested to record changes in pressure at the bottom of the lift during compaction when the soil increases its density. The engineering soil properties are measured for different compaction energies. However, due to

the low compaction energy and dry density generated and the small increments in density and stiffness during compaction, this compaction method is replaced by a dynamic compactor.

The compaction method using the dynamic compactor is divided into six compaction stages to simulate the number of passes of a real compactor and to induce a uniform compactive effort at the surface of the layer. The zero stage corresponds to the soil in its loose state, the first stage corresponds to the soil after being under the first compactor pass, the second stage corresponds to the soil after the second compactor pass, and so forth. At the end of each compactor stage or pass, the engineering soil properties are measured and recorded. The technical specifications of the vibratory compactor plate are shown in table 3.3.

Table 3.3: Technical specifications of the compactor

Specifications	HULK electric plate compactor
Motor	780W
Compaction force	5 kN
Plate dimensions	400 mm x 320 mm
Vibration	7.43 m/s^2
Weight	26 Kg

At the end of the test, it is not expected to reach the 95 % of the maximum dry density as the standard (Standard Specifications for Highway and Structure Construction – WisDOT 1996) requires due to the small size and weight of the compactor and the lift thicknesses tested. However the behavior of different soils under the same compactive effort, with different physical properties and lift thickness may be analyzed.

The step-by-step test procedure includes:

1. The soil is placed into the wooden box over the compacted layer, until the desired lift thickness is reached. A metric tape attached to the wall of the box helps to measure the high of the soil layer. At the center of the box MEMS accelerometers are deployed to be embedded into the soil every 5 cm in the soil lift as is shown in figure 3.5. The MEMS accelerometers are carefully covered by soil trying to maintain its vertical alignment according to section 3.4 for 0 g.
2. Once the soil has been placed in its loose stage, the engineering properties are measured to record the initial state.
3. Then, the soil is compacted uniformly using the free-falling steel plate or the electric dynamic compactor plate as is shown in figure 3.6. Three passes of the compactor plate per each stage represents one compactive effort supplied to the soil.
4. After the soil is compacted, the engineering soil properties are measured again to record the changes in physical and engineering properties.
5. This procedure of compaction and engineering properties measurement is repeated until the soil undergoes five compaction efforts.
6. During the compaction process, the soil undergoes nine passes of the compactor plate. The soil properties are measured again to record the final state of the compacted soil.

3.2.3. Engineering soil properties measurement and procedures.

The engineering soil properties measured in the tests are the dry density, water content, surface stiffness, penetration rate index (DPI), shear induced rotations, P-wave velocity and soil displacements. This section explains how the measurements are performed at each stage of the compaction test.

The step-by-step measurement procedure is:

1. The surface displacement is measured using a wooden ruler and a reference point as is shown in figure 3.7.
2. The surface stiffness is measured using the Soil Stiffness Gauge (SSG). Measurements are taken in two places to verify possible influences of the wooden box in the stiffness measured, one measurement is taken in the center of the box and other in the edge as is shown in figure 3.8.
3. The dry density and water content profiles are obtained using a Nuclear Density Gauge (NDG) at different depths depending of the lift thickness. Figure 3.9 shows the data acquisition of dry density and water content using the NDG.
4. The shear induced rotations are measured by MEMS accelerometers and recorded by a digital data acquisition using a code written in Labview. The voltage before and after a compaction stage is recorded and transformed to rotations using the MEMS acceleromters's sensitivity as is explained in section 3.4.
5. The P–wave velocity measurements are performed in the center of the box. The waves are triggered using an instrumented hammer. The time arrival of the elastic wave traveling through the soil is detected by the MEMS accelerometers and

recorded by an oscilloscope. Figure 3.10 shows the MEMS accelerometer and the location of the test into the wooden box.

6. The rate of penetration is evaluated by the dynamic cone penetrometer (DCP - figure 3.11). This test is invasive for the size of the specimen, therefore if is performed in different places trying to minimize disturbing the soil specimen. It was identified during the experiments that the DCP test influences the surface stiffness measurements and the soil displacements due to induced cracks in the surface of the soil when the DCP device is removed. The location to perform the DCP test has to be at least 300 mm from the center of SSG, radius of influence of the SSG reported by Sawangsuriya et al. (2002).
7. The final MEMS displacements with respect to the bottom of the layer are measured when the specimen is removed from the testing cell.

3.3. Soil engineering properties measurement techniques

To monitor the engineering soil properties, several measurement techniques and sensors are used:

- *Nuclear density gauge (NDG)* to measure the density and water content of the soil,
- *Soil stiffness gauge (SSG)* to evaluate the surface stiffness
- *Dynamic cone penetrometer (DCP)* to assess the shear strength of the compacted soil
- *P-wave velocity tests* to estimate the soil stiffness profile.
- *Pressure plate* to measure the vertical pressure at the bottom of the soil layer.

This section explains each of the techniques utilized to monitor the soil properties during compaction and the references used to analyze them.

3.3.1. Nuclear density gauge (ASTM D 6938-08a)

The nuclear density gauge is an easy and rapid method to evaluate the density and water content of the compacted soil layer at the site. This test allows taking a large quantity of measurements to have a better statistical control of the construction site (Bowels 1979). The NDG uses a radioactive isotope source located inside the device which is placed at the soil surface as is shown the scheme of figure 3.12. The gamma rays produced by the radioactive source are detected in the bottom of a rode that goes into the ground (McCarthy 2002). When the soil is dense, it absorbs more radiation than a loose soil; therefore, the density is obtained by evaluating the decay in radiation which is proportional to the total density of the soil (Holtz et al. 2010). The NDG may work using one of three methods: backscatter, direct or air gap (Rollings and Rollings 1996). The bulk density may be measured using backscatter or direct method while the water content is measured only in backscatter (Winter and Clarke 2002).

To avoid errors in the dry density profile measured by the NDG Winter and Clarke (2002) propose a theoretical method to determine the density profile in a layered media where the density varies within each layer. The method (figure 3.12) consists in to take the average density between two adjacent readings of the point being measured. If the average density $\overline{\rho_i}$ is measured at equal intervals Δz, The dry density at depth z_i is determined as:

$$\rho_i = i \cdot \bar{\rho_i} - (i-1) \cdot \bar{\rho}_{i-1} \quad \text{(Eq 3.1)}$$

where ρ_i is the dry density at depth z_i, and each average density is measured by the NDG.

3.3.2. Soil stiffness gauge (ASTM D 6758)

The soil stiffness gauge is a portable device which is used to determine the surface stiffness of a compacted layer. The stiffness is determined inducing very small displacements to the surface of the ground by a dynamic force vibrating at 25 different frequencies (Humboldt Mfg. Co. 2002). The resulting surface deflection as a function of time is recorded and averaged for the whole frequency range. The stiffness is computed using a rigid ring on a linear-elastic, isotropic and homogeneous half space theory (Lenke et al. 2003). Due to the small strain amplitudes induced by the SSG, the soil is assumed to respond as an elastic and linear material. The obtained soil surface stiffness may be used to back calculate the soil elastic modulus using Eq 3.2 (Sawangsuriya and Edil 2005).

$$K_{SSG} = \frac{1.77\ E_{SSG}\ R}{1-\nu^2} \quad \text{(Eq 3.2)}$$

where K_{SSG} is the stiffness measured by the SSG, E_{SSG} is the elastic modulus, R=57.2 mm is the radius of the ring, and ν is the Poisson ratio taken as 0.15 for small soil deformations.

The SSG has a radius of influence of 30 cm and is sensitive to soil stiffness from 12.5 cm deep. However, the stiffness measured by the SSG may be influenced by the underlying layer

when it is located between 12.5 and 27.5 cm depth. The amount of influence depends of the stiffness ratio between the layer measured and the underlying layer (Sawangsuriya et al. 2002).

The soil surface stiffness measured by the SSG has been correlated with other tests such as the falling weight deflectometer (FWD), dirt-seismic pavement analyzer (D-SPA), and spectral analysis of surface waves (SASW - Sawangsuriya and Edil 2005). Besides the elastic modulus of the SSG has being compared with tests such as the resilient modulus test, the resonant column test, the seismic test and triaxial compression test (Sawangsuriya et al. 2003).

3.3.3. Dynamic cone penetrometer (ASTM D 6951)

The dynamic cone penetrometer is a test used to measure the rate of penetration of a 20-mm, 60^{o} cone into the soil mass. The cone is located at one edge of a 16-mm steel rod. The rod is driving by an 8-kg hammer that drops over a height of 575 mm pushing the cone (Sawangsuriya and Edil 2005).

The DCP test gives the penetration index (DPI) which gives an indication of the soil shear resistant against penetration (Edil and Sawangsuriya 2006). In general, this test is used to identify boundaries of soil layers, evaluate the structural behavior of soil embankment and existing pavements structures (Abu–Farsakh et al. 2005). In the literature the DPI index has been correlated with other mechanical and engineering parameters (Rollings and Rollings 1996; Gas Technology Institute 2005; Sawangsuriya and Edil 2005). The procedure and calculation of the DPI are described in the ASTM D 6951 following the following relation:

$$DPI = \frac{\sum_i^N (DPI_i)}{N} \quad \text{(Eq 3.3)}$$

where N is the total number of DPI (penetration per blow) recorded at a given depth of interest.

The ASTM D 6951 also gives an option to use a small hammer of 4.6 kg when the 8 kg hammer produces excessive penetration in loose soils. To use the small hammer, the DPI index has to be multiplied by a hammer factor of 2 in order to standardize the measurements as the ASTM D 6951 requires.

3.3.4. Pressure plate

This device is used to measure the soil pressure induced by a surface load. The pressure is measured with a 19 cm diameter circular plate of loaded vertically (figure 3.13). A rubber membrane filled with water is located under the circular plate which is connected to a pressure transducer to transform hydraulic pressure to electrical signal. The voltage is recorded and transformed to pressure using the calibration curve of figure 3.14.

3.3.5. Shear induced rotations in soil using MEMS accelerometers

Miniature Electro-Mechanical Systems (MEMS) are devices with an integrated circuit used to measure accelerations in form of voltage; the output voltage is proportional to accelerations which depend of the supply voltage (Wang et al. 2008). In addition to

acceleration, MEMS accelerometers may also detect the rotation of the main sensing axis with respect of a vertical axis (Kim et al. 2011).

They use a suspended proof mass which detects how the misalignment of the component of gravity changes with the MEMS rotations (Sellers and Taylor 2008). The accelerations may be measured in 2D or 3D depending of the type of accelerometer used, moreover the new generation accelerometers may be wireless with a sensitivity up to 0.0009 degrees. These sensors make them a useful tool for monitoring geotechnical systems as Srinivasan et al. (2010) report.

Schuettpelz et al. (2009) studied the application of MEMS accelerometers to measure velocity of elastic waves through soils as well as the measurement of induced rotations. Moreover Hoffman et al. (2006) evaluate the use of MEMS as low cost accelerometers in near surface monitoring of geotechnical engineering systems performing shear wave velocity test.

In this study, the DE–ACCM2G accelerometers are used, which are capable to measure accelerations in two independent axis with a sensitivity of 0.75 V/g at a supply voltage of 5 V. The configuration shown in figure 3.15 was selected for 0 rotations. The voltage measured by MEMS is transformed to rotations using the following relationship (Schuettpelz et al. 2009).

$$MEMS\ rotation_i = |\arcsin(V_i - V_0)| \qquad \text{(Eq 3.4)}$$

where V_i is the MEMS voltage after rotation and V_0 is the voltage of the MEMS when its sensing axis is aligned with a vertical axis.

3.3.6. P-wave velocity in a vertical homogeneous media

The P-wave velocity test is a non-invasive test to measure the stiffness of the soil mass using the relation between the constrained modulus and the density of the soil (Richart et al. 1970).

$$V_p = \sqrt{\frac{M}{\rho}} \qquad \text{(Eq 3.5)}$$

where V_p is the P-wave velocity; M is the constrained modulus of the soil and ρ is the soil density.

The P-wave velocity is influenced by effective stress, void ratio, cementation, suction, stiffness of the minerals and water content (Santamarina 2001; Fratta et al. 2005; Sawangsuriya and Fratta 2006). Fratta et al. (2005) developed a preliminary laboratory investigation to determine the soil density and water content using the P-wave velocity test and the electromagnetic wave-based time domain reflectometry technique.

The time arrival of a P-wave traveling vertically through the soil layer is detected by an embedded MEMS accelerometer and recorded by an oscilloscope. Figure 3.16 shows the scheme of the P-wave velocity test as is reported by Schuettpelz et al. (2009). The P-wave is produced by an instrumented hammer hitting a coin deposited in the surface of the soil. The

differences in time arrival of the P-wave at each MEMS divided by the vertical separation taken as 5 cm, yield the P-wave velocity. The AIC Picker technique described in Zhang et al. (2003) is used to determine first-arrivals in the wave traces. The technique is designed to identify automatically the P-phase picks for a warning system (Sleeman and Eck 1999). The global minimum of the onset point of a seismic signal identifies the first arrival of the P-wave following this relation:

$$AIC\ (t) = t\ \cdot \log\left[var\{a(1,k)\}\right] + (N - t - 1) \cdot \log\left[var\{a(t+1,N)\}\right] \qquad \text{(Eq 3.6)}$$

where t is the time; N is the number of points of the data series and a is the acceleration measured by the signal

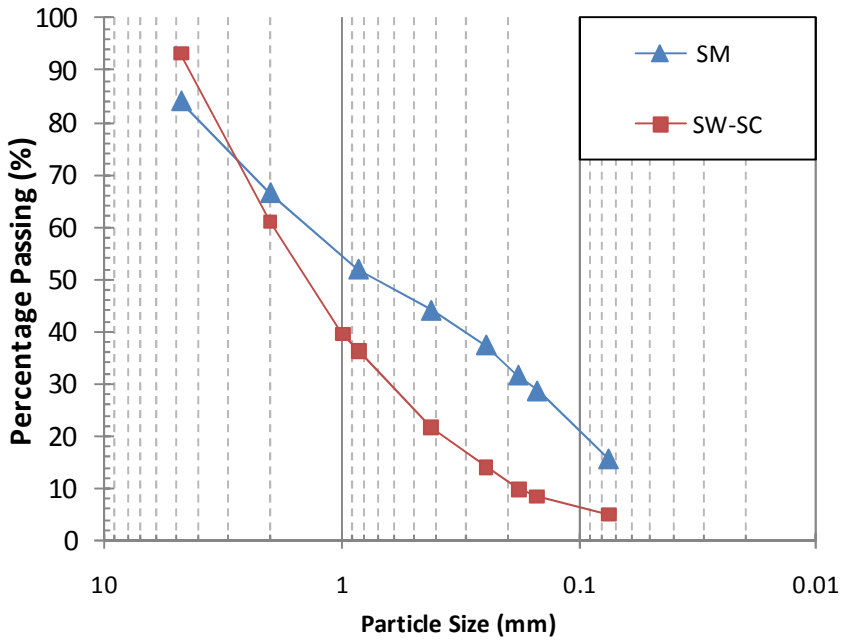

Figure 3.1: Particle size distribution of the tested soils

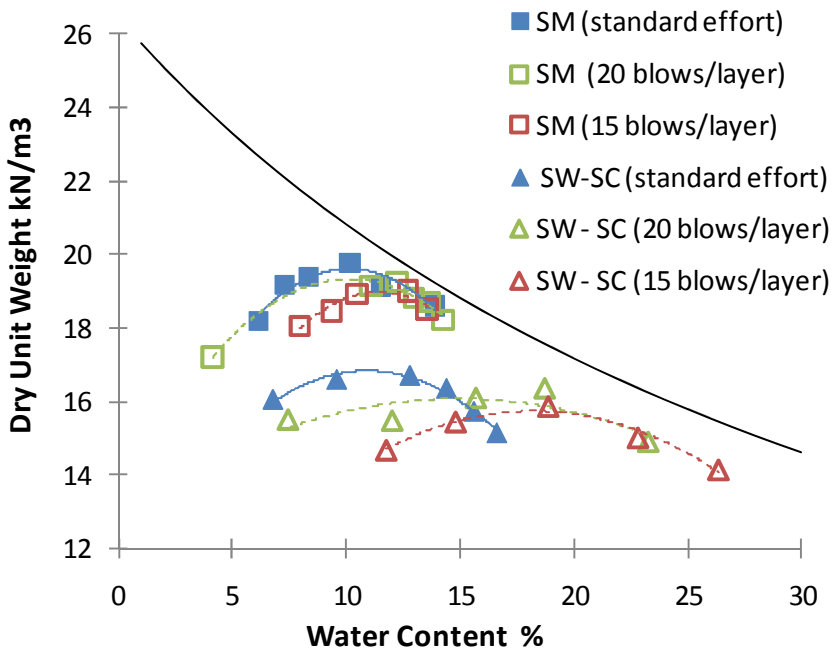

Figure 3.2: Compaction curve of the tested soils for different compaction efforts. The "standard effort" corresponds to the ASTM D 698 standard

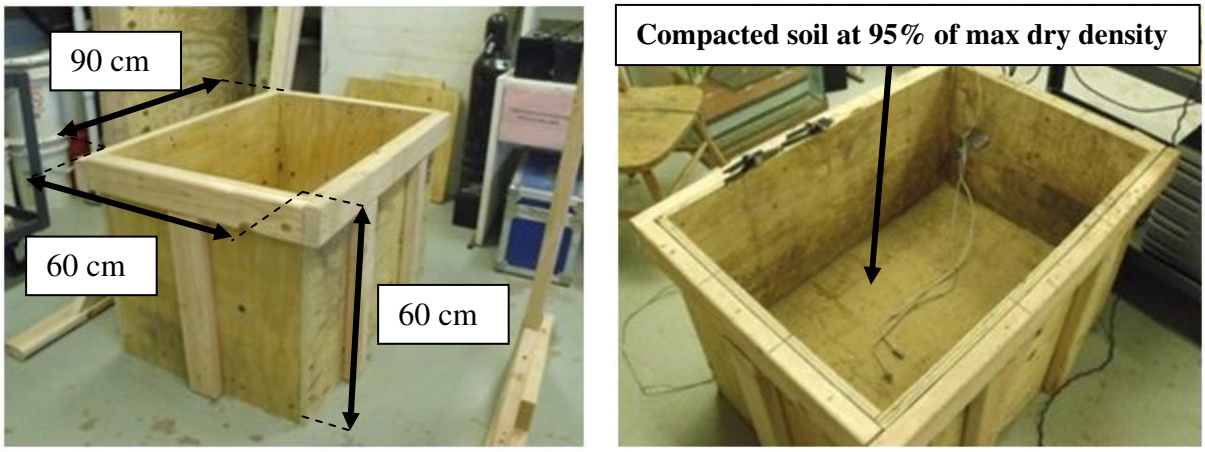

Figure 3.3: Wooden box set up to perform the soil compaction monitoring test

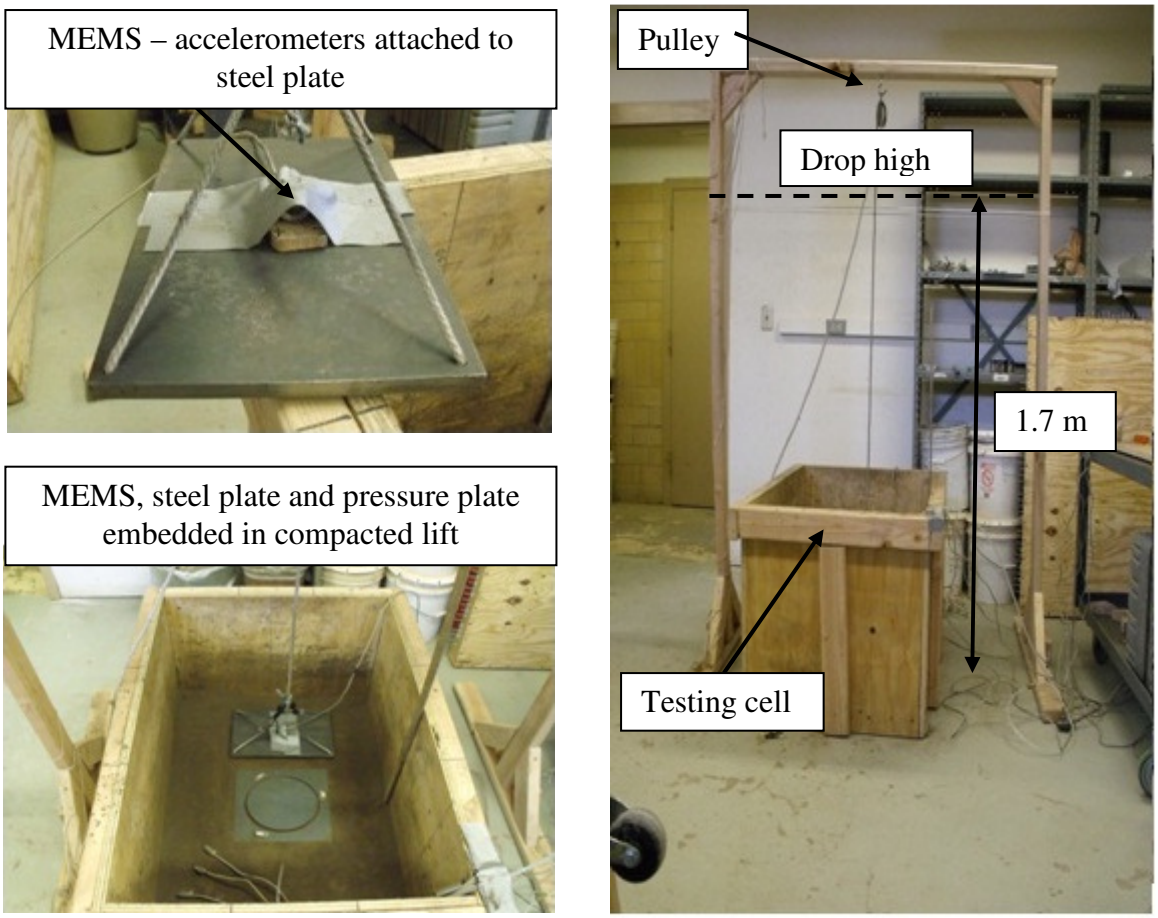

Figure 3.4: Preliminary test configuration

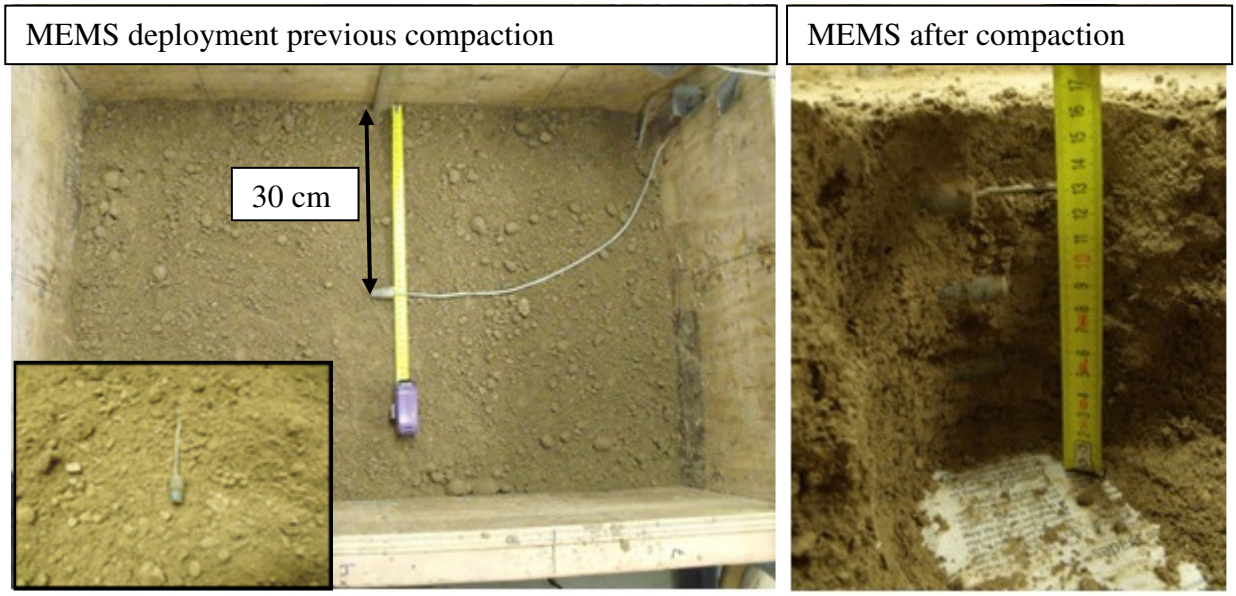

Figure 3.5: Deployment of MEMS accelerometers into the tested soil before and after compaction

Figure 3.6: Compaction process using the compactor plate

Figure 3.7: Measurement of the surface displacement

Center measurement	Edge measurement
	

Figure 3.8: Measurement of the surface stiffness using the SSG

Figure 3.9: Measurement of the density profile using the NDG

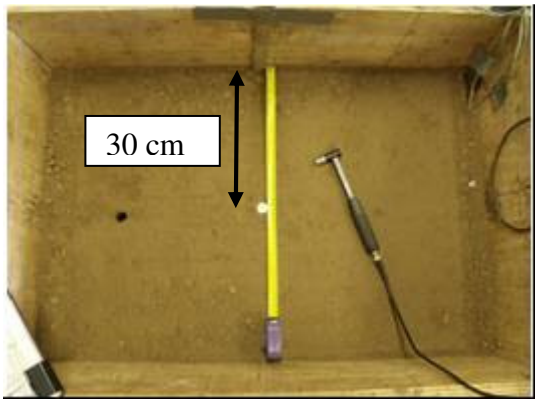

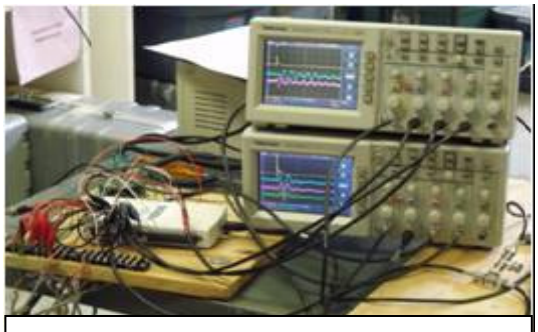

Data acquisition system

MEMS Accelerometers used to monitor the P–wave velocity

Figure 3.10: Measurement of the P–wave velocity in depth

Figure 3.11: Measurement of the DIP using the DCP

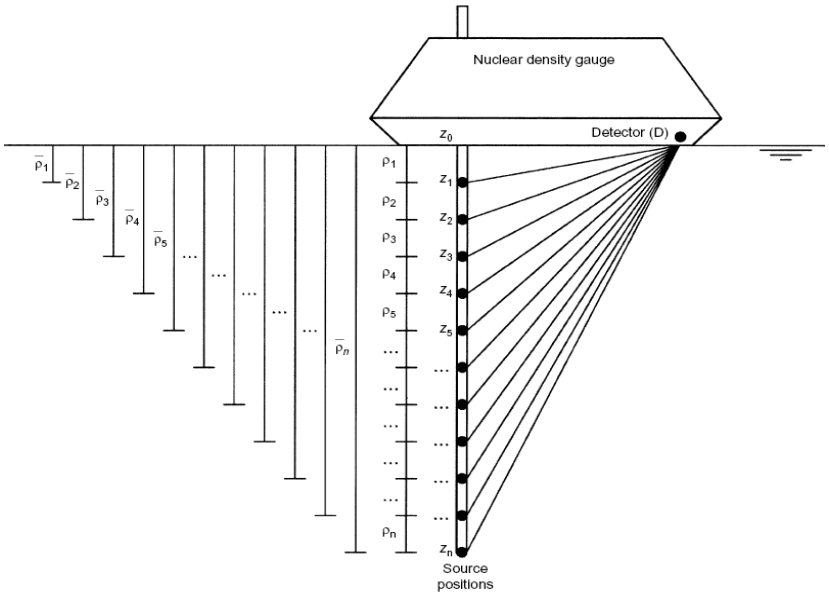

Figure 3.12: Density profile measurement according to Winter and Clarke (2002)

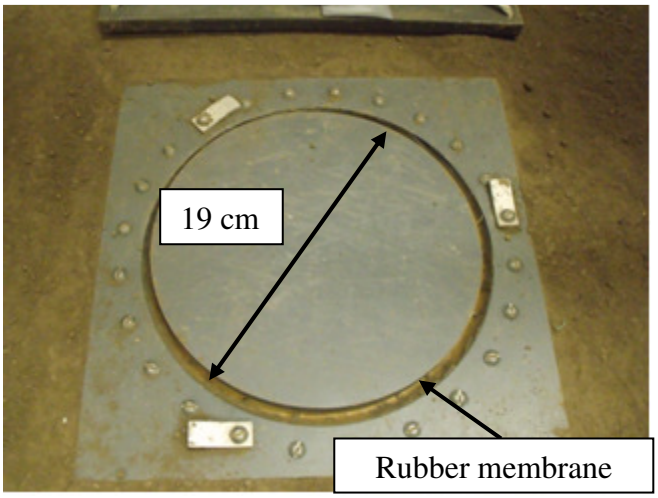

Figure 3.13: Pressure plate embedded in the bottom compacted layer

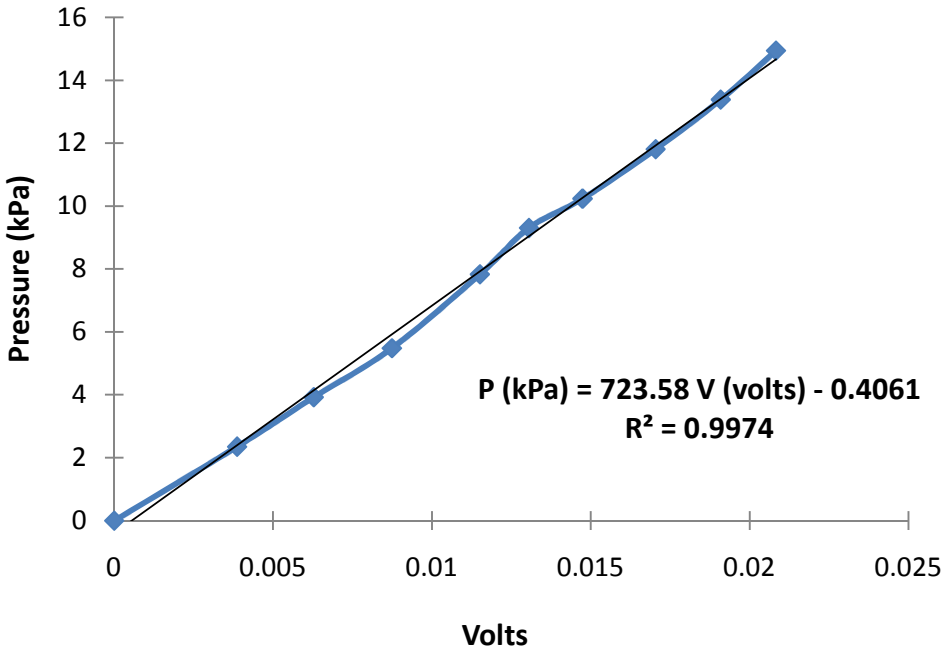

Figure 3.14: Calibration curve of the pressure plate

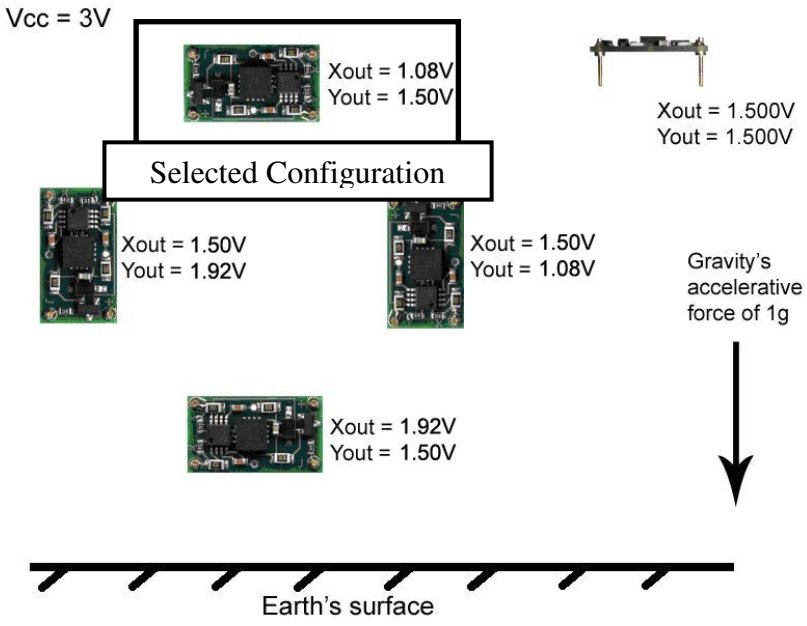

Figure 3.15: Rotation and calibration measurements with MEMS accelerometers (Excitation: 3 V_{DC} - Source: Dimension Engineering 2009)

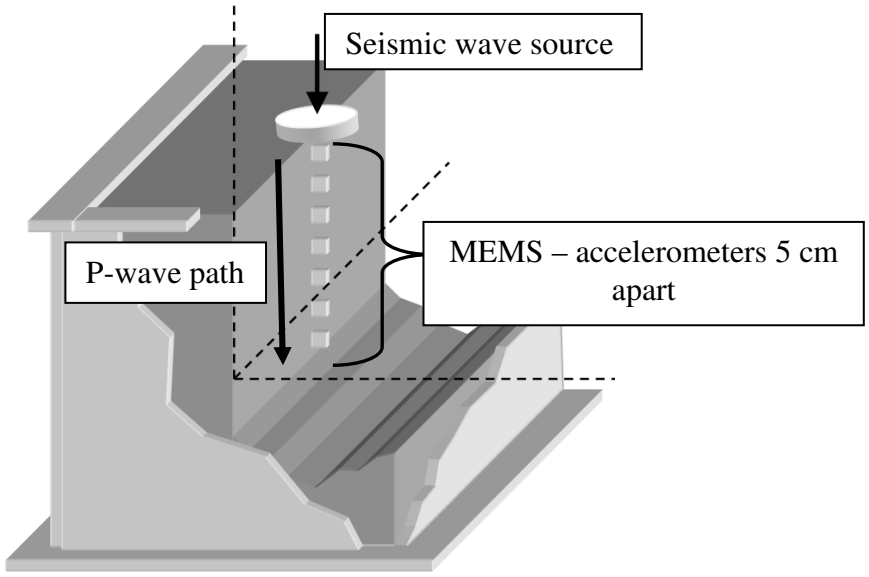

Figure 3.16: Scheme of the P–wave velocity test (Modified from Schuettpelz et al. 2009)

4. RESULTS AND ANALYSIS OF COMPACTION MONITORING

This section presents the results and data interpretation of the evolution of the physical and engineering parameters of compacted soils. The presentation of the material in this chapter is divided into four main analyses according to the soil properties studied:

- Soil displacements and soil disturbance
- Soil density
- Soil shear strength
- Stiffness

The test results were analyzed to evaluate the influence of the lift thickness, water content and soil type in the final engineering soil properties under a controlled compactive effort. The analysis focuses in identifying the influence of compactive effort and lift thickness in the final soil engineering properties.

4.1. Soil displacements and soil disturbance

The soil surface displacement and the vertical displacement of reference points within the soil give an indication of the degree of compaction and how the density profile is distributed across the lift. The vertical displacement of the soil surface is measured and recorded after each compaction pass while the final soil displacements is recorded using the MEMS accelerometers embedded into the soil layer as markers. They are measured when the specimen is removed from the testing cell. In addition, induced shear rotations give an indication of the soil disturbance caused by the compactor. These disturbances are measured by MEMS accelerometers.

4.1.1. Soil surface displacement

The soil surface displacement is presented in figure 4.1 and the percentage of soil surface displacement with respect to the lift high is presented in figure 4.2 as a function of the number of passes for different lift thicknesses, moisture content and soil type. The silty sand reaches a soil surface displacement after 8 passes of about 3 to 4 cm for all lift thickness, whereas in the sand the soil surface displacement is between 1.5 and 3.5 cm, depending of the lift thickness being compacted. The soil surface displacement increases with the lift thickness but the increment seems to be larger in the silty sand and smaller in the sand. When the soil is compacted with large lift thicknesses, the percentage of displacement is less than when the soil is compacted with a small lift thickness. In other words, a lift thickness of 15 cm yields a relative soil surface displacement of 25% for silty sand and 12% for the sand respectively, while a lift of 35 cm thick yields 10% of relative displacement for both soils. This implies that when the soil is compacted using a small lift thickness, the soil reduces more its volume at the same compactive effort than for a thick lift, although the soil surface displacement is larger in thick lifts.

These observations indicate that even when the soil surface displacement after 8 passes is larger in thick lifts; it is the relative displacement (vertical displacement divided by total lift high) which controls the level of compaction within the soil mass. Relative displacements of 25% and 12% for the silty sand and the sand indicate large degree of compaction.

Molding water content seems to have little influence in the soil surface displacement because both soils have approximately the same range of surface displacement when they are

compacted at the dry side or wet side of optimum. Nevertheless the vertical strain for the soils compacted at the wet side tends to be slightly larger than for the dry side. This is due to the lower void ratio of the wet soils when they are placed in its loose state and then compacted. Santamarina et al. (2001) and Fratta et al. (2005) report that the stiffness of a soil mass decreases when the degree of saturation increases (for the same void ratio). This lower stiffness may be caused by the larger water content, that decreases the matrix suction in the soils and allows more deformation under the same compactive effort.

4.1.2. Vertical displacement measurements

The displacements of the MEMS accelerometers embedded in the soil layer are measured after 8 passes of the compactor, when the soil is removed from the testing cell. The measurements are made taking as a reference the boundary between bottom the layer compacted at the 95% of maximum density and the layer being tested. These displacements might give an indication of the soil degree of disturbance profile across the lift. Figure 4.3 presents the displacement of MEMS accelerometers after 8 passes of the compactor. The data points at the center show the initial high of each MEMS accelerometer before compaction (initial condition), while the two set of points next to it show the height of each MEMS accelerometer after 8 passes for the soil compacted at the dry side and wet side of optimum respectively.

For both soils tested, the higher MEMS accelerometer displacement seems to be at the surface of the soil layer and decreases with depth. The data also suggest that the soil

displacement seems to be larger in the silty sand than in the sand at the same compactive effort.

The silty sand compacted at the wet side of optimum seems to have larger soil displacements than compacted at the dry side (for 35 cm lift thickness). While the sand seems to have a larger displacement when is compacted at the wet side of optimum for a lift thickness of 15 cm, and dry side of optimum for a lift thickness of 20 cm. Besides the displacement in the sand, when is compacted using a lift thickness of 35 cm is similar for both water contents.

Larger displacements in the silty sand when is compacted at the wet side of optimum follows the same pattern than the soil surface displacement due to the lower soil stiffness when the soil has more water content. However the data suggest that the final displacement for the sand depends of the water content and the lift thickness. It seems that when the lift thickness is increased, the displacement is larger when the soil is compacted at the dry side. This may be due the variable relationship of the dry density and water content (compaction curve) of the sand. The water content when the sand is compacted at low energies seems to have a small effect in the dry density due to its shape (figure 3.2). As the soils are compacted with a lower compactive effort that the standard effort (600 kN m/m^3) the change in water content might not have larger influence in the final soil displacement for the sand.

4.1.3. MEMS accelerometer-calculated rotations

Using embedded MEMS accelerometers within the soil layer it was possible to evaluate the induced rotations produced by the compactive efforts. These MEMS accelerometer-

calculated rotations may give an indication of the soil disturbance after each compaction pass and thus the depth of compaction effectiveness.

Figure 4.4 and 4.5 shows the shear rotation in absolute value for different lift thicknesses, soil type and water content. All rotations are below 5 degrees for all types of soil, lift thickness and water content. MEMS accelerometer-calculated rotations are larger close to the soil surface particularly for lift thickness of 15 and 20 cm. Despite the noisy data, figures 4.4 and 4.5 also show that induced rotations tend to decrease with depth and with the number of passes.

The degree of disturbance is higher when the soil is compacted using thin lifts, because given the same energy per pass, there is less material to compact and less energy losses than in the case of thick lifts. In addition, generated mechanical disturbances remain trapped within the compacted lift being. The interaction of the resulting vibration generated by the compactor produces a larger rearrangement of soil particles than for a thick lift.

In thick lifts, the compaction energy has more distance to dissipate its energy across the lift; therefore the energy that reaches the bottom part of the lift depends of the lift height and weight of the compactor. This explains why the measured displacements and the calculate-rotation decrease with depth. Furthermore with greater number of passes, the soil gains density and stiffness across the lift; this reduces the energy losses in the elastic waves. However, due to the larger density and large interlocking force between particles, the soil

particles need more energy to be rearranged, producing a decrease of the density gain with the number of passes.

The depth of soil disturbance produced during the first three passes by the small compactor used in this study (table 3.3), seems to be around 15 cm for a thick lift (35 cm) while for thin lifts (15 and 20 cm) the soil disturbance seems to be larger than 15 cm.

Even though the data are noisy, the soils compacted at the dry side close to the optimum seems to have a higher degree of disturbance than when are compacted at the wet side. This is because the compactive energy has more energy to disturb the soil particles when the soil is compacted at the dry side. This is because for a given frequency, a lower stiffness in the soil produces a larger damping (Santamarina et al. 2001). Therefore as the soil has lower stiffness when has more water content, the energy dissipation is larger, producing smaller disturbance amplitudes to rearrange the soil particles than in the case of dry of optimum.

4.2. Soil density

The density profile gives an indication of the distribution of soil density in depth when a compactive effort is applied. The density profile is obtained using the Nuclear Density Gauge (NDG) and is presented as relative density (RD) which is the result from the density measured by the NDG divided by the maximum dry density obtained from the Standard Proctor test. Figures 4.6 and 4.7 show the density profiles for different compactive efforts (number of passes), soil type, molding water content and lift thicknesses.

It is common knowledge that the density profile increases with the number of passes due to the reduction of void ratio during the compaction process (Olson 1963; Rollings and Rollings 1996; Holtz et al. 2010). In these laboratory tests, the density gain starts to decrease after the second pass for the silty sand and after the first pass for the sand. That is, there is a diminishing return of improving density with greater number of passes as D'Appolonia et al. (1969) reports. The final average density reached by the silty sand (16 kN/m^3) is larger than the average density reached for the sand (12.8 kN/m^3) after 8 passes.

Due to the different increments in soil density under the same compactive effort, and to the difference in final relative density reached by the tested soils, the compaction method using the vibratory plate (pounding) seems to work better for the silty sand than for the sand. Furthermore, figure 4.8 shows the average relative density for the sand compacted by pounding (during preliminary tests) at the optimum water content. The tested lifts are 15, 20 and 25 cm thick, the density is measured at the middle of the layer for different supplied energies generated by the steel plate. The final relative density reached by the sand at the middle of the layer using pounding in five passes is about 4 to 8 % larger than using the vibratory plate as a method of compaction for 15 and 20 cm lift thicknesses respectively. This larger relative density using pounding is explained by the smaller influence of the dynamic force produced by the vibratory plate in the middle of the layer in comparison with the influence of the shock wave produced by the steel plate. The stress level produced by dynamic load within the soil layer, contributes to the rearrangement of soil particle and to produce higher densities and confining pressures. Therefore, as the elastic wave generated by

pounding in the sand has larger energy the final relative density is larger than when the vibratory compactor is used.

When the lift thickness and molding water content are changed the gradient of the density profile is different for the tested soils. When the soils are compacted using lower water content, the density profile increases with depth for a lift thickness of 15 cm and decreases with depth for 35 cm lift thickness, this is true particularly for the silty sand. For 20 cm lift thickness, the density profile seems to be constant with depth. This finding suggests that the increment in density is more homogeneous across lift when the soils are compacted close to the optimum water content and using a lift high of 20 cm.

When the silty sand is compacted wet of optimum (figures 4.6 and 4.7), the density reaches larger values than when is compacted at the dry side, besides the density profile decreases with depth for all lift thicknesses, producing zones of lower density at the bottom of the lift. However for sand, the case seems to be slightly different for a lift thickness of 15 cm, due to the increment on water content results in zones of lower density at the surface of the lift. This may be produced by a phenomenon in coarse graded soils called “overcompaction” (D’Appolonia et al. 1969) where at the top part of the lift, due to the low effective stresses, the soil particles vibrated loose producing poorly compacted zones regardless of the number of passes.

To quantify the change of the density profile, figure 4.9 shows the increment in relative density after 8 passes of the compactor and the vertical difference of relative density between

the upper part of the layer and the lower part. The data suggest that when the lift is increased the vertical difference in relative density between the upper and lower part of the lift increases as well. The highest value of 7% for the relative density between the upper part and lower part of the lift is when the silty sand is compacted at the wet side of optimum using a 35 cm lift thickness. The sand on the other side shows more variability and a low relative density difference between the top and bottom part of the lift. The larger increment in density is close to the surface and the lower increment is at the bottom of the lift as is shown in figure 4.9. This behavior is prominent in the silty sand while the sand the increment in density seems to be smaller and more homogeneous across the lift.

Regardless of the lift thickness tested, the bottom part of the lift seems to have lower degree of compaction than the upper part. This is produced mainly by two factors. The first factor is due energy losses across the lift of the compactive disturbance that interacts with the soil lift. The second factor is that at the bottom part of the lift, the state of effective stress is slightly larger, therefore the particle interlocking shear strength is larger at the bottom of the lift than at the surface and more energy is needed to increase the density. This means that the compactive effort at the bottom part of the lift needs larger compactive energies to produce a rearrangement of particles and increase the density of the soil. Furthermore, when the water content is increased the energy losses of the elastic wave are larger than when are compacted using lower water contents.

4.3. Soil shear resistance

The dynamic penetration index (DPI) obtained with the dynamic cone penetrometer test (DCP) gives the number of blows necessary to penetrate a certain distance into the soil. The penetration index or DPI may give an indication of the soil shear resistant across the lift.

4.3.1. Dynamic Cone Penetration Testing

Figures 4.10 and 4.11 shows the DPI index as a function of depth for different lift thicknesses, soil type and water content. To compute the DPI index, it can be using two different dropping masses (4.6 or 8 kg). The smaller hammer allows testing loose soils, but as the ASTM D 6951 standard requires the DPI to be multiplied by a hammer factor of 2. Even though the smaller hammer is used for loose soils, the dynamic cone penetrometer device reaches entire soil layer, independent of the lift thickness and water content tested.

The DPI values start to decrease and to be more homogeneous across the lift after 4 to 5 passes of the compactor, particularly when is compacted at the wet side of optimum. As the amount of compactive energy received by the soil during the tests is smaller than the energy used in the standard proctor test; the compaction curve for the soil being tested is different than the compaction curve obtained with the proctor test. Furthermore the optimum water content taken from the standard compaction curve is different when the soil is compacted with less energy. The lower energy compaction curve is shifted to the right; it reaches lower maximum dry density and higher optimum water content as is shown in the scheme of figure 4.12. Therefore, when the soil is compacted at the wet side of the optimum water content obtained from the standard effort; it may be possible that for the same water content in the

lower compaction curve (lower energy), it is closer to the optimum than when the soil is compacted at the dry side. This situation produces larger densities (figures 4.6 and 4.7) which and thus higher shear strength.

The DPI values after 8 passes of the compactor in the silty sand increase when the lift thickness is increased, taking values of up to 100, 140, 200 mm/blow for lift thicknesses of 15, 20, 35 cm respectively. This increment in the final DPI values with increasing the lift thickness suggests that thick lifts yield lower shear strength than thin lifts. As the density profile decreases with depth in thick lifts, the effective stress state decreases as well, leaving zones of low soil shear resistant than in thin lifts the density is larger and more homogeneous with depth.

The sand specimen on the other side does not seem to have enough shear resistance to stop the cone penetration, since with one blow the penetration reaches the bottom part of the soil layer, even after eight passes of the compactor.

4.4. Soil stiffness

The soil stiffness was evaluated within the soil layer and at the surface using two different methods. The soil surface stiffness is evaluated with the soil stiffness gauge (SSG) and the stiffness within the soil layer is evaluated using P-wave velocity measurements.

4.4.1. Soil surface stiffness

Figure 4.13 shows the soil surface stiffness for different lift thicknesses, soil type and water content. With increasing number of passes, the surface soil stiffness increases due to the soil gain density reducing its void ratio. According to the tested lift thickness, this increment in soil surface stiffness seems to be always positive for the silty sand reaching a final value between 30 and 50 MN/m. However, the sand reaches a maximum value between 15 and 20 MN/m after the second or third pass. After that, the sand reaches a plateau that it is maintained up to 8 passes.

The data suggest that the soil surface stiffness of the silty sand compacted using the vibratory plate reaches higher values when the lift thickness is smaller for the same compactive effort and water content. However it has to be considered the influence of the underlying layer compacted at 95% of the maximum density in the SSG readings. According to Sawangsuriya et al. (2002), the readings of the SSG, it may produce larger measurement of stiffness for thin lifts on a layered system. If the lift thickness is smaller than a critical height, the stiffness measured by the SSG is influenced by the underlying layer. Sawangsuriya et al. (2002) indicate that the depth at where the SSG start to identified the soil stiffness is 12.5 cm or thicker. However if the SSG is used in a layered media, the underlying soil layer influences the SSG measurement between 12.5 and 27.5 cm depth depending of the stiffness ratio between layers (Sawangsuriya et al. 2002). Same problems have been reported when measuring the in-situ soil stiffness in intelligent compaction procedures (Anderegg and Kaufmann 2004; Rinehart and Mooney 2007 and 2009). Rinehart and Mooney (2009)

suggests that for an Amman and Bomang IC rollers working in a layered soil media the critical depth depends of the stiffness ratio between the layers.

Figure 4.13 and 4.14 shows the soil surface stiffness for the sand compacted using the vibratory plate and by pounding respectively. The soil surface stiffness for the sand using both methods does not seem to be influenced by the underlying layer, because the soil surface stiffness does not change when the sand is compacted using the vibratory plate at each lift thickness and increase with increasing lift thickness when the sand is compacted by the drop plate. This may be produced because the sand reaches larger densities when is compacted using the drop plate than using the vibratory compaction plate. Moreover, the measured stiffness in thin lifts depends of the stiffness ratio of the two compacted layers being higher for larger stiffness ratio. This implies that the stiffness ratio between the bottom compacted layer and the layer being tested is larger for the silty sand and smaller for the sand.

Figure 4.15 shows the stiffness ratio between the stiffness of the soil after compaction divided by the stiffness of the soil before compaction for different lift thickness and water content. The stiffness ratio for the silty sand reaches larger values than the sand at the same compactive effort. This indicates that for a given compactive effort, the silty sand has larger stiffness ratio than the sand. Therefore the hypothesis proposed by Sawangsuriya et al. (2002) that the stiffness ratio between the bottom layer of the silty sand, compacted at the 95 % of the maximum dry density and the silty sand layer being compacted might have larger stiffness ratio influencing the SSG readings appears to be confirmed.

Molding water content does not seem to have a great influence in the final soil surface stiffness since both water content tests shows the same behavior for a given soil. However, the soil compacted at wet of optimum seems to have a slightly lower soil surface stiffness. This observation agrees with section 4.1.1 where the vertical strain is slightly larger for the soils compacted with larger water contents due to lower stiffness. Furthermore, Santamarina (2001) and Fratta et al. (2005) report that the elastic modulus does depend of the water content, where larger water contents produces smaller stiffness.

The data obtained with the SSG present some points where the soil surface stiffness reduces when the number of passes increases. This interesting observation may have been caused by the testing procedure used. Despite the DCP tests are performed after the SSG is placed to record the stiffness in one particular compaction stage, it is for the next compaction stage where the SSG reading are affected by previous DCP tests regardless the added compaction effort between stages. When the DCP device is removed from the specimen it induces some cracks in the surface of the soil diminishing the soil surface density and thus the stiffness. These cracks affect further influencing readings of the SSG.

4.4.2. P – wave velocity profile

Figures 4.16 and 4.17 show the P-wave velocity profile for different lift thicknesses, soil types and water content. As the P-wave velocity is function of the mechanical properties of the media; it also increases with the number of passes. The P-wave velocity in the silty sand increases from about 100 to 300 m/s while in the sand increases form about 100 to 200 m/s after 8 passes.

The final P-wave velocity across the lift seems to be larger for the silty sand than the sand under the same compactive effort, suggesting that the silty sand reaches higher stiffness than the sand at the same compactive effort. This is because the P-wave velocity depends largely of the state of effective stress and the void ratio of the compacted soil as well as the water content (Santamarina 2001; Fratta et al. 2005; Sawangsuriya and Fratta 2006). Due to silty sand has larger fine content than the sand, it reaches larger density profile across the lift (Figures 4.7 and 7.8) and it results in larger P-wave velocities due to the smaller void ratio. Furthermore, the silty sand has lower water content than the sand which also may explain why silty sand reaches larger P- wave velocities.

Due to the change on the state of stress, density and void ratio across the lift, the P-wave velocity profiles is different for a given soil, water content and lift thickness. Despite the state of stress increases with depth in a compacted soil, the P-wave velocity profile for the tested soils using a lift thickness of 35 cm decreases with depth. This behavior is clearer for the soils compacted wet of optimum than for a soil compacted dry of optimum; the P-wave velocity profile seems to be slightly more homogeneous with depth when the soil is compacted at the dry side.

The larger P-wave velocity close to the surface is caused by an increment in the density and thus reducing the lift high. This reduction in the lift thickness affects the MEMS separation, especially close to the soil surface (Figure 4.3). The reduction in the MEMS separations close to the surface produces larger unrealistic P-wave velocity. Nevertheless in the bottom part of

the lift the MEMS separation apparently is not highly affected and the P-wave velocity measurement may to be more representative.

In order to solve this issue, after 8 passes of the compactor the P-wave velocity profile may be corrected considering the final MEMS displacement form figure 4.3. Figure 4.18 shows the final corrected P-wave velocity profile for each lift thickness, soil type and water content after 8 passes of the compactor. The silty sand reaches larger final P-wave velocities than the sand, which proves that silty sand has larger stiffness at the same compactive effort than the sand. Besides, soils compacted at the wet side of optimum the P-wave velocity profile decreases with depth due to the soil reaches larger density (reduces the void ratio) closer to the soil surface (figure 4.6 and 4.7). The data also show a slightly increment in the P-wave velocity when the lift thickness decreases due to the larger density reached by the soil when the lift thickness is smaller. The sand on the other side does not have an increment in P-wave velocity even after 8 passes of the compactor; this explains why the soil surface stiffness also does not increase with the number of passes in figure 4.13.

4.5. Data analysis and comparison with field compaction monitoring

The laboratory data are combined and correlated using theoretical relationships from the literature to establish how the engineering soil properties change with the degree of compaction and to support the main discussions of previous sections.

The compaction monitoring tests at laboratory scale performed in this study give an indication of the effectiveness of soil compaction for different lift thickness soil type and

molding water content. However, the low degree of compaction (density and stiffness) reached after the test, in addition to the type of compactor equipment used at the laboratory (size and weight), makes it difficult to extrapolate the main findings of this research to a real case. In order to try to solve this issue, the results are compared with a similar field experiment of soil compaction performed by Kim et al. (2011).

4.5.1. Correlations and comparison of the engineering soil properties

In order to analyze, the response of soils under compaction, the data are combined to evaluate how the P-wave velocity and soil elastic modulus change with density. The induced soil vertical strain is related with the soil surface stiffness for each compactive effort, soil type and water content. Furthermore, the elastic modulus obtained using the P-wave velocity is compared with the elastic modulus from the SSG.

The dry density (determined by NDG) and P-wave velocity (determined by P-wave velocity tests using embedded MEMS-accelerometers) are averaged across the lift for each lift thickness, soil type, water content and compactive effort. The void ratio (e) is determined using the averaged dry density and the soil physical properties (table 3.1) using the following relation:

$$\rho_{dry} = \frac{G_s \, \rho_w}{1 + e} \qquad \text{(Eq 4.1)}$$

where ρ_{dry} is the average dry density of the soil layer for a given soil, water content, and lift thickness; ρ_w is the density of the water and e is the void ratio.

The elastic modulus of the soil layer is determined using the equation proposed by Richart et al. (1970) (Eq 3.5) and the phase relationships of a soil mass. The final equation is as follow:

$$V_p = \sqrt{\frac{E_{soil}\dfrac{(1-\upsilon)}{(1+\upsilon)(1-2\upsilon)}}{\rho_{dry}(1+w)}} \qquad \text{(Eq 4.2)}$$

where V_p is the P-wave velocity; E_{soil} is the soil elastic modulus; ρ_{dry} is the soil dry density measured by the NDG; w is the molding water content and υ is the Poisson ratio taken as 0.15 for soils with small deformations. On the other hand, the soil surface elastic modulus E_{SSG} determined from the SSG test is obtained using Eq 3.2 with a ring radius of 52.7 mm and a Poisson ratio of 0.15.

The soil elastic modulus across the lift (E_{soil}) is compared with the soil surface elastic modulus determines by the SSG (E_{SSG}) in figure 4.19. It seems to exist an acceptable correlation between the tests; the soil elastic modulus (E_{soil}) increases when the E_{SSG} increases as well. Nevertheless, the elastic modulus across the lift is one order of magnitude smaller than the E_{SSG}. This difference is due to the decrease in density with depth, besides one fourth of the total soil surface stiffness data (tests for the silty sand compacted at the dry and wet side of optimum using 15, 20 cm lift thickness) are influenced by the underlying layer, giving higher values of stiffness, while the P-wave velocity and thus the elastic

modulus are not influenced by the stiffness of the bottom layer. Furthermore, the volume and type of measurement (induced displacement) are different in both tests.

The average P-wave velocity and the soil surface stiffness follow the same pattern when they are related with the void ratio (figure 4.19). As is discussed in previous sections, a decrease on the void ratio produced by compaction (soil densification) increases the P-wave velocity and the soil surface stiffness (K_{SSG}) as well. The relationship between the void ratio and the average P-wave velocity across the lift and the soil surface elastic modulus in the sand seems to be influenced by the lift thickness as is shown in figure 4.19. An increment in lift thickness produces a decrease in the void ratio due to a larger initial density of the sand before compaction.

As the soil gains density, the P-wave velocity and the soil surface stiffness increase with the compactive effort. In order to quantify this increment, figure 4.19 demonstrates the relation between the stiffness modulus of SSG (K_{SSG}) and the average P-wave velocity across the soil layer. The relation shows a poor correlation (i.e., $R^2 = 0.34$). This result is principally due to two factors. First; the P-wave velocity profiles give unrealistic measurements close to the surface, giving larger P-wave velocity and second; the SSG measures are influenced by the bottom layer when the silty sand is tested giving larger soil stiffness.

Figure 4.20 shows the soil surface stiffness (K_{SSG}) as a function of the vertical strain for each soil type and lift thicknesses. These data document that under the same vertical strain, the silty sand shows higher soil surface stiffness than the sand. Furthermore, the silty sand

increases its surface stiffness when is compacted at the dry side of optimum at the same vertical strain. That is, soils compacted at the dry side of optimum present larger stiffness than if they are compacted at the wet side; this explains why the soil displacements are larger when the soil has larger water content. Sand slightly increases its surface stiffness when the vertical strain increases and the difference between the two molding water content is less perceptible.

4.5.2. Comparison with field compaction monitoring

Figure 4.21 shows the results for the pressure plate located at the bottom of the sand layer compacted by pounding during the preliminary tests and figure 4.22 shows the result of the pressure plate at the bottom of the lift for the soil being compacted using a smooth-drum vibratory roller (Kim et al. 2011). The maximum pressure measured at the bottom of the soil layer during compaction decreases with increasing the lift thickness. This is mainly caused by the stress distribution produced by the compaction force across the lift, where lower stresses arrive to the bottom of the layer when the lift thickness increased.

Also in figure 4.22 is shown the stress distribution of a rectangular footing (which represents the contact width B of the compactor and the length of the drum), calculated by the Boussinesq's solution. These lines show that the contact width of the compactor may be estimated in 20 cm for a smooth drum vibratory roller (Caterpillar^{TM} Model CS-563E) as Kim et al. (2011) reports.

The field testing and laboratory tests show that MEMS induced rotations (soil disturbance) decreases with depth and with the number of passes as the soil gain density and stiffness. The

compactor used at laboratory scale (40 by 32 cm vibratory compaction plate with a 5 kN compaction force) has a depth of influence of about 15 cm in loose soil whereas at real scale operations the depth of influence of a smooth-drum vibratory roller (109 kN operating weight) is about 35 cm in clean sand and 40 cm in silty sand as is shown in figure 4.23 (Kim et al. 2011).

According to the laboratory experiments, the bottom part of thick lifts (35 cm) presents regions of low density. This agrees with Kim et al. (2011) who report that lift thicknesses larger than 30 cm may present zones of undercompaction for coarse graded soils as is shown by the DPI profiles in figure 4.24 and because the PDI index starts to increase after 30 cm depth when the silty sand is compacted with a lift thickness of 60 cm. A difference of 7 % of relative density with depth has being found at laboratory scale compaction when the silty sand was compacted at the wet side of the optimum water content obtained from the standard proctor test.

Figure 4.25 shows the comparison of elastic moduli evaluated by P-wave velocity and SSG at the field compaction monitoring. There are some points where the soil surface elastic modulus is larger than the elastic modulus obtained from the average P-wave velocity. This result indicates zones of undercompaction at the bottom of the layer; however the type of measurement and volume where the measures are performed are different in both tests.

Despite of the large difference in the amount compactive effort between the laboratory and at the field test are completely different, both set of experiments suggests that the soil gain

larger density at the upper part of the thick lift where the effectiveness depth of influence of the compactor produces more soil disturbance. Furthermore, in despite the compaction force in field operations is 22 times larger than the use in laboratory, the soil still presents zones of undercompaction at the bottom of lift thickness about 30 cm. That is, energy of compaction is not the only controlling parameter in the determination of lift thickness but the effect contact area appears to control the results as well.

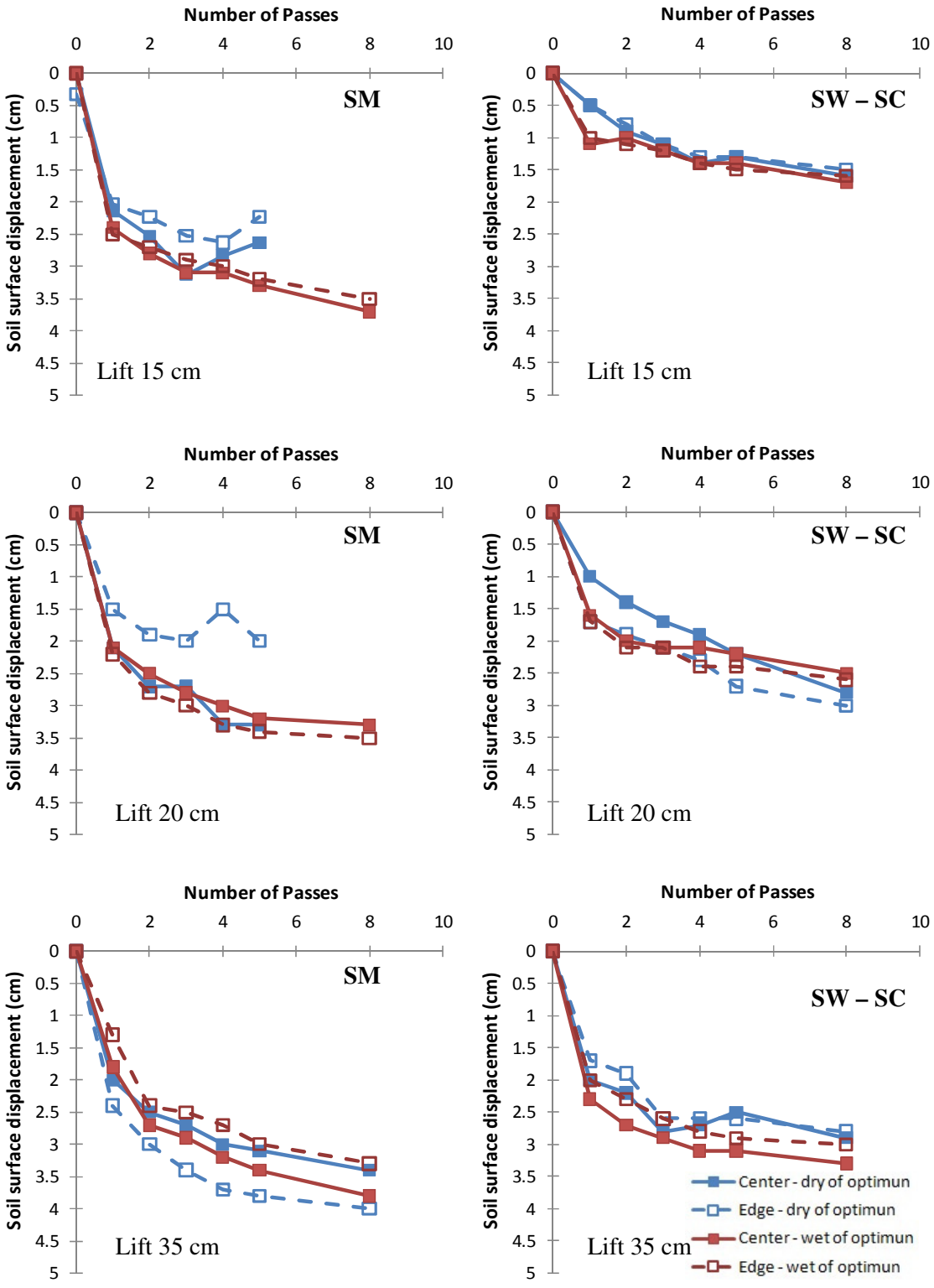

Figure 4.1: Soil surface displacement as a function of the number of passes at different water content

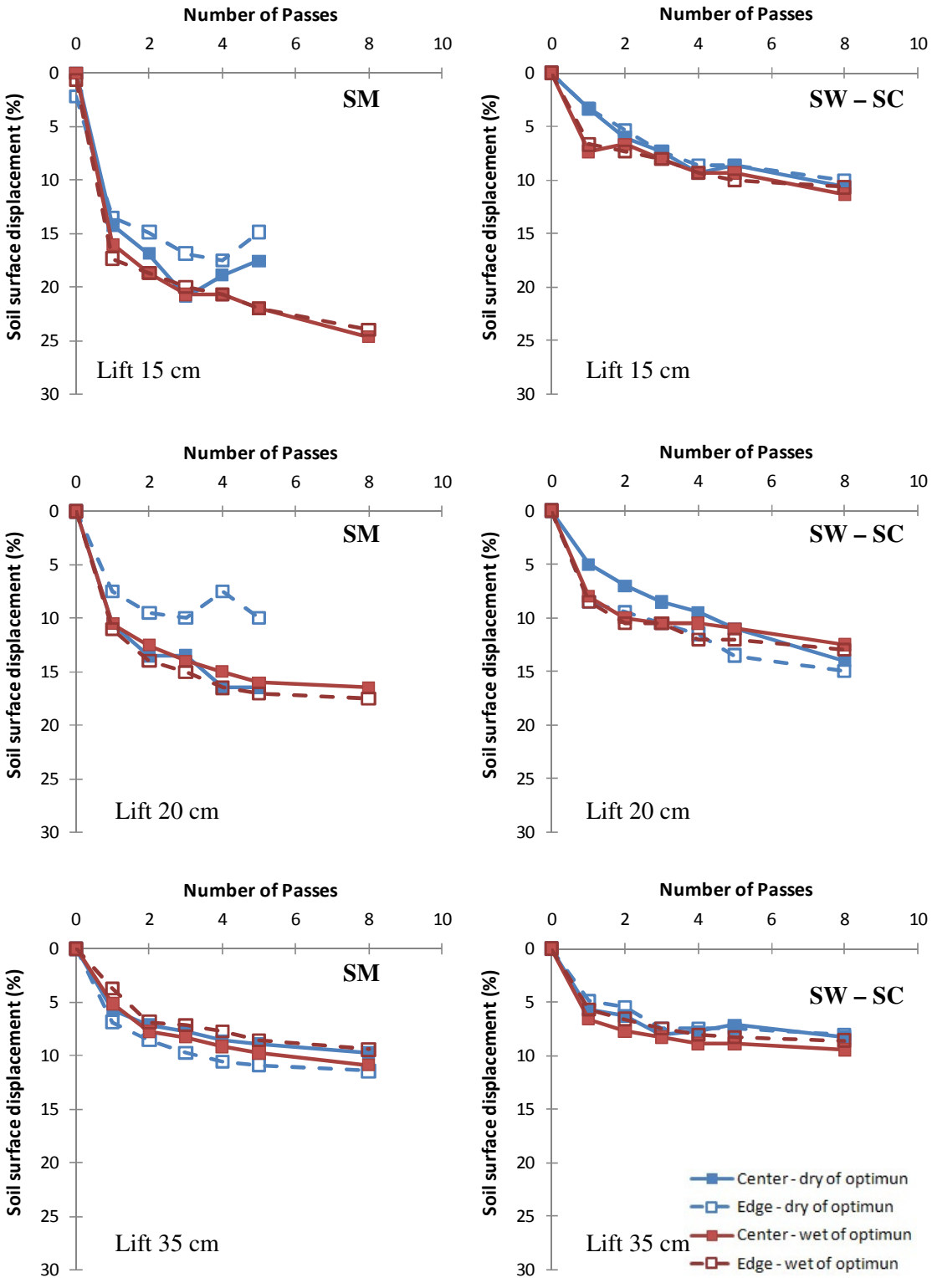

Figure 4.2: Percentage of soil surface displacement with respect of the lift thickness as a function of the number of passes at different water content

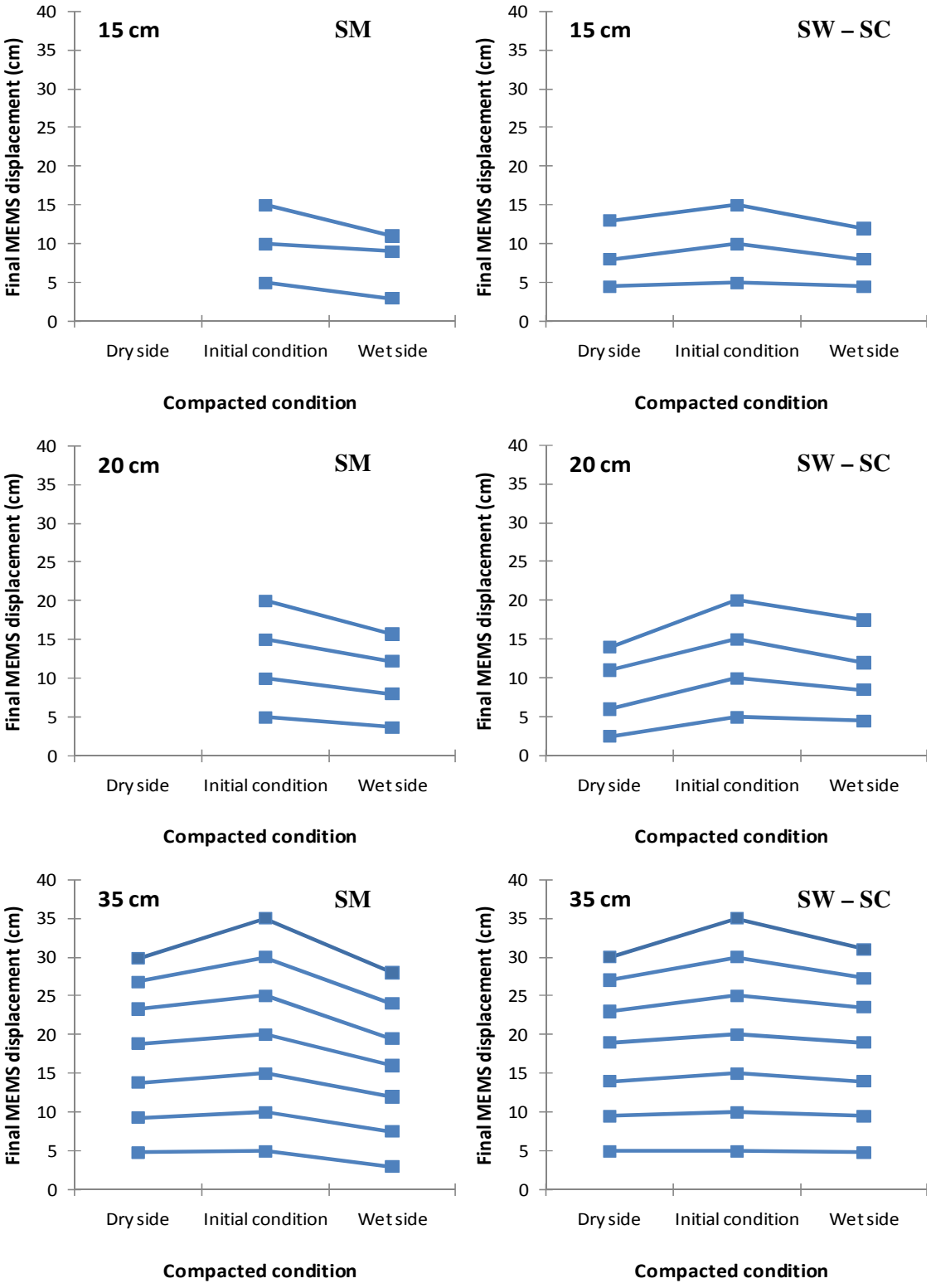

Figure 4.3: MEMS accelerometer-measured displacement after 8 passes of the compactor for different molding water content and soil type

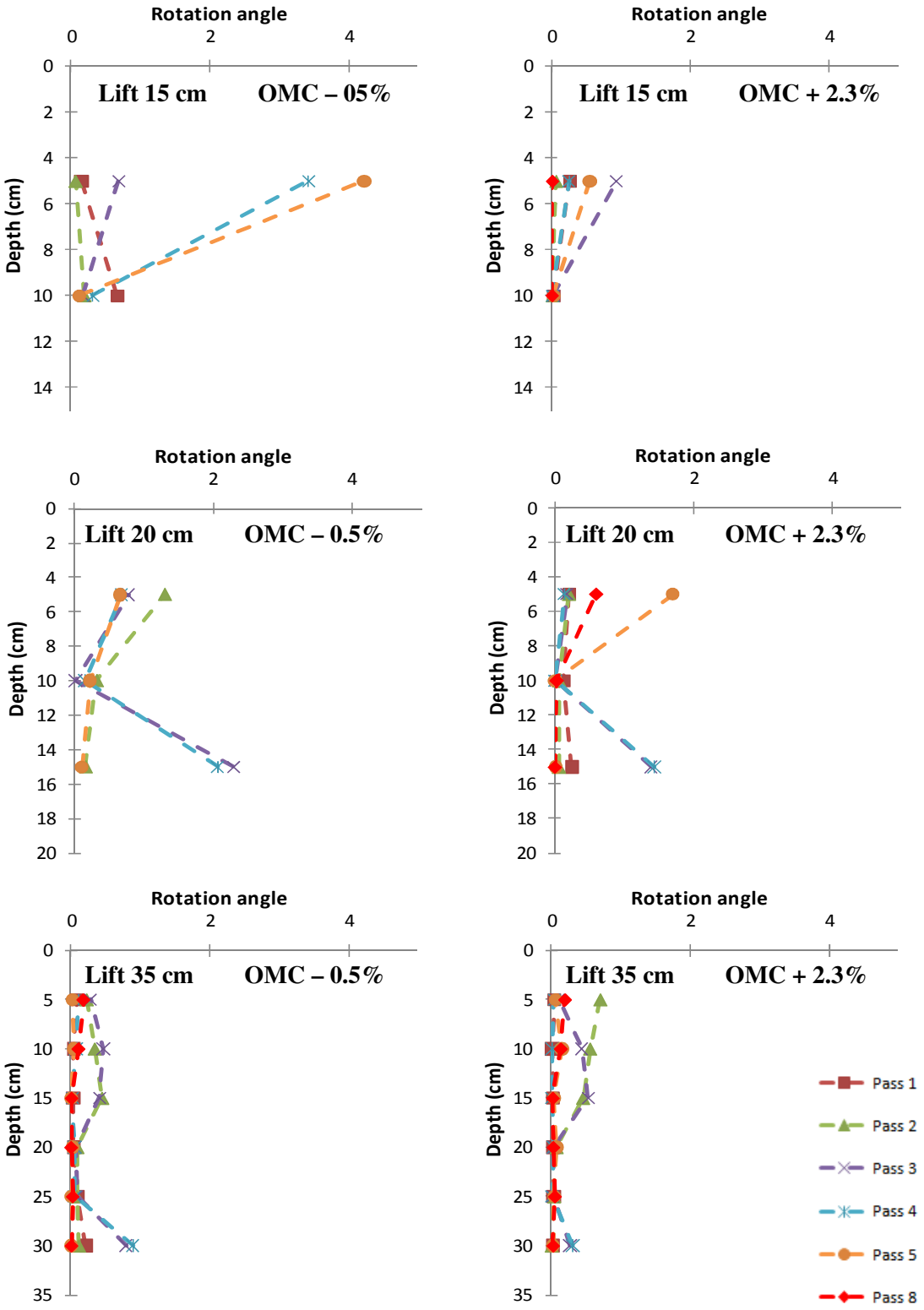

Figure 4.4: Results of MEMS rotation profile for the silty sand compacted in the dry side and wet side of optimum

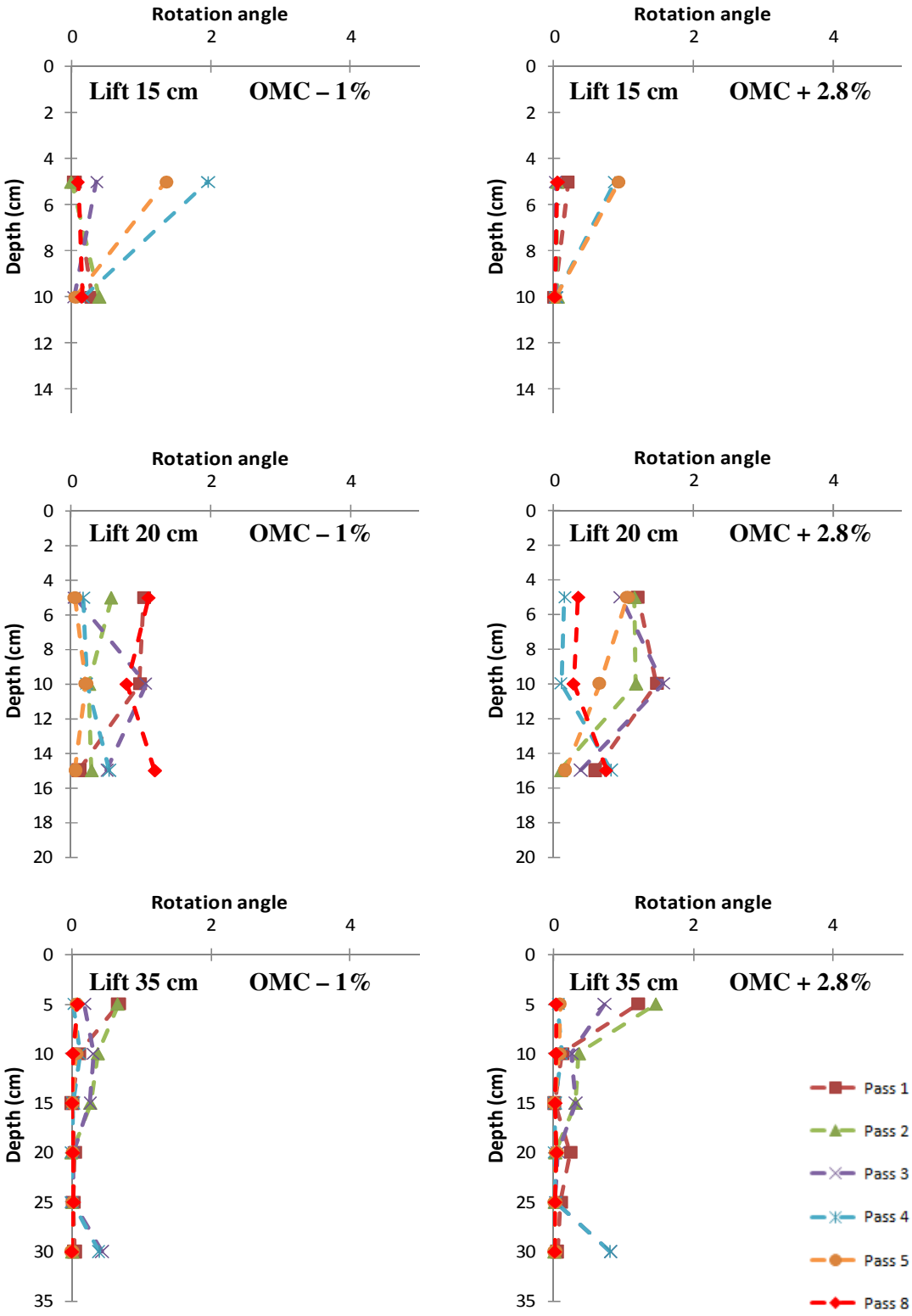

Figure 4.5: Results of MEMS rotation profile for the sand compacted in the dry side and wet side of optimum

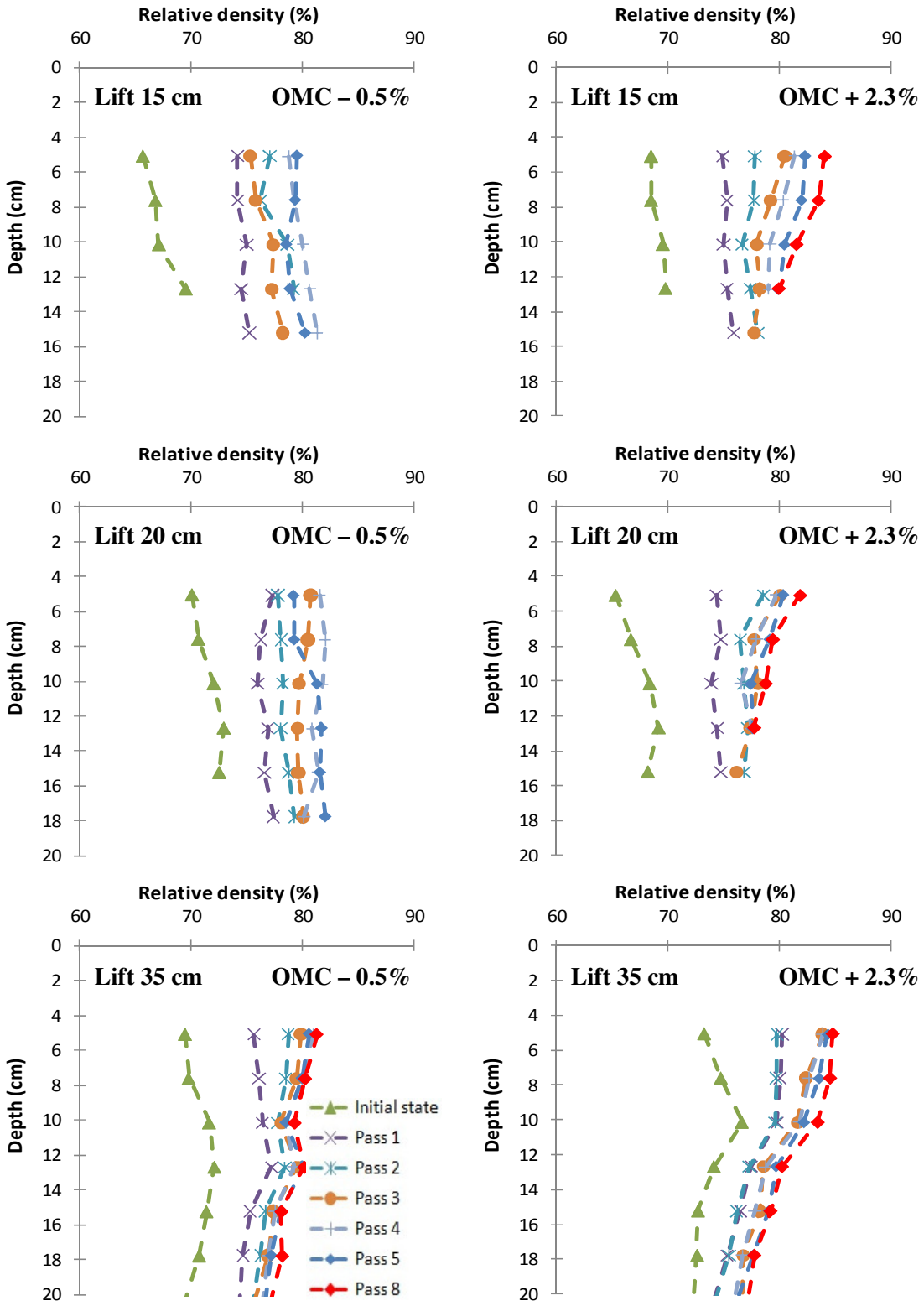

Figure 4.6: Results of soil density profile for the silty sand compacted in the dry side and wet side of optimum moisture content

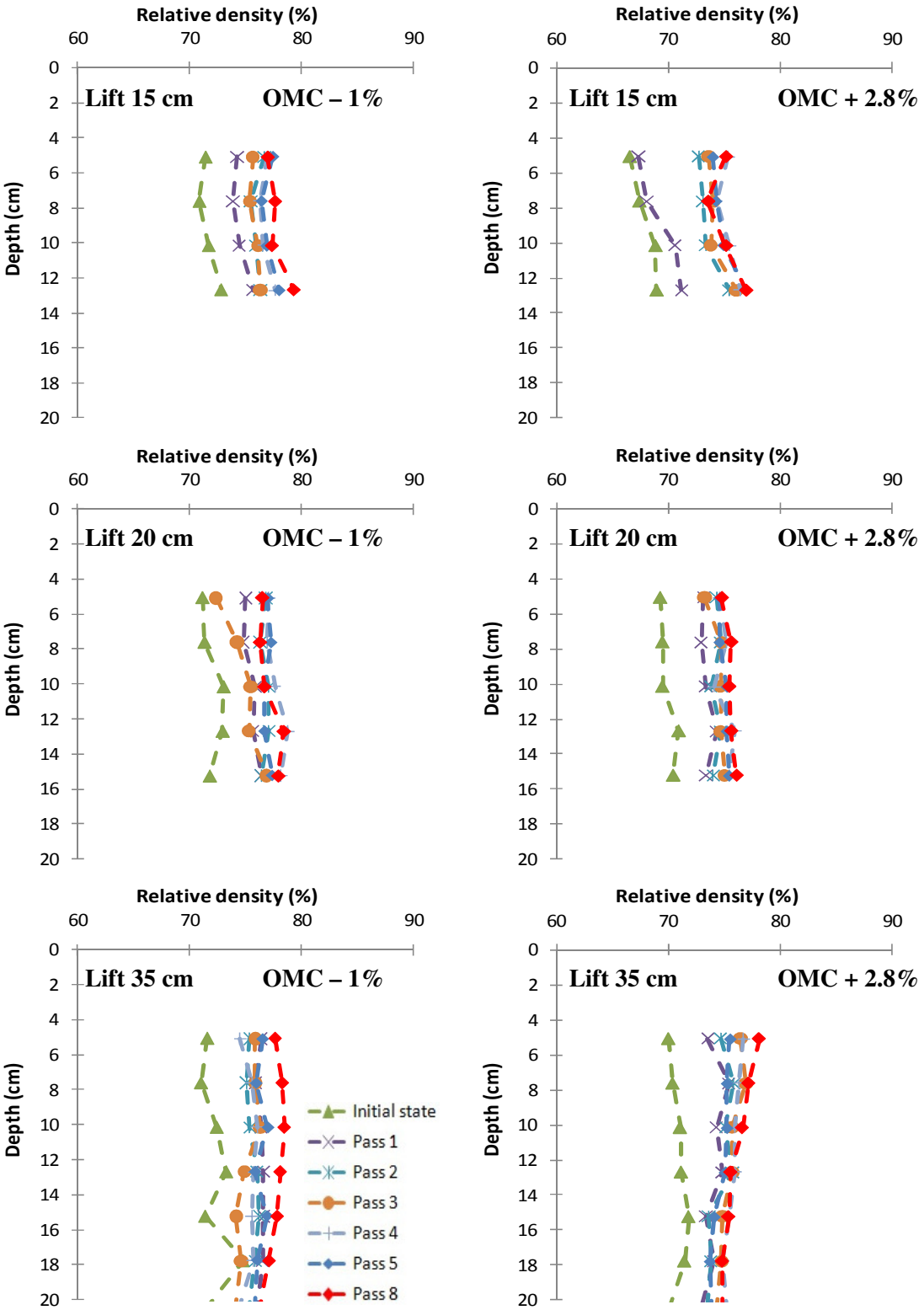

Figure 4.7: Results of soil density profile for the sand compacted in the dry side and wet side of optimum moisture content

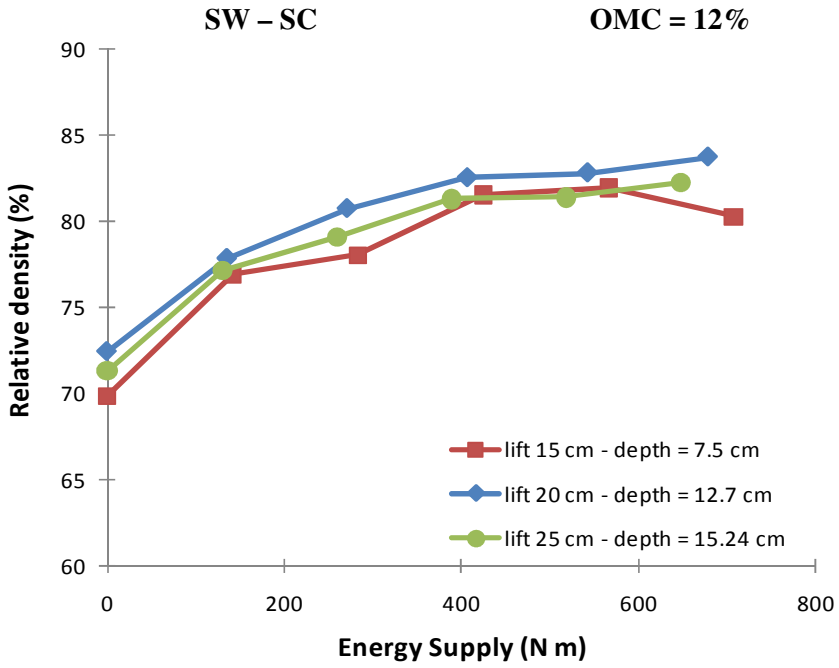

Figure 4.8: Results of sand density at the middle of the layer using pounding as a compaction method

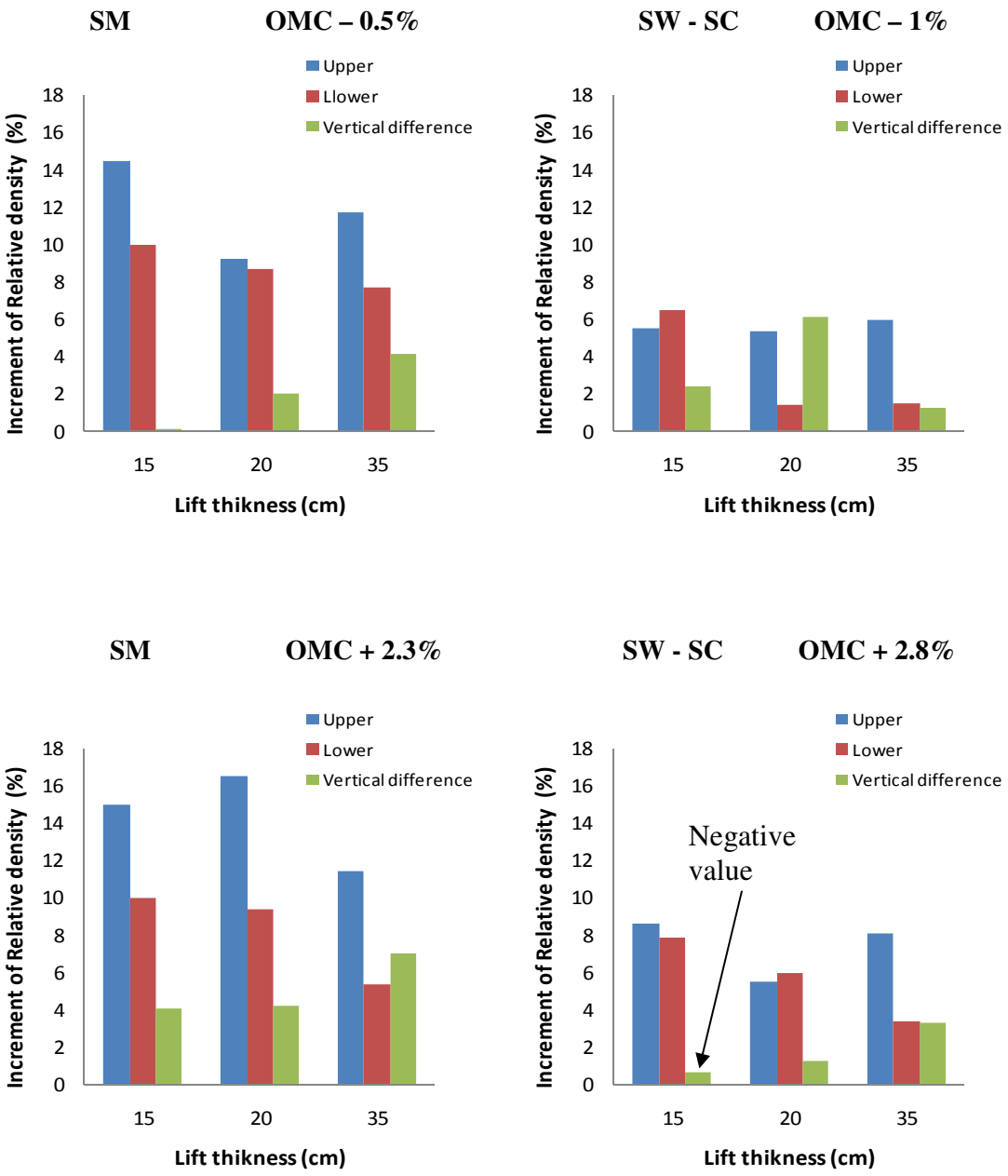

Figure 4.9: Increment in relative density after 8 passes at the upper and lower part of the lift and the vertical difference between the upper and lower relative density

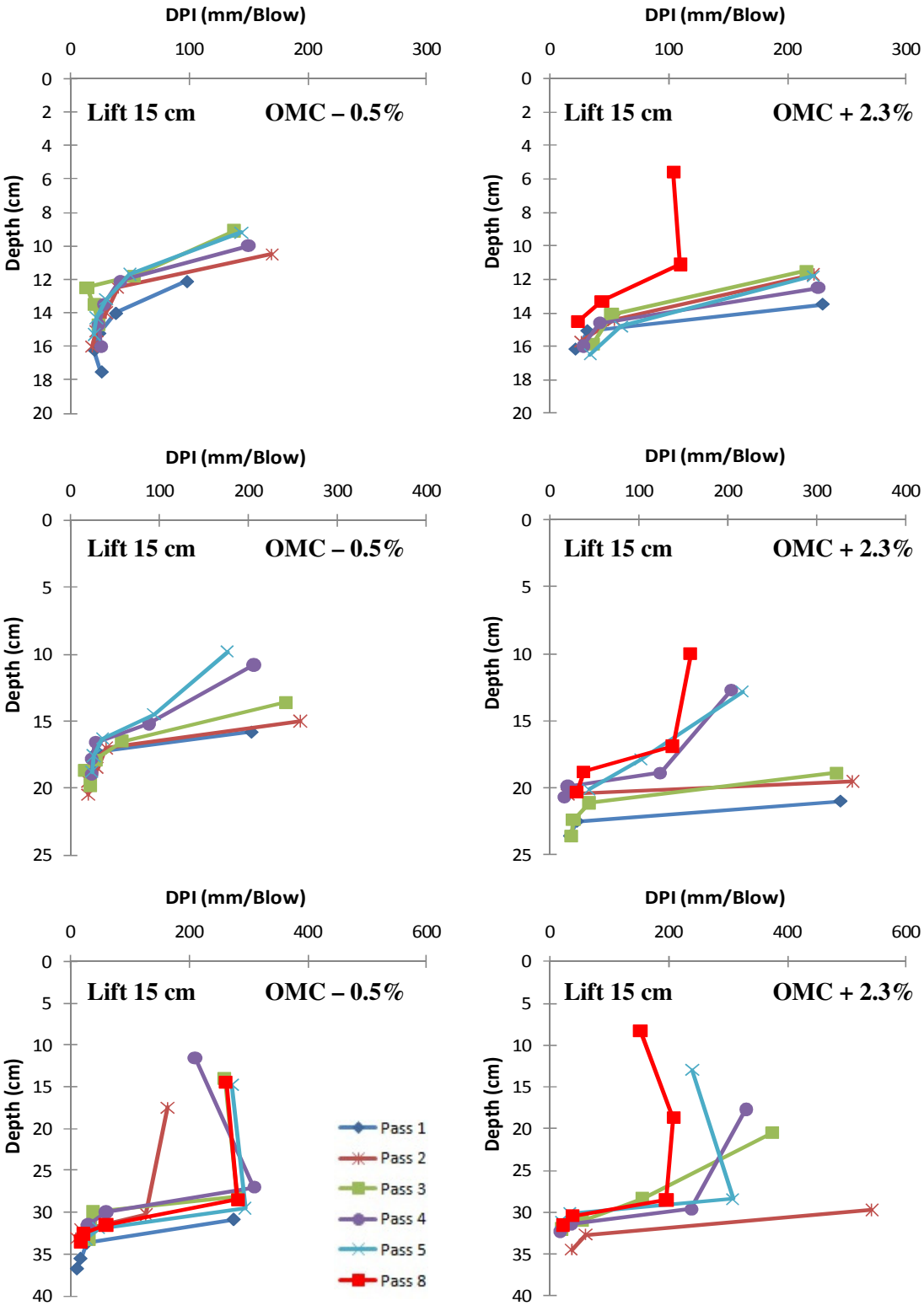

Figure 4.10: Results of DPI profile for the silty sand compacted in the dry side and wet side of optimum

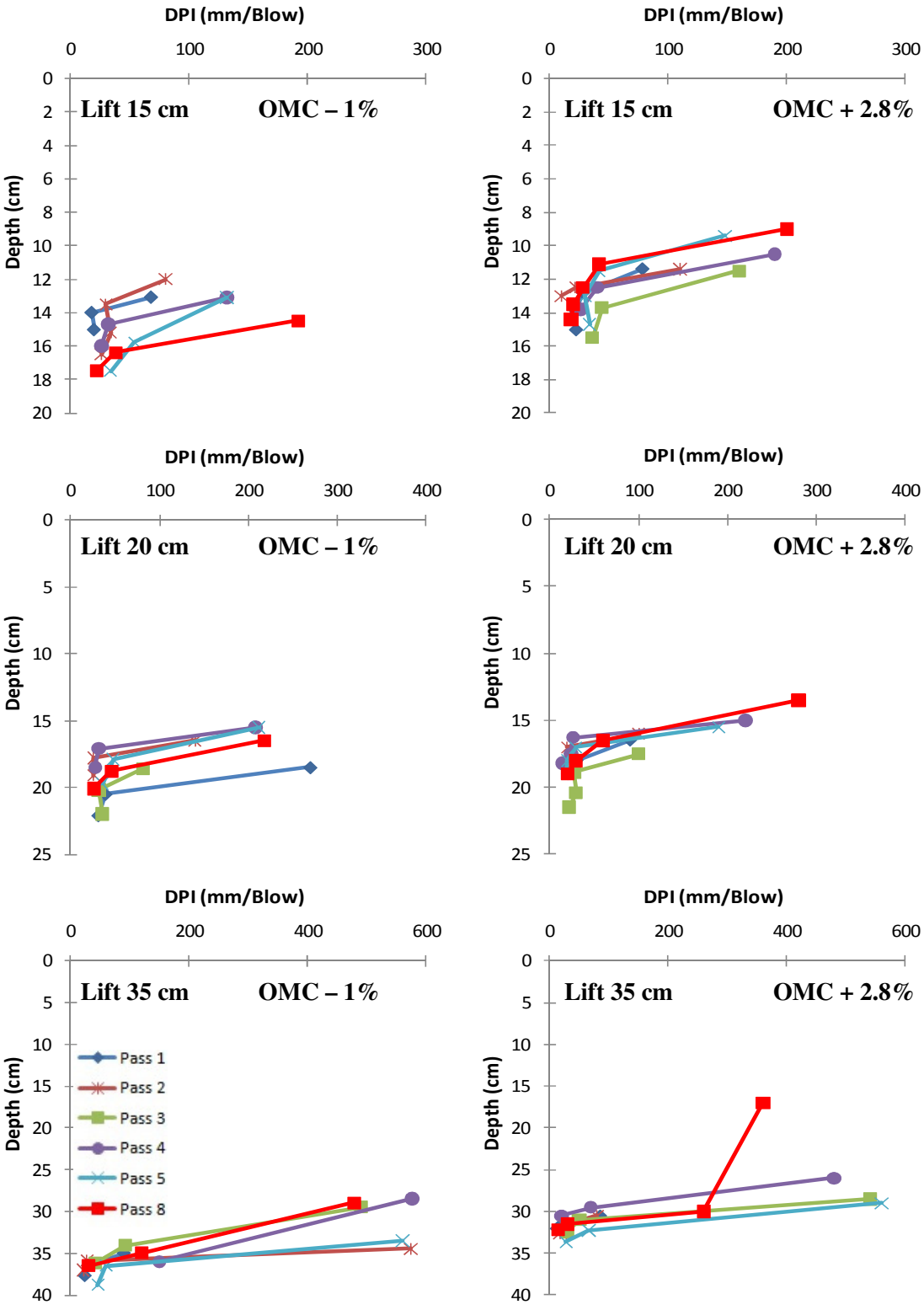

Figure 4.11: Results of DPI profile for the sand compacted in the dry side and wet side of optimum

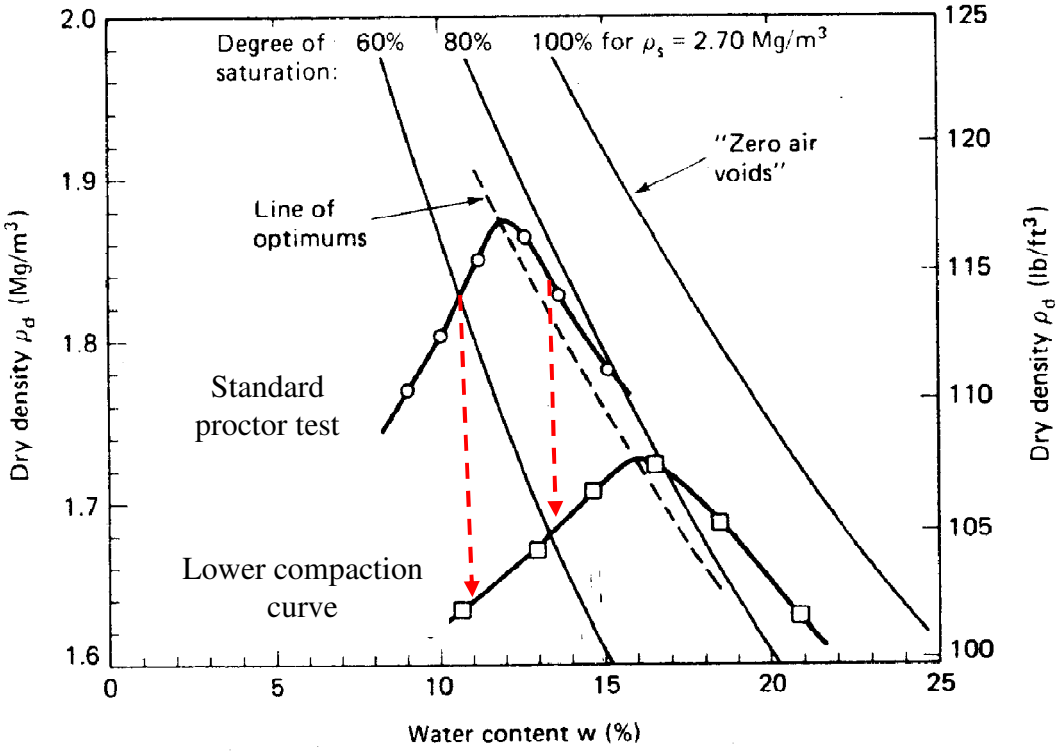

Figure 4.12: Scheme of a theoretical compaction curve obtained with lower energy than the standard proctor test and the theoretical molding water content at the lower energy curve. (modified after Holtz et al. 2010)

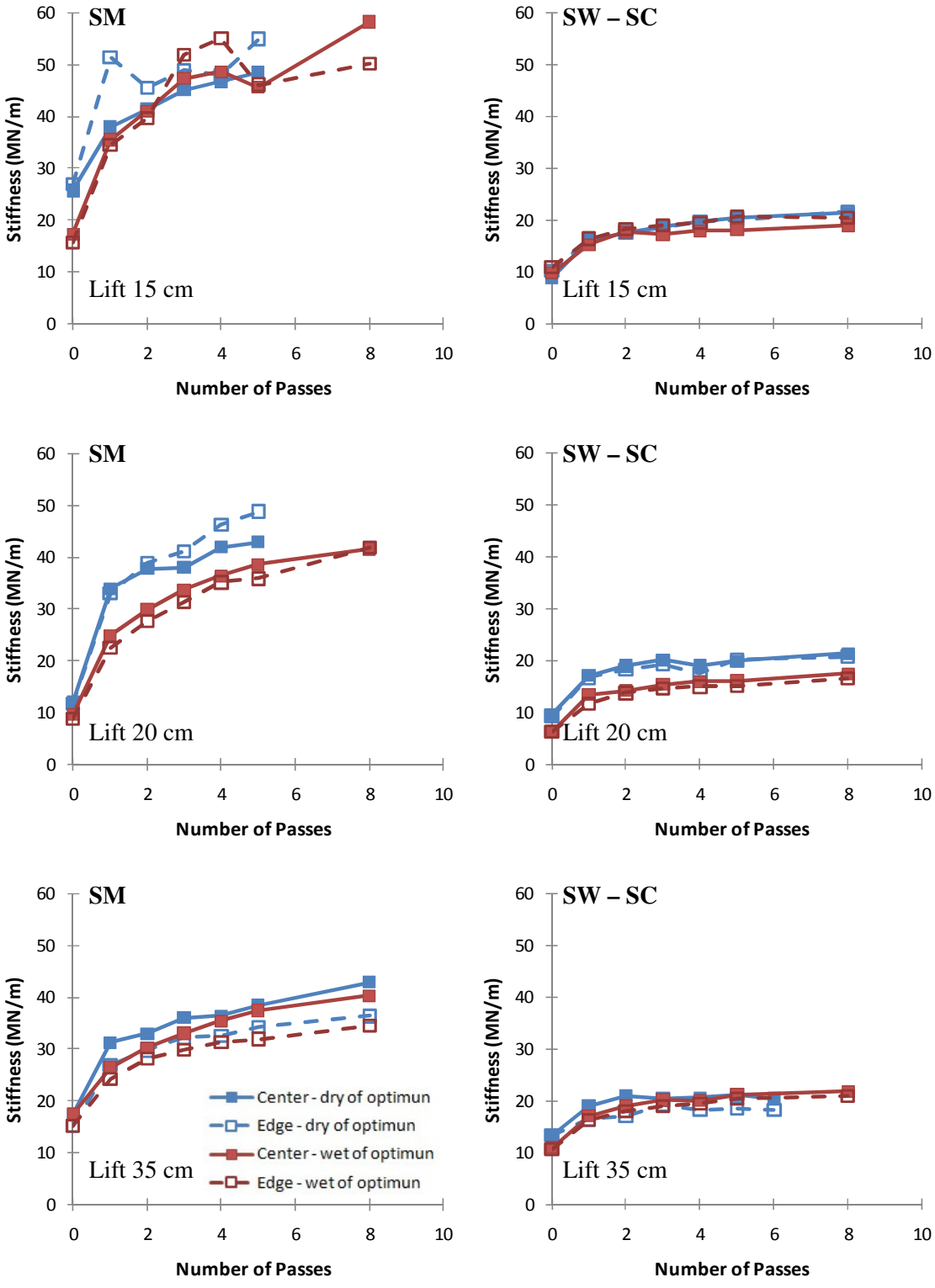

Figure 4.13: Soil surface stiffness as a function of the number of passes at different water content

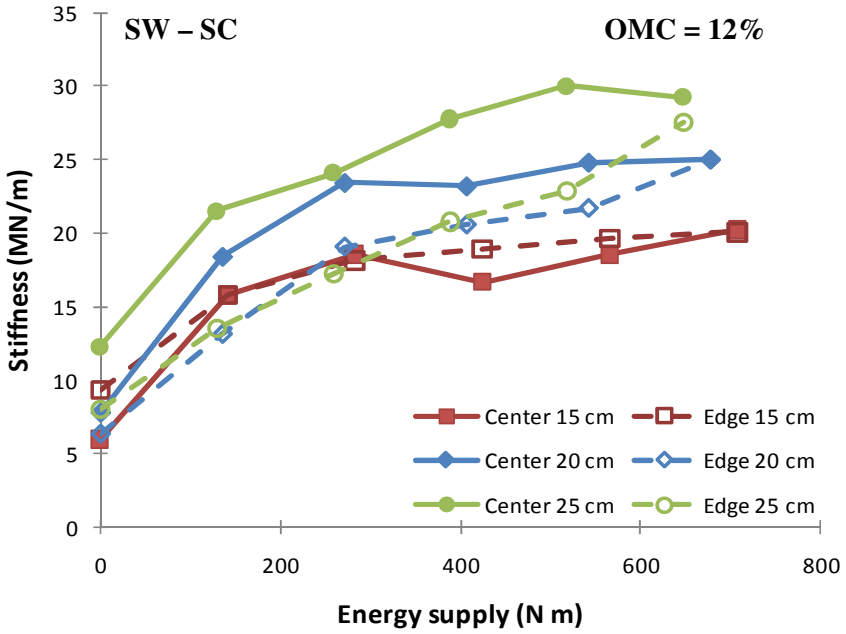

Figure 4.14: Results of soil surface stiffness as a function of energy supply using pounding as a compaction method

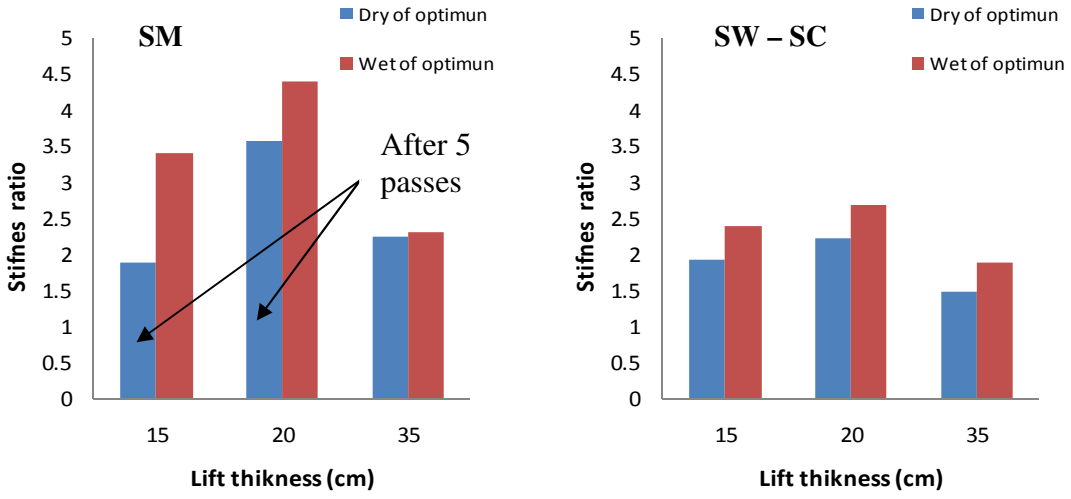

Figure 4.15: Surface stiffness of the soil after compaction (8 passes) divided by the surface stiffness before compaction (0 passes) for different lift thicknesses and soil type

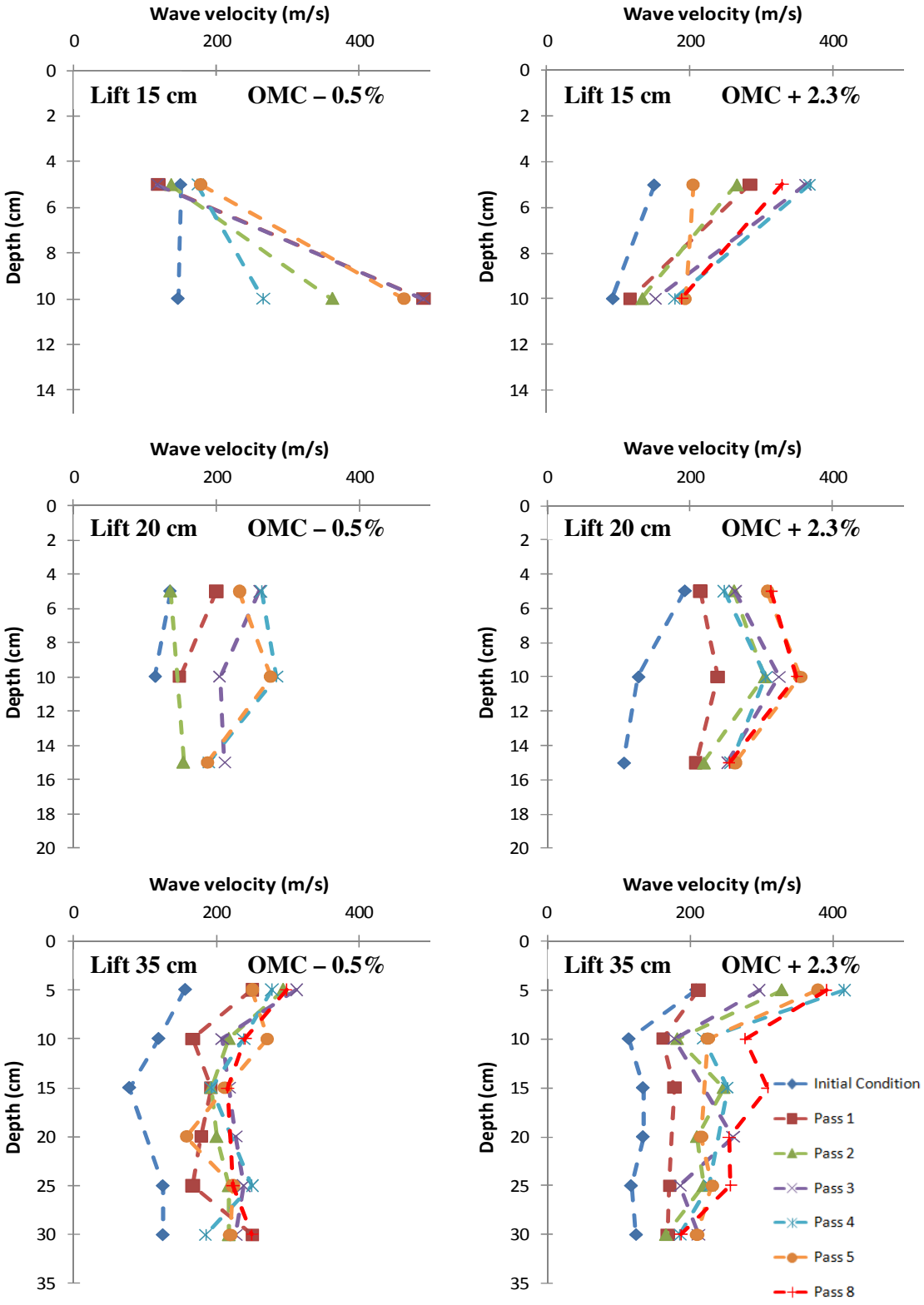

Figure 4.16: Results of soil P-wave velocity profile for the silty sand compacted in the dry side and wet side of optimum

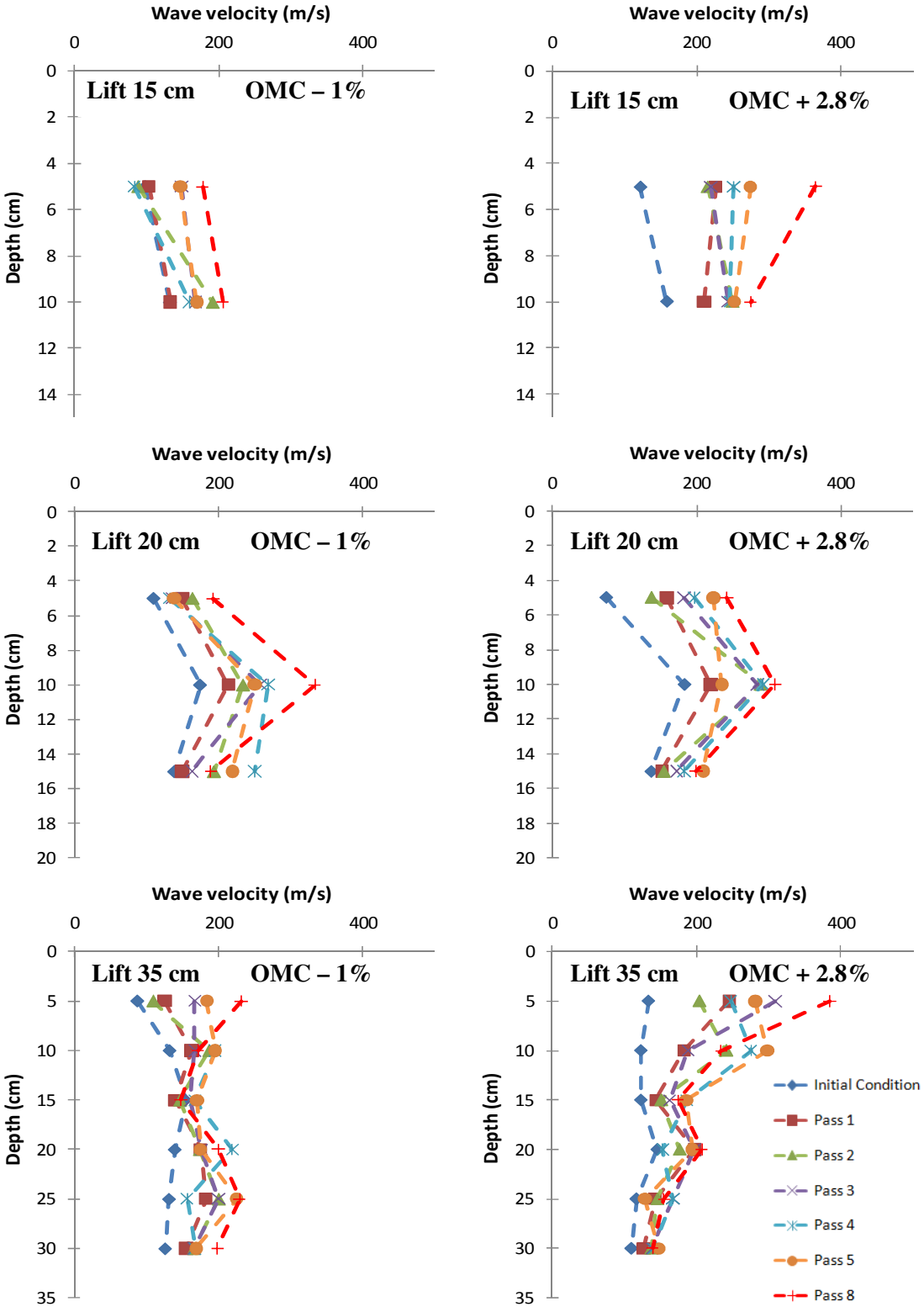

Figure 4.17: P-wave velocity profiles for the sand compacted in the dry side and wet side of optimum

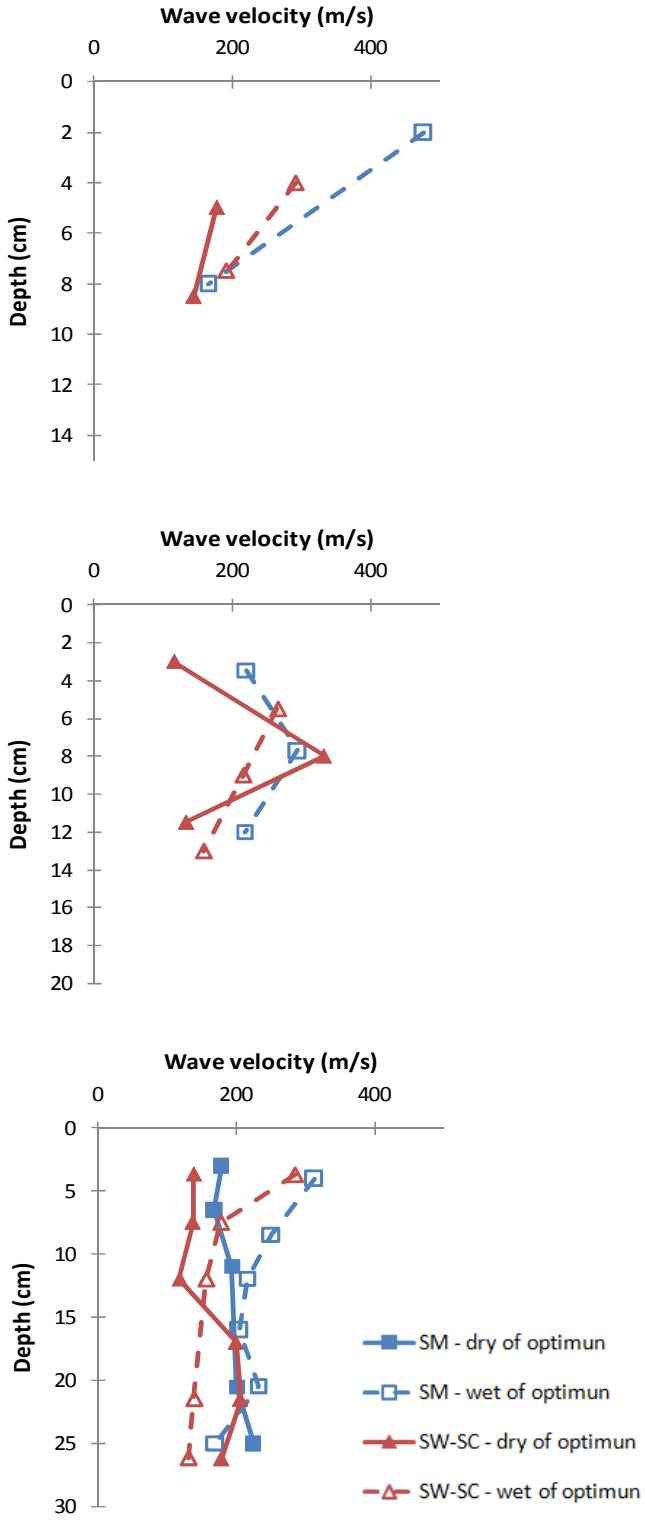

Figure 4.18: Corrected P-wave velocity profiles for lift thickness, soil type and water content after 8 passes of the compactor

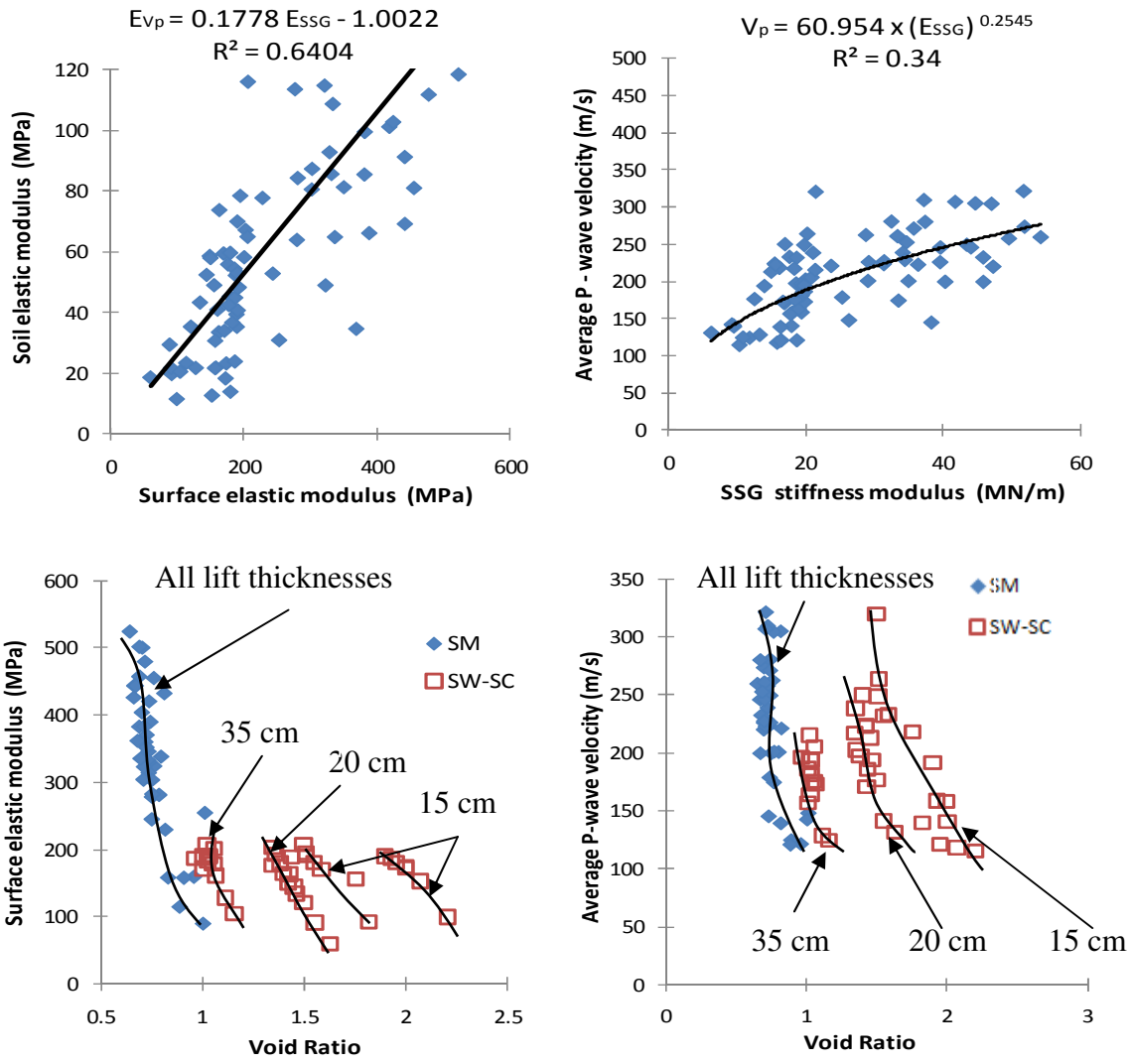

Figure 4.19: Correlations between the P-wave velocity, soil elastic modulus, soil surface stiffness, soil surface modulus and the void ratio

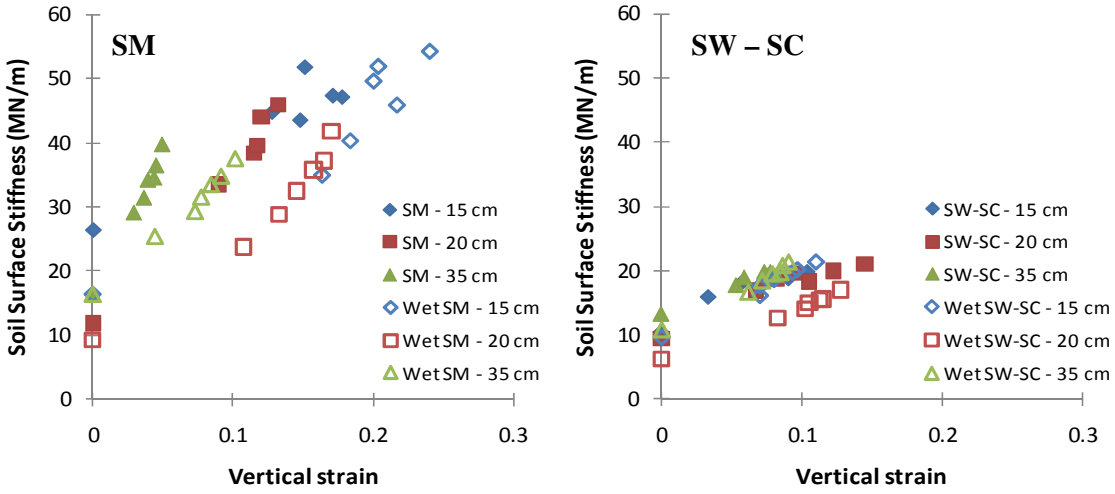

Figure 4.20: Soil surface stiffness as a function of the vertical strain for different soil type and water content.

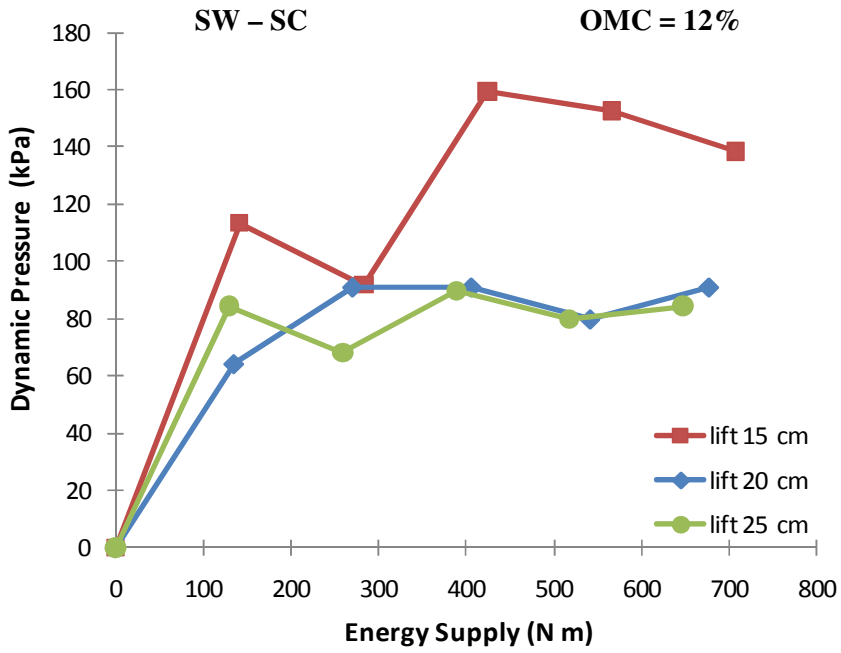

Figure 4.21: Maximum dynamic pressure measured at the bottom of the lift for the sand compacted by pounding

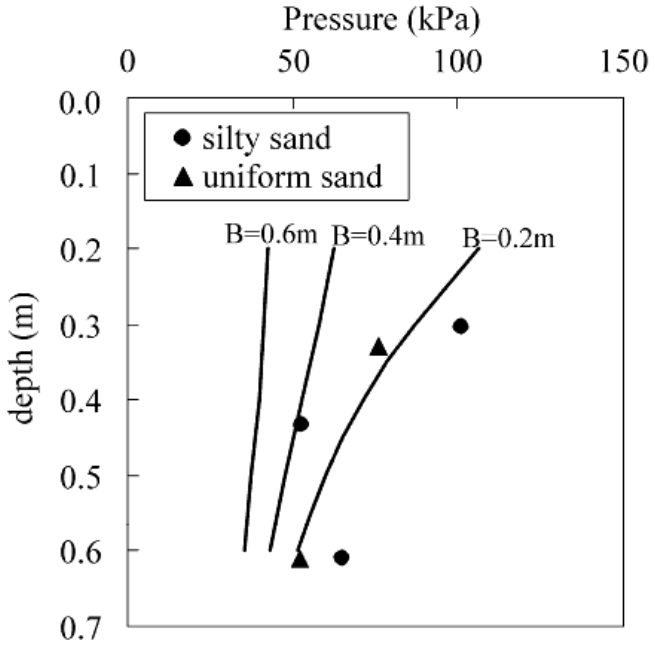

Figure 4.22: Pressure at the bottom of the lift during compaction using a smooth drum vibratory roller (Caterpillar™ Model CS-563E) (Kim et al. 2011)

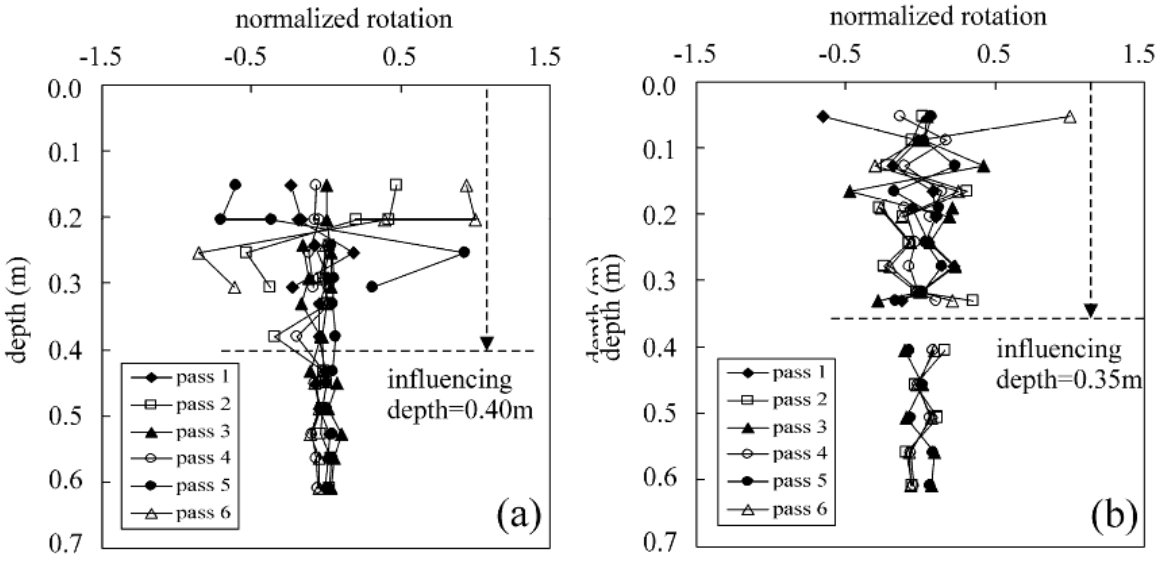

Figure 4.23: MEMS induced rotation normalized during compaction for silty sand (a) and uniform sand (b) using a smooth drum vibratory roller (Caterpillar™ Model CS-563E) (Kim et al. 2011)

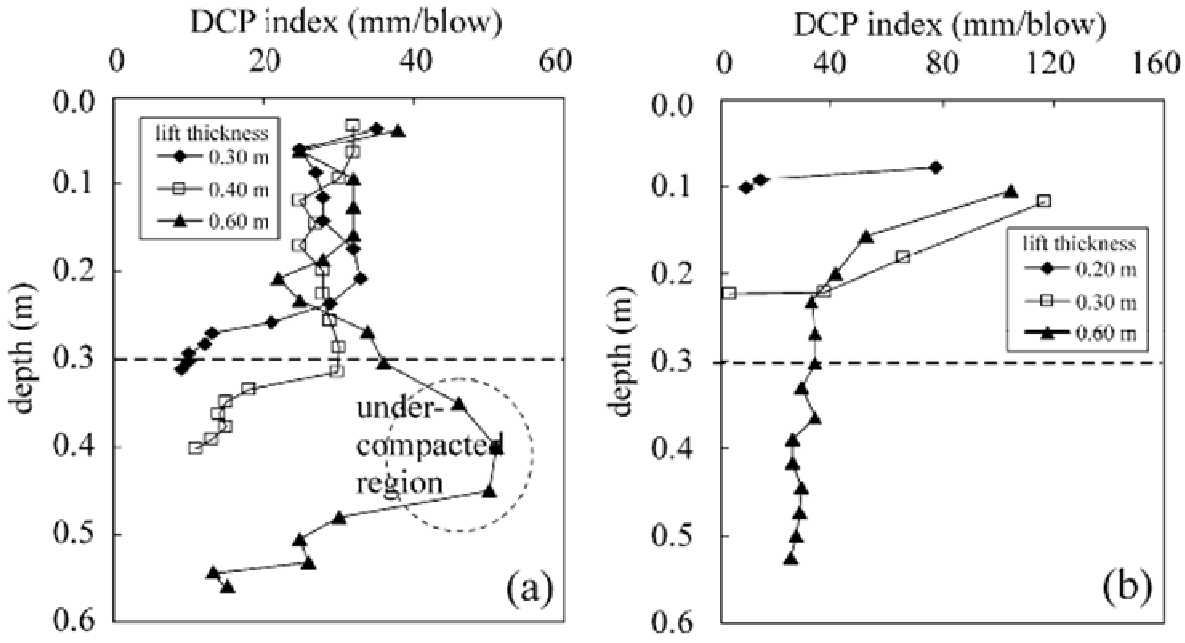

Figure 4.24: Results for the dynamic cone penetrometer in silty sand (a) and uniform sand (b) after compaction using a smooth drum vibratory roller (CaterpillarTM Model CS-563E) (Kim et al. 2011)

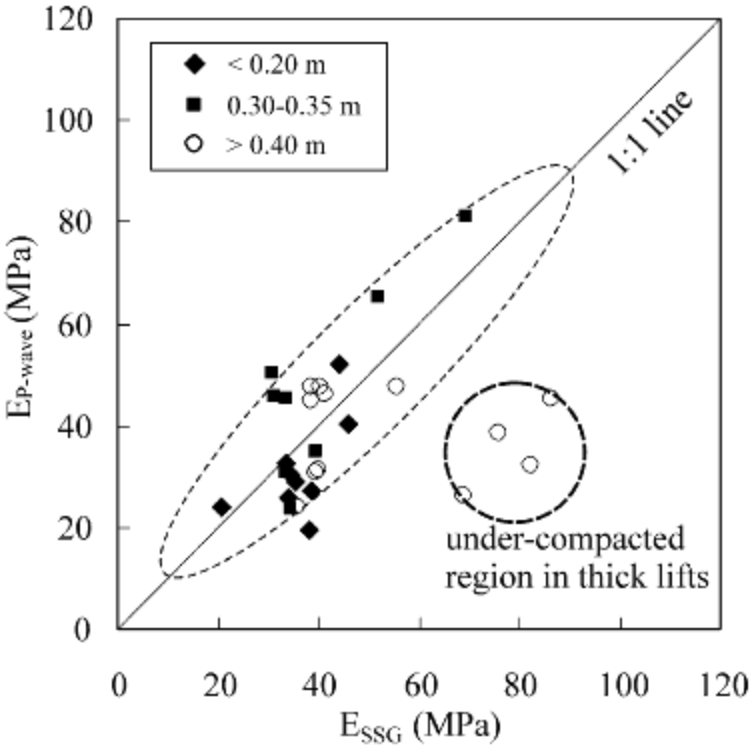

Figure 4.25: Comparison of elastic moduli evaluated by P-wave velocity and SSG (Kim et al. 2011)

5. CONCLUSIONS AND RECOMMENDATIONS

In this research a soil compaction monitoring program at laboratory scale was designed, tested and analyzed to monitor the change of engineering soil properties under a controlled compactive effort. The lift thickness, type of soil, and molding water content were changed to study how these field compaction variables influence the effectiveness and degree of compaction.

The engineering soil properties monitored were soil density, soil stiffness, soil induced rotations, soil shear resistant, and soil vertical displacement. As the degree of compaction and the compactor equipment used in laboratory are different than field condition, the data were compared with a field experiment of compaction monitoring performed using typical compactor equipments and different lift thicknesses.

The results of the soil compaction monitoring at laboratory scale show that:

- When the soil is compacted using thin lift thicknesses, the soil reduces more its void ratio at the same compactive effort than for thick lift thicknesses, although the soil surface displacement and the total reduced volume is larger in thick lifts.
- For tested sandy and silty soils tested, the higher soil displacement within the lift seems to be at the surface of the soil layer and decreases with depth. The data also suggest that the soil displacement seems to be larger in the silty sand than in the sand at the same compactive effort.

- The effective depth of influence for the compactor used at laboratory scale during the first three passes, seems to be about 15 cm for thick lifts (35 cm) while for thin lifts (15 and 20 cm), the depth of influence seems to be slightly larger than 15 cm.
- Due to the different increment in soil density under the same compactive effort and to the difference in final relative density reached by the tested soils, the compaction method using the vibratory plate seems to work better for the silty sand than for the sand. Furthermore pounding as a compaction method in sand yields larger densities than using the vibratory compaction plate.
- When the lift thickness and molding water content are changed, the gradient of the density profile is different. The density profile seems to be more homogeneous when the soil is compacted using a lift thickness of 20 cm and decreases with depth for thick lifts. This difference in the density profile is even larger when the water content increased.
- Regardless of the lift thickness, the bottom part of the lift seems to have lower degree of compaction than the upper part principally by energy losses across the lift and differences in state of effective stress produced by a heterogeneous density profile.
- It appears that the larger shear resistant is produced when the molding water content is closer to the optimum of a lower compaction curve than the standard effort due to the low energy applied to the specimens. Besides thick lifts yield lower shear strength than thin lifts.
- The stiffness ratio between the bottom layer and the layer being tested seems to be larger in the silty sand than in the sand. This explains why the SSG readings increase when the lift decrease for the silty sand while for the sand seems to be more constant.

- Due to the change on the density and thus on the state of effective stress and void ratio across the lift, the P-wave velocity profiles is different for a given soil, water content and lift thickness.
- The P-wave velocity on a soil under compaction increases when the soil gains density and the void ratio decrease. Besides the soil surface stiffness also increases when the void ratio of the soil decreases.
- At a given vertical strain, the silty sand shows higher soil surface stiffness than the sand. Besides the soils show higher soil surface stiffness when the water content is decreased.
- The MEMS-accelerometers induced rotations decreases when the compactive effort and the depth increase. Besides the maximum pressure at the bottom of thick lifts is smaller than thin lifts.
- Despite the difference in scale between the field and laboratory experiment, the bottom part of thick lift (larger then 30 cm), presents regions of undercompaction. This means that the energy of compaction is not the only controlling parameter in the determination of lift thickness but the effect contact area appears to control the results as well.

6. REFERENCES

Abu-Farsakh, M. Y., M. D Nazzal, K. Alshibli, and E. Seyman. (2005). *Application of dynamic cone penetrometer in pavement construction control*. Journal of the Transportation Research Board, No. 1913, 53–61.

Anderegg, R., and K. Kaufmann. (2004). *Intelligent compaction with vibratory rollers*. Transportation Research Record. Transportation Research Board, Washington, D.C. No. 1868, 124–134.

Bowels, J. E. (1979). *Physical and Geotechnical Properties of Soils*, McGraw Hill, 478 pages.

Campbell, G., and K. Bristow. (2002). *Underground power cable installations: Soil thermal resistivity*. Australian Power Transmission and Distribution, Chapel Hill, QLD: PTD Publications, 46-48.

Caterpillar (2011). Company Web Site; URL: http://www.cat.com (Accessed on august 16, 2011).

Cui, X. (2010). *Real-time diagnosis method of compaction state of subgrade during dynamic compaction*. Geotechnical Testing Journal. Vol. 33, No. 4. 5 pages

Daniel, D. and C. H. Benson. (1990). Water content-density criteria for compacted soil liners. Journal of Geotechnical Engineering. Vol. 116, No.12, 1811-1830.

D'Appolonia, D. J., R. V. Whitman, and E. D. D'Appolonia. (1969). *Sand compaction with vibratory compaction equipment*. Journal of the Soil Mechanics and Foundations Division, Vol. 95, No. SMl, 263-284.

Edil, T. B., and A. Sawangsuriya. (2006). *Use of stiffness and strength for earthwork quality evaluation*. ASCE Geotechnical Special Publication (GSP): Site and Geomaterial Characterization, GeoShanghai Conference 2006, Shanghai, China.

Fratta, D., K. Alshibli, W. M. Tanner, and L. Roussel. (2005). *Combined TDR and P-wave velocity measurements for the determination of in situ soil density-experimental study*. Geotechnical Testing Journal. Vol. 28, No. 6, 553-563.

Fredlund, D.G., and H. Rahardjo. (1993). *Soil mechanics for unsaturated soils.* Willey inter-science. 517 pages.

Gas Technology Institute. (2005). *Evaluation of Soil Compaction Measuring Devices*. Final Report GRI-04/0067. 1700 South Mount Prospect Road. Des Plaines, IL 60018. 132 pages.

Hoffman, K., R. Varuso, and D. Fratta. (2006). *The use of low-cost MEMS accelerometers for the near-surface monitoring of geotechnical engineering systems*. Paper presented at GeoCongress 2006, February 26 - March 1.

Holtz, R. D. (1990). State of the Art Report 8: Guide to Earthwork Construction. Transportation Research Board. National Research Council. Washington DC. 107 pages.

Holtz, R. D., W. D. Kovacs, and T. C. Sheahan. (2010). *An introduction to geotechnical engineering*. Prentice Hall, 853 pages.

Hoppe, E.J. (1999). *Guidelines for the Use, Design, and Construction of Bridge Approach Slabs*. Report VTRC 00-R4, Virginia Transportation Research Council, Charlottesville, VA. 39 pages.

Humboldt Mfg. Co. (1999). *User Guide – Model H-4140 Soil Stiffness / Modulus Gauge*. 7300 West Agatite Avenue. Norridge, Il 60706. USA. 21 pages.

Kim, K., D. Fratta, H. Wen. (2011). *Field Measurements of Compaction Energy in Thick Lifts of Coarse - Grained Soils*. Paper submitted to the Journal of the Transportation Research Board.

Lambe, T. W. and R. V. Whitman. (1969). *Soil mechanics*, John Wiley & Sons. 553 pages.

Lenke, L. R., R. G. McKeen, and M. P. Grush. (2003). *Laboratory evaluation of GeoGauge for compaction control.* Transportation Research Record, No. 1849, 20-30.

Mayne, P. W., J. S. Jones Jr., and J. C. Dumas. (1984). *Ground response to dynamic compaction*. Journal of Geotechnical Engineering. Vol. 110, No. 6, 757-774.

McCarthy, D. F. (2002). *Essentials of soil mechanics and foundations*. Prentice Hall. 788 pages.

Mitchell, J. K., and K. Soga. (2005). *Fundamentals of soil behavior*. John Wiley & Sons. 588 pages.

Mooney, M. A., and R. V. Rinehart. (2007). *Field Monitoring of Roller Vibration during Compaction of Subgrade Soil.* Journal of Geotechnical and Geoenvironmental Engineering. Vol. 133, No. 3, 257-265.

Mooney, M. A., and R. V. Rinehart. (2009). *In situ soil response to vibratory loading and its relationship to roller-measured soil stiffness*. Journal of Geotechnical and Geoenvironmental Engineering. Vol.135, No.8, 1022-31.

Olson, R. E. (1963). *Effective stress theory of soil compaction*. Journal of the Soil Mechanics and Foundations Division. Vol. 89, No.SM2, 27-45.

Richart, F. E., J. R. Hall, and R. D. Woods. (1970). *Vibrations of soils and foundations*. Newmark, N. M., W. J. Hall. 414 pages.

Proctor, R. R. (1933). *Fundamentals principles of soil compaction.* Engineering news-record. Vol. 111, No. 9, 245-248.

Rahman, F., M. M. M. Hossain, M. M. Hunt, and S. A. Romanoschi. (2008). *Soil stiffness evaluation for compaction control of cohesionless embankments*. Geotechnical Testing Journal. Vol. 31, No. 5, 442-451.

Rinehart, R. V., and M. A. Mooney. (2009). *Measurement depth of vibratory roller-measured soil stiffness*. Geotechnique. Vol. 59, No.7, 609-619.

Rollings, M. P., and R. R. Rollings. (1996). *Geotechnical materials in construction*. McGraw-Hill, 525 pages.

Santamarina, J. C. (2001). *Soils and waves particulate materials behavior, characterization and process monitoring*. Wiley, 488 pages.

Sawangsuriya, A., P. J. Bosscher, and T. B. Edil. (2002). *Laboratory evaluation of the soil stiffness gauge.* Transportation Research Record. No. 1808, 30-37.

Sawangsuriya, A., T. B. Edil, and P. J. Bosscher. (2003). *Relationship between soil stiffness gauge modulus and other test moduli for granular soils*. Transportation Research Record. No. 1849, 3-10.

Sawangsuriya, A., and T. B. Edil. (2005). *Evaluating stiffness and strength of pavement materials*. Proceedings of the Institution of Civil Engineers: Geotechnical Engineering. Vol. 158, No. 4, 217-230.

Sawangsuriya, A., and D. Fratta. (2006). *Discussion of "correlations between P-wave velocity and Atterberg limits of cohesive soils*. Canadian Geotechnical Journal Vol. 43, No. 6, 653-655.

Schuettpelz, C. C., D. Fratta, and T. B. Edil. (2009). *Evaluation of the Influence of Geogrid Reinforcement on soil Rotation and Stiffness in Compacted Based Curse Soil*. Transportation Research Record. No. 2116, 76 - 84.

Schuettpelz, C. C., D. Fratta, and T. B. Edil. (2009). *Mechanistic method for determining the resilient modulus of base course materials based on elastic wave measurements*. Journal of Geotechnical and Geoenvironmental Engineering. Vol. 136, No. 8, 1086 - 1094.

Seed, H. B., and C. K. Chan. (1959). *Structure and strength characteristics of compacted clays*. Journal of Soil Mechanics and Foundation Division. Vol. 85, No.SM5, 87-128.

Sleeman, R., and T. van Eck. (1999). *Robust automatic P-phase picking: an on-line implementation in the analysis of broadband seismogram recordings*, Phys. Earth Planet. Interiors No. 113, 265-275.

Sellers, J. B., and R. Taylor. (2008). *MEMS basics.* Geotechnical News. Vol. 26, No. 1, 32-33.

Srinivasan, S., A. J. Muck, and P. W. Chou. (2010). *Real-time slope and wall monitoring and reporting using 3-D MEMS-based, in-place instrumentation system*. Paper presented at GeoFlorida 2010: Advances in Analysis, Modeling and Design Conference, February 20- February 24.

Terra System Incorporated .(2011). Company Web Site; URL: http://www.terrasystemsonline.com (Accessed on august 16, 2011).

Tinjum, J. M., C. H. Benson, and L. R. Blotz. (1997*). Soil-water characteristic curves for compacted clays.* Journal of Geotechnical and Geoenvironmental Engineering. Vol. 123, No. 11, 1060-1069.

Turnbull, W. J., and C. R. Foster. (1956). *Stabilization of materials by compaction*. Journal of the Soil Mechanics and Foundations Division. Vol. 82, No. SM, 934-1-934-23.

Wang, Y. H., C. H. Ma, and W. M. Yan. (2009). *Characterizing bond breakages in cemented sands using a MEMS accelerometer*. Geotechnical Testing Journal. Vol. 32, No. 2, 186-195.

Wen, H., W. Martono, T. Edil, T. R. Clyne, and R. Patton. (2010). *Field evaluation of recycled pavement materials at MnROAD*. GeoShanghai International Conference 2010- Paving Materials and Pavement Analysis, June 3 - June 5.

Winter M.G. and B. G. Clarke. (2002). *Methods for determining representative density-depth profiles using nuclear density gauges.* Geotechnique. Vol. 52, No.7, 519-525.

Yoo, T.-S., and E. T. Selig. (1979). *Dynamic of vibratory-roller compaction*. *Journal of the Geotechnical Engineering Division*. Vol. 105, No. GT10, 1211-1231.

Zhang, H., C. Thurber, and C. Rowe. (2003). *Automatic P-wave arrival detection and picking with multiscale wavelet analysis for single-component recordings*. Bulletin of the Seismological Society of America. Vol. 93, No.5 - 10, 1904-1912.

Zou, W., Z. Wang, and Z. Yao. (2005). *Effect of dynamic compaction on placement of high-road embankment*. Journal of Performance of Constructed Facilities. Vol. 19, No. 4, 316-323.

Appendix 1: Laboratory data reduction

Lift thickness - 15 cm

Soil type USCS	Lifts thickness (cm)	Specific gravity	Moister content (%)	SSG stiffness (MN/m)	SSG elastic muduli (MPa)	Average P-wave velocity (m/s)	Elastic Moduli from P-wave (MPa)
SM	**15**	**2.72**	**10**	26.30	253.88	147.95	30.83
				44.69	431.43	304.38	144.77
				43.45	419.51	249.09	101.08
				47.04	454.17	303.78	148.39
				47.28	456.44	219.78	80.91
				51.72	499.30	320.77	170.91
SM	**15**	**2.72**	**12.5**	16.45	158.82	121.26	21.76
				34.96	337.49	200.46	64.78
				40.30	389.09	199.47	66.06
				49.57	478.54	257.38	111.67
				51.85	500.61	273.11	127.74
				45.86	442.77	199.36	69.10
				54.20	523.25	259.17	118.33
SW-SC	**15**	**2.61**	**12.09**	10.36	99.98	114.98	11.44
				15.83	152.84	118.14	12.59
				17.95	173.26	140.40	18.21
				18.06	174.37	158.30	23.16
				18.72	180.69	121.28	13.81
				19.41	187.35	158.56	23.79
				19.72	190.35	191.85	35.21
SW-SC	**15**	**2.61**	**14.5**	9.56	92.25	139.79	19.62
				16.17	156.12	218.16	48.92
				17.65	170.41	232.76	59.35
				18.68	180.35	231.60	59.55
				19.79	191.02	248.78	69.87
				20.24	195.37	263.63	78.35
				21.45	207.10	319.84	115.92

Soil type USCS	Lifts thickness (cm)	Specific gravity	Moister content (%)	Relative Density (%)	Dry Density (Kg/m^3)	Soil Density (kg/m^3)	Void ratio
SM	**15**	**2.72**	**10**	67.25	1351.92	1487.11	1.01
				74.62	1499.93	1649.92	0.81
				77.79	1563.76	1720.13	0.74
				76.78	1543.49	1697.84	0.76
				79.99	1607.89	1768.68	0.69
				79.32	1594.43	1753.87	0.71
SM	**15**	**2.72**	**12.5**	69.11	1389.16	1562.81	0.96
				75.27	1513.06	1702.19	0.80
				77.52	1558.23	1753.01	0.75
				78.71	1582.26	1780.04	0.72
				79.96	1607.41	1808.33	0.69
				81.18	1631.83	1835.81	0.67
				82.25	1653.46	1860.14	0.65
SW-SC	**15**	**2.61**	**12.09**	47.81	814.78	913.29	2.20
				49.88	849.93	952.68	2.07
				51.08	870.39	975.61	2.00
				51.09	870.56	975.81	2.00
				51.91	884.61	991.56	1.95
				52.30	891.19	998.93	1.93
				52.89	901.23	1010.19	1.90
SW-SC	**15**	**2.61**	**14.5**	54.33	925.84	1060.09	1.82
				55.62	947.83	1085.26	1.75
				59.28	1010.18	1156.66	1.58
				60.08	1023.84	1172.30	1.55
				61.09	1041.03	1191.98	1.51
				61.01	1039.63	1190.38	1.51
				61.32	1044.96	1196.48	1.50

Lift thickness - 20 cm

Soil type USCS	Lifts thickness (cm)	Specific gravity	Moister content (%)	SSG stiffness (MN/m)	SSG elastic muduli (MPa)	Average P-wave velocity (m/s)	Elastic Moduli from P-wave (MPa)
SM	**20**	**2.72**	**10**	11.84	114.27	124.65	23.31
				33.51	323.49	174.40	48.87
				38.29	369.69	145.10	34.54
				39.56	381.90	225.73	85.38
				44.05	425.25	245.55	102.64
				45.84	442.53	232.02	91.12
SM	**20**	**2.72**	**12.5**	9.25	89.26	142.38	29.33
				23.71	228.92	220.72	77.65
				28.76	277.67	261.99	113.43
				32.47	313.49	280.12	130.89
				35.74	345.02	270.67	122.28
				37.21	359.26	308.80	160.59
				41.75	403.09	306.41	159.66
SW-SC	**20**	**2.61**	**12.09**	9.47	91.38	141.28	21.68
				16.92	163.31	171.03	33.40
				18.62	179.73	197.31	45.27
				19.63	189.48	185.91	39.32
				18.34	177.07	217.03	55.75
				19.97	192.81	202.47	48.21
				21.06	203.33	238.35	67.12
SW-SC	**20**	**2.61**	**14.5**	6.26	60.44	131.17	18.52
				12.56	121.27	176.35	35.24
				13.98	134.98	193.85	43.20
				14.99	144.73	212.80	52.33
				15.49	149.55	223.91	58.56
				15.61	150.71	222.39	57.86
				16.98	163.94	249.80	73.66

Soil type USCS	Lifts thickness (cm)	Specific gravity	Moister content (%)	Relative Density (%)	Dry Density (Kg/m^3)	Soil Density (kg/m^3)	Void ratio
SM	**20**	**2.72**	**10**	71.65	1440.34	1584.37	0.89
				76.72	1542.27	1696.49	0.76
				78.36	1575.10	1732.61	0.73
				80.02	1608.47	1769.32	0.69
				81.29	1634.10	1797.51	0.66
				80.83	1624.76	1787.24	0.67
SM	**20**	**2.72**	**12.5**	67.56	1358.01	1527.76	1.00
				74.42	1496.08	1683.09	0.82
				77.17	1551.18	1745.08	0.75
				77.88	1565.60	1761.30	0.74
				77.93	1566.56	1762.38	0.74
				78.63	1580.58	1778.15	0.72
				79.40	1596.19	1795.72	0.70
SW-SC	**20**	**2.61**	**12.09**	60.05	1023.28	1147.00	1.55
				63.13	1075.78	1205.84	1.43
				64.28	1095.44	1227.88	1.38
				62.88	1071.58	1201.14	1.44
				65.43	1115.00	1249.80	1.34
				65.00	1107.70	1241.62	1.36
				65.31	1112.94	1247.49	1.35
SW-SC	**20**	**2.61**	**14.5**	58.25	992.58	1136.51	1.63
				61.33	1045.08	1196.61	1.50
				62.22	1060.20	1213.93	1.46
				62.54	1065.71	1220.24	1.45
				63.21	1077.09	1233.27	1.42
				63.31	1078.86	1235.30	1.42
				63.88	1088.65	1246.50	1.40

Lift thickness - 35 cm

Soil type USCS	Lifts thickness (cm)	Specific gravity	Moister content (%)	SSG stiffness (MN/m)	SSG elastic muduli (MPa)	Average P-wave velocity (m/s)	Elastic Moduli from P-wave (MPa)
SM	**35**	**2.72**	**10**	16.31	157.47	120.68	21.61
				29.06	280.57	200.70	63.83
				31.36	302.78	223.10	80.47
				34.13	329.47	238.48	92.70
				34.44	332.47	228.67	85.51
				36.36	351.00	222.39	81.20
				39.61	382.43	245.35	99.39
SM	**35**	**2.72**	**12.5**	16.34	157.76	139.13	30.62
				25.31	244.32	178.59	52.74
				29.18	281.68	225.83	84.20
				31.41	303.26	227.01	87.23
				33.37	322.14	260.47	114.66
				34.65	334.54	252.22	108.60
				37.38	360.90	279.64	134.64
SW-SC	**35**	**2.61**	**12.09**	13.31	128.46	128.59	21.67
				17.78	171.62	156.60	33.89
				19.00	183.44	163.52	36.60
				19.86	191.70	172.71	40.63
				19.43	187.59	181.06	44.79
				19.86	191.75	186.36	47.98
				19.36	186.92	196.40	54.36
SW-SC	**35**	**2.61**	**14.5**	10.88	105.00	124.81	20.44
				16.70	161.24	172.74	40.87
				18.49	178.47	175.38	42.39
				19.56	188.80	193.43	52.10
				19.78	190.93	194.60	52.91
				20.85	201.30	205.46	58.12
				21.40	206.61	215.28	64.86

Soil type USCS	Lifts thickness (cm)	Specific gravity	Moister content (%)	Relative Density (%)	Dry Density (Kg/m^3)	Soil density (kg/m^3)	Void ratio
SM	**35**	**2.72**	**10**	70.87	1424.53	1566.99	0.91
				75.67	1521.18	1673.29	0.79
				77.20	1551.88	1707.06	0.75
				77.84	1564.69	1721.16	0.74
				78.09	1569.76	1726.74	0.73
				78.40	1575.90	1733.49	0.73
				78.85	1584.98	1743.48	0.72
SM	**35**	**2.72**	**12.5**	73.85	1484.60	1670.18	0.83
				77.21	1552.14	1746.16	0.75
				77.08	1549.47	1743.16	0.76
				79.03	1588.72	1787.31	0.71
				78.91	1586.32	1784.61	0.71
				79.71	1602.33	1802.63	0.70
				80.39	1615.95	1817.94	0.68
SW-SC	**35**	**2.61**	**12.09**	72.46	1234.72	1384.00	1.11
				76.40	1302.00	1459.41	1.00
				75.67	1289.45	1445.34	1.02
				75.29	1283.04	1438.16	1.03
				75.53	1287.05	1442.65	1.03
				76.37	1301.46	1458.81	1.01
				77.91	1327.63	1488.14	0.97
SW-SC	**35**	**2.61**	**14.5**	71.00	1209.89	1385.33	1.16
				74.13	1263.29	1446.46	1.07
				74.59	1271.03	1455.33	1.05
				75.35	1284.11	1470.31	1.03
				75.61	1288.38	1475.20	1.03
				74.51	1269.69	1453.80	1.06
				75.73	1290.52	1477.64	1.02

Appendix 2: Sample data form

Soil compaction test worksheet

Preliminary information	
Date	
Lift thickness (cm)	
Energy	
Soil Name	
Number of MEMS	
Separation MEMS (cm)	

Water content control

	Before Test	After Test
Water Content (%)		

Soil surface stiffness and soil surface displacement

	Stiffness (MN/m)		Displacement (cm)	
Passes	**Center**	**Edge**	**Center**	**Edge**
0				
1				
2				
3				
4				
5				
8				

Soil density profile (NDG)

NDG	Dry Density (kN/m^3)						
Depth (cm)	0	1	2	3	4	5	8
5.08							
7.62							
10.16							
12.7							
15.24							
17.78							
20.32							

Soil water content (NDG)

NDG	Water content (%)						
Depth (cm)	0	1	2	3	4	5	8
5.08							
7.62							
10.16							
12.7							
15.24							
17.78							
20.32							

Dynamic cone penetrometer test

DCP							
Pass 1		Pass 2		Pass 3		Pass 4	
Blows	**Pen (cm)**	Blows	**Pen (cm)**	Blows	**Pen (cm)**	Blows	**Pen (cm)**
0		0		0		0	
1		1		1		1	
2		2		2		2	
3		3		3		3	
4		4		4		4	
5		5		5		5	
6		6		6		6	
7		7		7		7	

Pass 5		Pass 6	
Blows	**Pen (cm)**	Blows	**Pen (cm)**
0		0	
1		1	
2		2	
3		3	
4		4	
5		5	
6		6	
7		7	

Appendix 3: Matlab codes

ACI pickers P-wave velocity detection

```
clear
format long

 % Enter MEMS number and number of passes of the compactor of each mems,
sensitivity mems
 numsig= 3; %Number of accelerometers
 Npass=6; %Number of compactor passes

 % Import data from the Excel file
fileimport='PWVelocity.xls';

 % Save data to
filesave='PWVelocity.xls';
sheet='PWV-15 cm';

for Nn=1:Npass

if Nn==1

    N='pass0';
    R3='C3';

end

if Nn==2

    N='pass1';
    R3='D3';

end

if Nn==3

    N='pass2';
    R3='E3';

end

if Nn==4

    N='pass3';
    R3='F3';

end
```

```
if Nn==5

    N='pass4';
    R3='G3';

end

if Nn==6

    N='pass5';
    R3='H3';

end

if Nn==7

    N='pass6';
    R3='I3';

end

data=xlsread(fileimport,N,'B3:K10002');

for num = 1:numsig;

    % Vectors generation
for i=1:length(data)

    T(i,1)=data(i,1);
    A(i,1)=data(i,num+1);

End

% DETERMINATION AND MANIPULATION OF THE ACCELERATION SIGNALS
 %ACI pickers determination to identify the begining of each signal

clear antes despues ACI

for n=1:length(T)

    ll=1;

    while ll<=n;

        antes(ll,1)=A(ll,1);
        ll=ll+1;

    end

        lll=n+1;
```

```
    while  lll <= length(T);

            despues(lll,1)=A(lll,1);
            lll=lll+1;

       end

   ACI(n,1)=n*log(var(antes))+(length(T)-n-1)*log(var(despues));

End

Time arrival determination from the ACI curve (minimun point)
clear ACI1

nnn=1;

for nn=100:length(T);

    ACI1(nnn,1)=ACI(nn,1);
    nnn=nnn+1;

end



for j=1:length(T);

if ACI(j,1)== min(ACI1);

      Tin1 = T(j,1);    %Para agarrar la senal desde mas atraz -0.1

 End

End

arrival(num,Nn)= Tin1;

end

end

% Save file

xlswrite(filesave,arrival,sheet,'C3')
```